Synthesis and Structural Analysis of Macrocyclic Arenes: Experimental and Computational Insights

Saber Mirzaei
Marquette University

SYNTHESIS AND STRUCTURAL ANALYSIS OF MACROCYCLIC ARENES: EXPERIMENTAL AND COMPUTATIONAL INSIGHTS

by
Saber Mirzaei, B.Sc.

A Thesis submitted to the Faculty of the Graduate School,
Marquette University,
in Partial Fulfillment of the Requirements for
the Degree of Master of Science

Milwaukee, Wisconsin
May 2019

ABSTRACT
SYNTHESIS AND STRUCTURAL ANALYSIS OF MACROCYCLIC ARENES: EXPERIMENTAL AND COMPUTATIONAL INSIGHTS

Saber Mirzaei
Marquette University, 2019

Synthesis, properties and applications of macrocyclic molecules have been one of the interesting branches of organic chemistry during the past century. Several classes of macrocyclic molecules, based on their repeating unit and connectivity pattern, have been discovered. Macrocyclic arenes, cyclo[n]veratrylenes, calix[n]arenes and pillar[n]arenes, were among the most interesting and studied molecules. The major difference between these molecules is the methylene-bridged connectivity pattern. In the present thesis, I attempted to synthesize these molecules using novel approach which has been developed in our group and performing some structural analysis using experimental and computational techniques.

The first synthesized and investigated molecule is the cyclotetraveratrylene (CTTV) which has the ortho (1,2) methylene-bridged connectivity pattern. This molecule showed conformational flexibility at the room temperature. This phenomenon intrigued us to investigate its conformational changes upon the one-electron oxidation. The results of both experimental and computational studies revealed that the most stable conformer of this molecule is different in the neutral (sofa) and cation-radical (boat) states. However, due to instability of the cation-radical structure we have not been able to isolate the crystal structure of this system.

The second synthesized molecules possessing the meta (1,3) methylene-bridged connectivity pattern, calix[4]arenes. Herein, I synthesized a series of calix[4]arenes with different substituents to show how the solvent environment and crystal packing forces can totally change the most stable conformation of these molecules. The results revealed that in the solution the 1,3-alternate is the most stable conformer, however, in the solid state, the boat is more stable. This phenomenon can be attributed to the intermolecular interaction of calix[4]arenes in the solution with the solvent molecules and in the solid states as the inter-calix[4]arene-calix[4]arene interactions.

Pillar[n]arenes are the third class of macrocyclic arenes that were investigated in this study which have para (1,4) methylene-bridged connectivity pattern. Since the fortuitus discovery of pillar[5]arne in 2008, selective synthesis of higher sizes ($n > 5$) has remained as an intriguing challenge for organic chemists around the world. Herein, I developed a novel synthetic method which can help us to synthesize pillar[n]arenes ($n = 5, 6$) selectively with high yield. The experimental and computational results indicated that the solvent has significant role in the size of the synthesized product. While the dichloromethane can generate more pillar[5]arene, using chloroform as the solvent can lead to pillar[6]arene as the dominant product. This effect can be attributed to the templating effect of the solvent.

ACKNOWLEDGMENTS

Saber Mirzaei

My Lord! Enrich me with knowledge… (Quran, 20:114)

At first, all the praises and thanks be to Allah (God) who sent his prophets to guide us to the straight path. There is not a shred of doubt of his constant presence and profound influence on whole my life. The great emphasis of Allah in the Holy Quran and his last prophet, Mohammad (may peace be upon him), on pursuing knowledge and using our thoughts to figure out the logic of the world is the main reason for me to following my graduate carrier thousands of miles away from my home and my family.

I would like to thank my supervisor, Prof. Qadir K. Timerghazin, for his kindness and encouragement. Moreover, I am grateful to him for letting me to work in another lab under the supervision of Prof. Rajendra Rathore (deceased February 16, 2018). Working in two labs under the supervision of two sophisticated professors gave me a great opportunity to learn how I can combine the experimental and computational techniques to have better insight about the physical and chemical properties of materials. Moreover, I should mention the kindness and generosity of Prof. Rathore for accepting me in his group and giving me several challenging projects.

Moreover, I am thankful to my committee members Professors Scott A. Reid, Jier Huang and Nicholas Reiter for their useful comments. I also thank Dr. Sergey V. Lindeman for the helpful discussions and several single crystal X-ray structures and Dr. Sheng Cai for the help with NMR studies and instruments. Furthermore, I would like to thank the group member of both Dr. Timerghazin's Lab (Niloufar Hendinejad) and Dr. Rathore's Lab (Dr. Denan Wang, Dr. Maxim V. Ivanov, Dr. Mohammad Mosharaf Hossein, Dr. Lena V. Ivanova and Ainur Abzhanova) for their helps.

Finally, I would like to express my sincere appreciation to my family who encouraged me throughout my undergraduate in Iran, and my graduate carrier in the Marquette University. Furthermore, a special gratitude goes out to my younger brother, Mohammad Saeed Mirzaei, for his constant support and valuable advices.

تقدیم به بابا و مامان

رَبِّ ارْحَمْهُمَا كَمَا رَبَّيَانِي صَغِيرًا...

TABLE OF CONTENTS

LIST OF TABLES

LIST OF FIGURES

LIST OF SCHEMES

Chapter 1

INTRODUCTION

During the recent decades, the macrocyclic molecules attracted so many chemists and biochemists due to the numerous intriguing features including host-guest interaction, self-assembling, self-complexing and symmetrical structures. The symmetrical and typically cyclic structures of macrocycles make them an attractive cavity for guest molecules to bind. Moreover, the repeating unit of these systems make the characterization relatively easy which helping the synthetic chemist for the fast identification of the desired product. Several different classes of macrocyclic molecules are defined based on the repeating unit and the connectivity pattern of the monomers; cyclodextrins, crown ethers, cucurbit[n]urils, cyclo[n]veratrylene, calix[n]arenes and pillar[n]arenes are the major classes of the macrocyclic molecules.

Cyclodextrins: Cyclodextrins (CDs) were first reported in 1891 by Villiers and co-workers.[1] These cyclic molecules consisting of six (α-CD), seven (β-CD) and eight (γ-CD) glucose units with cavity size increasing with the number of glucose units. These water-soluble CDs, due to the presence of several hydroxyl groups, are commercially available. In contrast to its water-solubility, it should be noted that the internal cavity of these systems predominantly consist of carbon and hydrogen, which making a hydrophobic cavity. Therefore, the CDs can capture the hydrophobic molecules or hydrophobic part of a molecule inside the polar solvents like water.

As depicted in the **Figure 1.1**, the CDs can bind to the guests with same size as its cavity.[2] It has been revealed that the strong binding affinity of CDs can be attributed to

the unfavorable binding of water with the hydrophobic interior part of cyclodextrins.[1] The stronger hydrophobic-hydrophobic interaction and elimination of waters leads to the formation of complexes with different molecules from small size to large polymers.[3,4]

The guests prefer to enter the CDs from the wider rim as they face smaller stric hindrances. Moreover, if the guests possess extended structure, they can bind with two or even more CDs at the same time. Based on these host-guest interaction properties, Harada and co-workers tried to make cyclodextrin-based molecular machines.[5] They investigated the possibility of having a CD which can move back and forth along a polymer. In addition to organic molecules, CDs can bind to inorganic and organometallic complexes, especially, ferrocenes.[6] The oxidation state of the ferrocenes can control the binding or dissociating state of the complex. In the neutral state, they showed relatively strong binding constant. However, oxidizing the ferrocene leads to the dissociation of the complex. Iron containing metallocene can bind in different pattern with the different size of CDs (**Figure 1.2**).

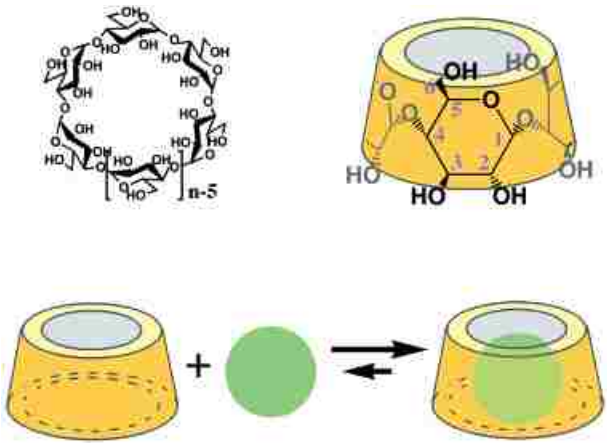

Figure 1.1 The structure of Cyclodextrins (CDs, n = 6, 7, 8) and its host-guest pattern. The picture adopted form the Ref. 2.

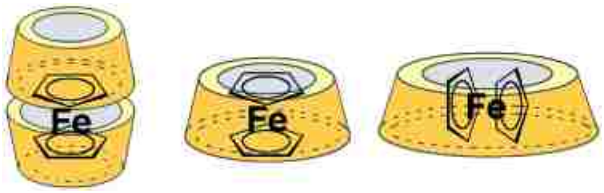

Figure 1.2 The complex of ferrocene with α (left), β (middle) and γ (right) CDs. The picture adopted form the Ref. 2.

Crown ethers: Since the first fortuitous identification of crown ethers by Pedersen in 1967, this family of molecules has been a topic of a long-standing interest.[7] Later in 1987 he won the Nobel prize in chemistry for his work in this area. The crown ethers are simple cyclic polyethers with -CH_2CH_2O- repeating units which based on the size have different affinity for alkali metals. As depicted in **Figure 1.3**, there is a systematic nomenclature for crown ethers which the first number representing the number of all atoms (except hydrogens) in the ring and second number showing the number of oxygens in the molecule.

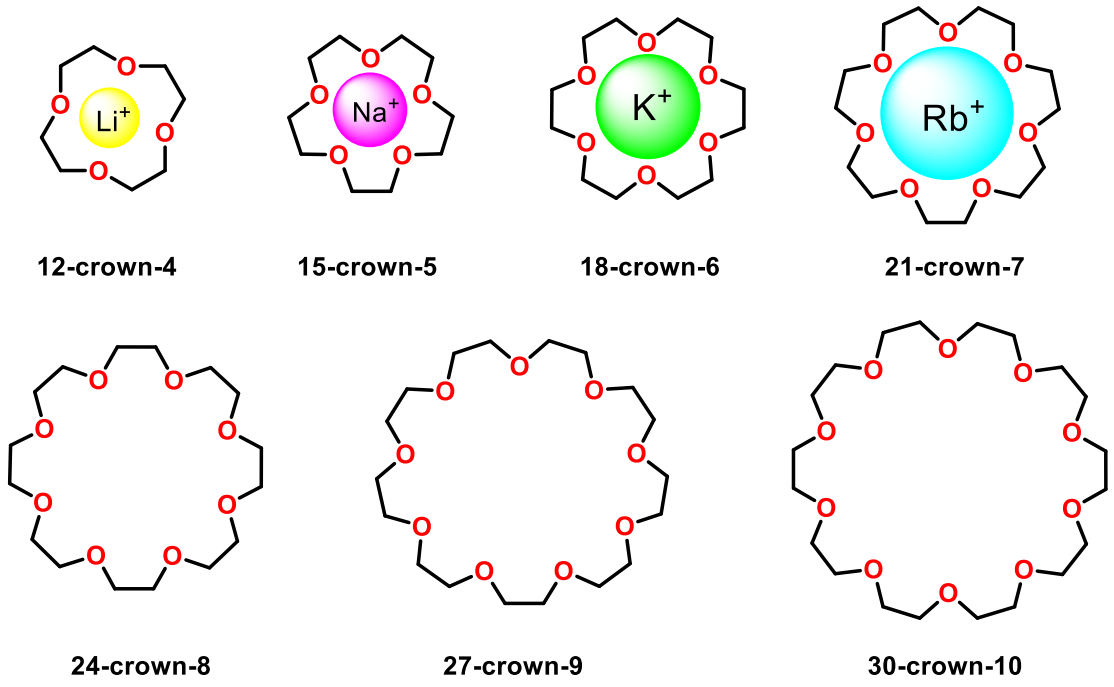

Figure 1.3 The chemical structure of some common crown ethers and the specific binding sites for alkali metals.

The lone pairs of oxygens can bind to the positively charged alkali cations like sodium and potassium. This binding affinity is very selective based on the size of the alkali metals. For example, the lithium cation cannot fit properly inside the 18-crown-6 or larger crown ethers. Therefore, these compounds can be used to selectively extract the desired metal from the solution. In addition to sharing lone pairs with the metals, oxygens play significant role in the solubility of crown ethers in different solvents. The possibility of forming hydrogen bonding with protic solvents and the presence of hydrophobic hydrocarbons made these compounds soluble in broad range of solvents including water and organic solvents.[8] This unique feature of crown ethers allows the researchers to use them for solubilizing metal containing salts (e.g., KF). The crown ethers bind with the positively charged metal and increase the solubility of counter anion which leads to the

dramatically increase of reactivity.[9] This phenomenon is very useful in the field of phase transfer catalysis.[10] In addition of complexation with alkali metals, it has been revealed that some of the crown ethers can bind strongly with other species trough the hydrogen binding. For instance, the 18-crown-6 (see **Figure 1.3**) is well-known for its selective binding with potassium; however, less appreciated, this macromolecule can bind with the protonated amines both in solution and gas phases.[11–13]

Cucurbit[n]urils: The similarity of methylene-bridged glycoluril macrocycles to the *cucurbitaceae* family of plants was the prominent reason for naming these pumpkin-shaped molecules cucurbit[n]urils (CB[n]) by Mock and co-workers in 1981.[14,15] Cucurbit[n]urils are the result of the condensation of glycoluril and formaldehyde under the acidic condition (**Figure 1.4**). The CB[6] was the only identified size of cucurbit[n]urils for around two decades (**Figure 1.5**). It should be noted that this molecule has been synthesized for the first time in 1905,[16] however, due to the solubility problems, has not been characterized since 1981.[14] Later, the research groups of Kim and Day developed new synthetic method for synthesizing different sizes of CB[n] molecules.[17–19] They found the importance of temperature in controlling the size of CB[n]s. To the contrary of higher temperatures (> 110 °C) which leads to the CB[6] as the only product, the lower temperatures (75-90 °C) can lead to CB[n] with different sizes.[18] The crystal structures of CB[n] with different sizes revealed that despite the significantly different cavity sizes, all CB[n] have same depth (~9 Å). It should be noted that the cavity size of CB[10] is too large to bind strongly with the smallest synthesized size cucurbit[n]uril (n = 5).[19] Moreover, in some crystal structures, water molecules are trapped inside the cavity which are removed upon the binding with the guests.

The CB[n] family and their applications have been the subject of several reviews during the past decades.[20–22] These macrocyclic molecules gained large interest due to the several reasons including: commercial availability, existence in several different sizes (n = 5-10), selective and strong complexation with wide variety of guests and solubility in aqueous media. It should be noted that the one pot synthesis is another important reason for ever-growing applications of these macromolecules.

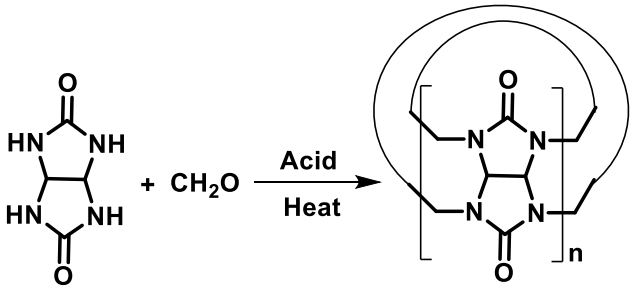

Figure 1.4 The general method for synthesis of CB[n].

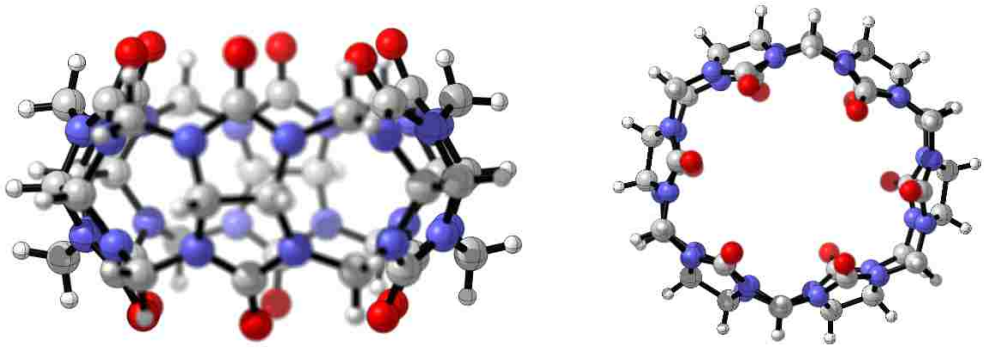

Figure 1.5 The 3-D representation of CB[6] from top (right) and side (left) views.

As depicted in **Figures 1.4** and **1.5**, the glycoluril molecules are inter-connected with two methylene (CH_2) groups to form the bridges. This unique feature of CB[n] macrocycles made the whole structure less conformationally flexible. Moreover, the

highly symmetrical structure created identical entrances for guests on both sides of the molecule. Therefore, the entropy change of the host does not affect the binding affinity of these macromolecules.

Cyclo[n]veratrylenes, Calix[n]arenes and Pillar[n]arenes: The chemistry of macrocyclic arenes, especially alkoxy substituted benzenes, was among the most interesting subjects of macromolecular systems during past decades.[23–26] The smallest family of these groups is the cyclotriveratrylene (CTV) which is the result of the connection of three veratrole (1,2-Dimethoxybenzene) using CH_2 groups as the bridge.[27] The NMR spectroscopy and single-crystal structure revealed that the most stable conformer of this molecule has crown-like structure.[27] There are two general possible approaches for the synthesis of this molecule; condensation of veratrole alcohol under acidic condition and condensation of veratrole using paraformaldehyde and Lewis/Brosted acids (**Figure 1.6**).[28–30]

The host-guest interaction of CTV and its derivatives are studied extensively.[31–35] The strong binding affinity of CTVs for fullerenes are well-known. The binding constant increasing with the increasing the size of the fullerenes ($C_{84} > C_{70} > C_{60}$) which has been attributed to the better non-covalent π-π interaction between bigger fullerenes and CTV.[36] The other cyclo[n]veratrylene (n = 4, 5, 6) are also synthesized. Among them the cyclotetraveratrilene (CTTV, n = 4) indicated the conformational flexibility in the solution. However, according to the variable temperature NMR and single X-ray crystal structure, it has been revealed that the most stable conformer for this macrocyclic molecule has sofa-shaped structure.[37] Also, changing the methoxy groups to hydroxyl did not affect the most stable conformer in the solution or crystal state.[37]

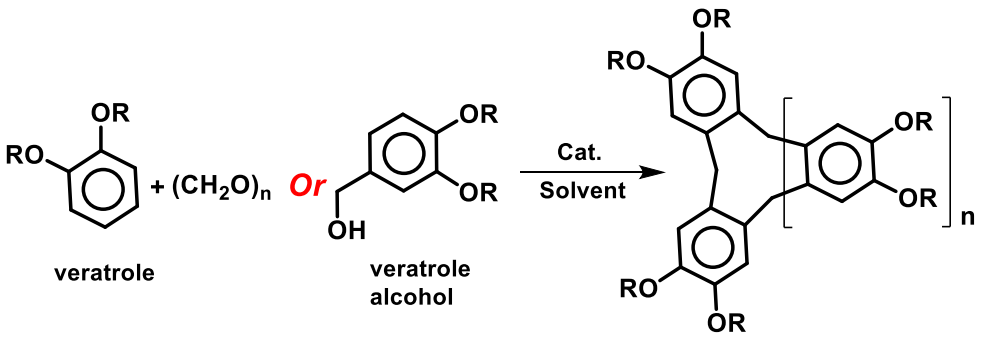

Figure 1.6 The general synthetic methods and structure of cyclo[n]veratrylene (n = 1-4).

Cyclo[n]veratrylene presenting the arenes-based macrocyclic compounds with the ortho (1,2) bridging pattern. Another macrocyclic molecule which containing the substituted arenes are calix[n]arenes, named due to calix-shaped structures. These macromolecules following the meta (1,3) methylene-bridged pattern. In comparison to cyclo[n]veratrylene, these family of molecules were synthesized in much greater extent and their properties are investigated prevalently in the literatures related to the macrocycles or supramolecular chemistry. It should be noted that several research groups extended the calixarene families to the other aromatic systems including furan (calixfurans),[38] pyridine (calixpyridines),[39] pyrrole (calixpyrroles),[39] indole (alixindoles),[40] naphthalene (calixnaphthalenes),[41] etc. Moreover, several groups reported the synthesis of calixarenes with the different groups as the bridge instead of methylene.[42–45] For example, thiacalixarene which the bridge CH_2 groups have been replaced with the sulfur.[44]

The smallest identified and characterized calixarene contains four substituted benzene ring (calix[4]arene). This molecule, due to the vast spectrum of application, attracted ever growing attention from the researchers. Interestingly, this molecule can

show four different conformers cone/boat, partrial-cone (paco), 1,2-alternate and 1,3-alternate (**Figure 1.7**). Depending on the substituents, these conformers can be rigid and separable or interconverting very fast in solution. However, the fast interconversion between these conformers will be halted at low temperature or binding with the guests.

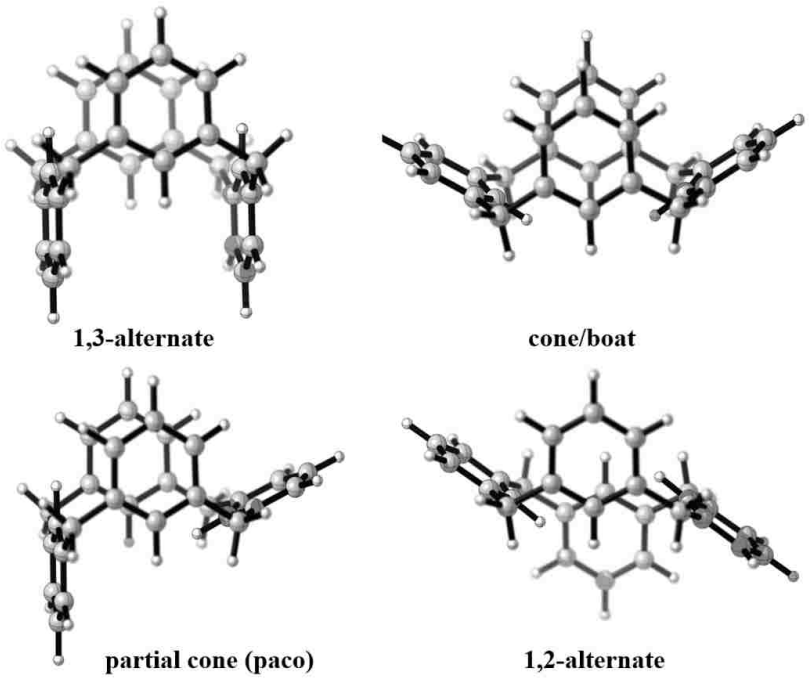

Figure 1.7 The 3-D representation of four different conformers of calix[4]arene; the position of all aromatic protons can be occupied with different groups (e.g. methoxy, methyl, etc.).

The presence of four aromatic rings as potential source of pi-electrons for π-π and π-cation interactions and a symmetrical rigid structure intrigued researcher to examine its abilities for binding with vast variety of guests. NO_x gases are one of the interesting possible guests which can interact strongly with the cavity of calixarenes. The colorless dimer of nitrogen dioxide (NO_2) can undergo disproportionation upon the reaction with

calixarenes to form π-cation (NO^+) interaction which leads to the color change.[46,47] This phenomenon provokes several groups to generate nitric oxide artificially using $NOBF_4$ or $NOSbCl_6$ salts and investigate its interactions with the different substituted calixarenes.[48–51] During the past decade, Rathore and co-worker tried to design and synthesize novel calix[4]arenes for strong binding with nitric oxide.[52–55] These molecules are designed to act as the NO detector or storage materials.

The practical applications of calixarenes are not confined to the NO detection. The high binding affinity of calix[4]arenes for ionic metals and neutral molecules intrigued so many researchers to investigate their applications for separation of toxic metal. The two alkali metals Cs and Sr are the byproducts of nuclear reactions which gain lots of attentions due to their radioactivity concerns.[56,57] Also, several different chemically modified calixarenes (e.g., calix[4]arene-crown and mercaptocalix[4]arenes) are synthesized to separate the hazardous materials (e.g., mercury) selectively.[58] Moreover, calixarenes were used for making several selective electrodes for cations like sodium (Na^+) and potassium (K^+).[59–62] The accurate identification of these ions is originating from their importance role in the biological systems. In addition of metals, Regen and coworkers attempted to build a thin-film membrane of calixarene to separate the He gas from the mixture of several gases.[63] Moreover, Chan et al., claimed that their selective electrode for *in situ* generated hydrazone can detect this neutral compound with acceptable range of accuracy.[64]

The latest family of arene-based macrocyclic compounds is discovered by Ogoshi and coworkers in 2008.[65] They named the newest family of macrocyclic molecules as the pillar[n]arene due to the rigid and tubular, pillar-shaped, structure of them. New bridging

pattern (para (1,4)), easy and one-pot synthesis, possibility of synthesis with different cavity sizes, versatile functionality and symmetrical structures are some of the unique features of pillar[n]arenes which gain the attention of chemist from all around the world.[26]

The first pillar[n]arene, a five membered macrocycle (pillar[5]arene), was synthesized and characterized accidentally as the byproduct of a reaction which has been designed to synthesize a polymer.[65] As depicted in the **Figure 1.8**, the reaction was a one-pot synthesis of a phenolic polymer using 1,4-dimethoxybenzene and paraformaldehyde as the starting materials and $BF_3 \cdot Et_2O$ as the Lewis acid catalyst. In contrast to $BF_3 \cdot Et_2O$, which showed the pillarene as the major product, employing other Lewis acids, $FeCl_3$ and $SnCl_4$, as the catalyst generated the polymer as the major product and pillarene was the minor product.[65]

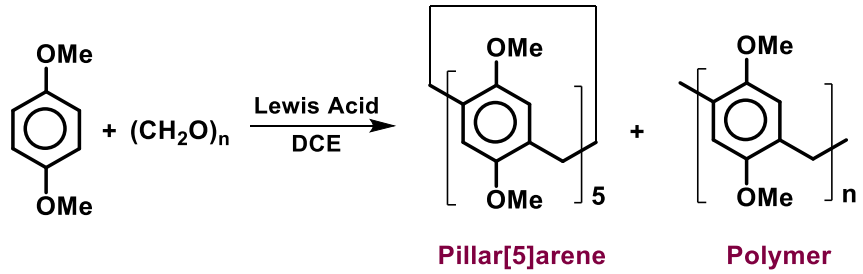

Figure 1.8 The first reported condition for the synthesis of pillarenes using DCE (1,2-dichloroethane) as the solvent (Ref. 65).

After the report of these results, several different groups tried to optimize the reaction conditions to increase the yield of the pillarenes in comparison to the

polymerized product. Ogoshi and coworker, changed the ratio of paraformaldehyde to increase the yield form 26% to around 73%.[66] Moreover, the results of Szumna et al. investigated reactions revealed highly solvent-dependent nature of this reaction.[67] Their results indicated that the 1,2-dichloroethane (DCE) is the best solvent for the synthesis of pillar[5]arene. However, employing other solvents (e.g., dichloromethane or chloroform) can lead to the higher pillarenes.[67] Therefore, the Hou and coworkers attempted to synthesize and characterize several higher pillar[n]arenes (n > 5).[68] Their results revealed the possibility of synthesis of higher pillar[n]arenes (n = 6-10) under the kinetically controlled reaction. However, the yield of seven-, eight-, nine- and ten-membered pillarenes did not exceed 3%.[68]

All the evidences pointed to the great influence of the solvent on the synthesis of pillarenes. Therefore, Ogoshi and coworkers attempted to find the best solvent for the synthesis of pillar[n]arene (n = 5, 6) selectively. They figured out the high potential of chlorocyclohexane (ClCy) as the solvent for the selectively synthesis of pillar[6]arene.[69] They define this effect as the template-effect of the solvent for selectively syntheses of pentamer (pillar[5]arene) or hexamer (pillar[6]arene) as the desired product. The bulky hydrocarbons, e.g., ClCy, can act as the both template and guest for closing the macrocyclic structure in bigger shape (hexamer). In contrast, small molecules, especially 1,2-dichloroethane (DCE), can push the reaction to the pentamer structure (**Figure 1.9**). However, for this special case, cyclohexylmethyl (CH_2Cy), the low yield was attributed to steric hindrance which prevent the formation of pentamer structure.[69]

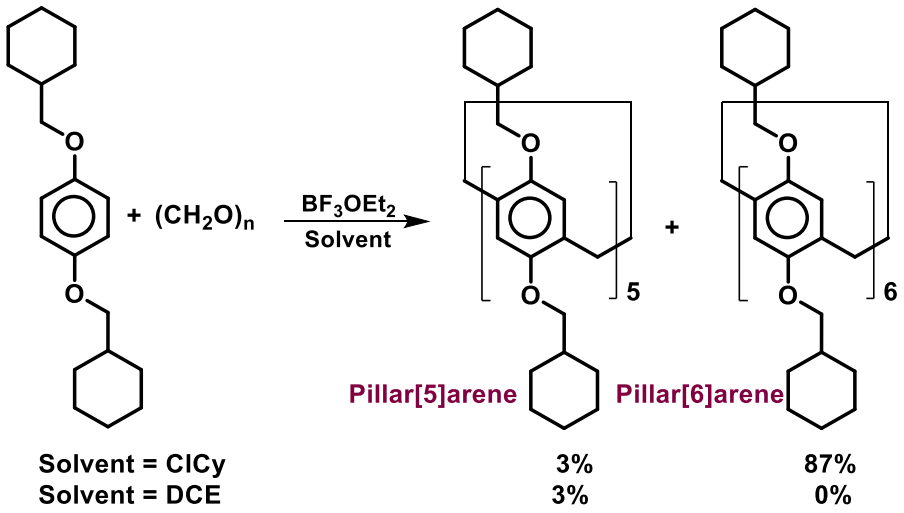

Figure 1.9 The effect of the solvent on the synthesis of pentamer (n = 5) or hexamer (n = 6) pillar[n]arene. The chlorocyclohexane (ClCy) and 1,2-dichloroethane (DCE) showed the templating-solvent effect for the synthesis of pillar[6]arene and pillar[5]arene, respectively.

Additionally, Ogoshi and co-workers investigated the conversion of pure pillar[5]arene and pillar[6]arene to each other by selecting the solvent under the Lewis acid catalyzed reaction. The results revealed that pillar[5]arene will be converted to the pillar[6]arene using the chlorocyclohexane (ClCy) as the solvent. Also, the pillar[6]arene has been converted to pillar[5]arene in the 1,2-dichloroethane (DCE) media. Moreover, Nierengarten and coworkers started from the timer of CH_2-bridged 1,4-diethoxybenzene as the starting material with this hope to synthesize pillar[6]arene with high yield.[70] However, the major product was pillar[5]arene in the 1,2-dichloroethane (CH_2Cl_2) media. The results of Ogoshi et al. and Nierengarten et al. revealed the dynamic nature of methylene bridge bonds formation/cleavage during the reaction (**Figure 1.10**).

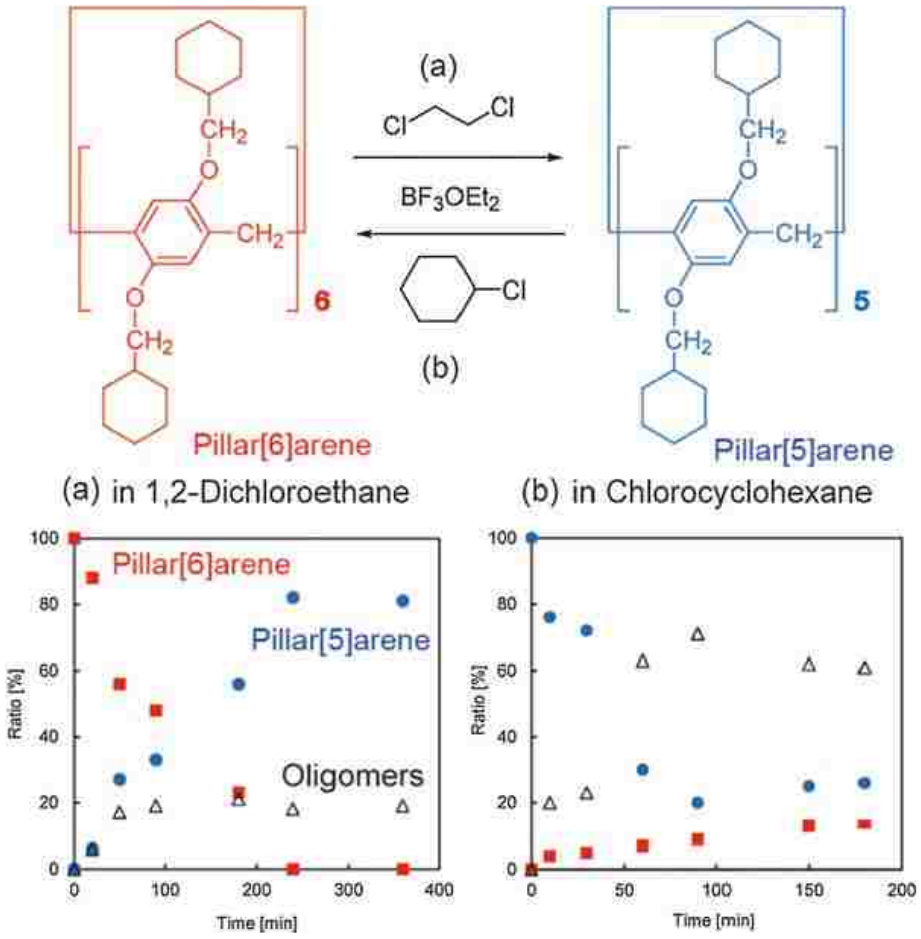

Figure 1.10 The dynamic nature of CH_2-bridge bonds formation/cleavage during the reaction (adopted form Ref.69).

The pillarenes have a great potential for carrying several different functional groups to change its solubility, interactions with guests and assemblies. The deprotection of ether part will lead to the reactive OH groups which can undergo several different reactions. This conversion, from alkoxy to hydroxyl, can be accomplished easily by employing Tribromoboron (BBr_3). The presence of OH groups helped the researchers to install different functional groups which lead to the synthesis of water-soluble pillarenes. Moreover, by optimizing the reaction conditions (equivalent of BBr_3 and temperature),

one can control the number of generated OH groups. However, due to generation of several different product, the separation of the desired product can be completely difficult. Therefore, another approach, using subsequent oxidation/reduction, has been proposed.[71–73] In this method, the final product bearing two hydroxyl groups on the same benzene ring which results in the cleaner reaction. Starting from the reagents carrying the bromide moieties is another proposed for post modification and installing different functional groups on the pillarenes.[74] Also, the co-cyclization of different studying materials let us to have pillarenes with limited number of modifiable groups.[75–77] However, synthesis and purification of desired product with acceptable yield remains as a challenging part of co-pillarenes synthesis.

The unique structure of pillarenes, in comparison to other macrocyclic arenes, make them very interesting candidates for (bio)chemist to investigate their host-guest properties. The presence of para-bridging CH_2 groups can generate highly ordered symmetric cylindrical structure, pentagonal and hexagonal for pillar[5]arene and pillar[6]arene, respectively. In contrast to pillar[5] and pillar[6]arene, the crystal structures of higher pillar[n]arenes (n = 8-10) showed two cavities with different sizes.[78] For example, pillar[9]arene showed on hexagonal and one pentagonal cavities. However, the applications of these higher pillarenes remained totally restricted due to the relatively hard synthesis and purification.

Pillarenes feature a π-electron rich cavity which has strong tendency toward the binding with neutral (e.g., n-hexane and n-heptane) and cationic (e.g., ammonium and pyridinium) systems. The binding affinity of pillarenes with these molecules are mainly attributed to the CH-π and cation-π interactions. The association constant for alkanes are

much lower than the cations. Though, replacing the hydrogens with electron-withdrawing groups (e.g., halogens) can increase the binding constant for linear hydrocarbons. In addition to the presence of electron-withdrawing groups, the shape of the hydrocarbons can greatly affect the possibility of their entrance to the cavity of pillarenes. For instance, the branched and cyclic hydrocarbons cannot form complex with the smallest synthesized pillar[n]arene (n = 5).[79] Moreover, changing the substituent of pillarene form alkoxy to other functional groups (e.g., carboxylic acid) can alter the binding constant significantly. In 2014, Xia and Xue reported the synthesis and binding affinity of pillar[5]arene with one para-carboxylic acid moiety.[80] Their results revealed very large binding constant (K = 1.52×10^5 M^{-1}) for monoamine derivative in chloroform. This value can be attributed to the hydrogen binding between the COOH and NH_2 groups (**Figure 1.11**).

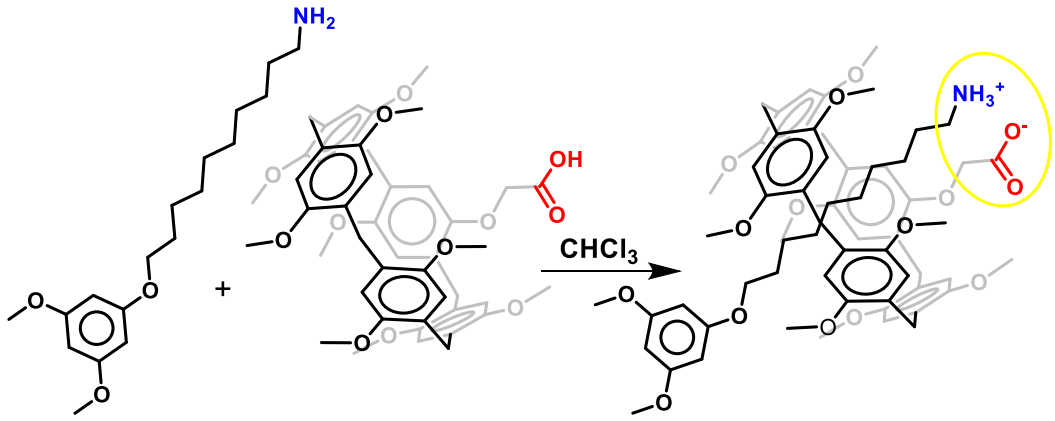

Figure 1.11 Modifying the pillar[5]arene ring to increase its binding affinity for guest molecules.

The cavity size of pillar[6]arene (6.7 Å) is bigger than the pillar[5]aren (4.7 Å). This larger cavity size can alter the host-guest interactions dramatically. For example,

Fan et al. reported the charge transfer complexation of carbonium tropylium ion tetrafluoroborate.[81] The NMR data indicated that the suitable cavity dimension of pillar[6]arene is responsible for the binding of this cation inside the host and subsequent color change (form color less to red). To the contrary of pillar[6]arene, the smaller (pillar[5]arene) and bigger (pillar[7]arene) cavities did not show any color change which indicating the disability of these pillarenes for forming stable complexes.[81]

In addition to interesting host-guest chemistry, the highly symmetrical structure of pillarenes intrigued researchers to investigate the supramolecular assemblies (1-D, 2-D and 3-D) of these macromolecules. One-dimensional assemblies will lead to the tubular structures. These tubular structures which are the result of covalent interconnection of different number of pillarene units will form tube-like systems. The smallest possible structure has been synthesized by connection of two pillar[5]arens.[79] Interestingly, this dimer molecule showed considerably larger binding constant for linear alkanes in comparison to its monomer. Later, several different sizes (up to 9-mer) have been synthesized by Stoddart and his coworkers.[82]

Chapter 2

ORTHO (1,2) METHYLENE-BRIDGED MACROCYCLIC ARENES: REDOX-INDUCED CONFORMATIONAL CHANGE OF CYCLOTETRAVERATRYLENE (CTTV)

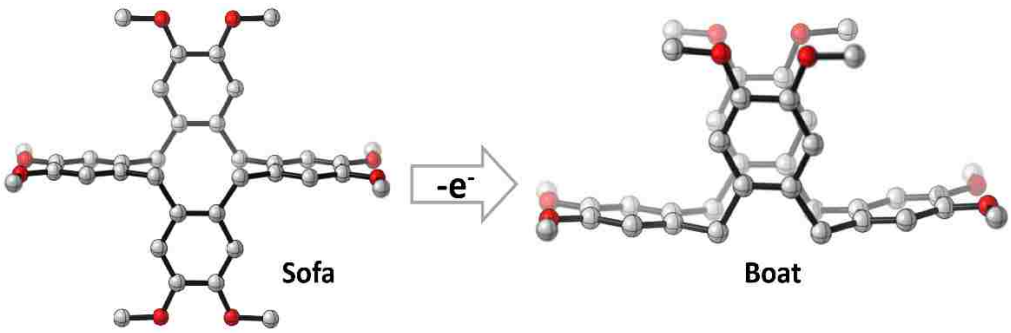

Electro-active polychromophoric assemblies that undergo clam-like electromechanic actuation represent an important class of organic functional materials. Here, we show that the readily available cyclotetraveratrylene (CTTV) undergoes oxidation-induced folding, consistent with interconversion from a non-cofacial “sofa” conformation to a cofacial “boat” conformer. It is found that the non-cofacial "sofa" conformer of CTTV forms stable electron donor-acceptor complexes with chloranil and DDQ. Electron-transfer induced conformational transformation in CTTV provides a framework for the rational design of novel organic functional molecules.

Introduction: The design and synthesis of organic functional molecules is critically important for numerous practical applications, such as molecular sensors, molecular switches, nonlinear optical materials, etc.[83–92] Among the various classes of functional materials, molecular actuators have attracted significant attention. Typically, a molecular actuator exhibits dramatic conformational changes when triggered by an external stimulus (e.g., heat, light, metal ion binding, or electron transfer), leading to a modulation in their physical properties (e.g. color, spin, electrical conductivity, and optical properties).

Among various external stimuli, electron transfer is of particular importance, especially in the case conformationally mobile bichromophores that can adopt a π-stacked arrangement of its chromophores. Extensive studies have established that upon ionization, charge-resonance stabilization of the cationic charge (i.e., hole) is dependent on the orbital overlap between the aromatic moieties of two chromophores.[93,94] Because orbital overlap is maximal when the chromophores are perfectly sandwiched,[93] many conformationally mobile chromophores undergo oxidation-induced actuation from "open" to "closed" conformation as schematically depicted in **Figure 2.1A**.

Many examples of molecular actuators are available in the literature,[87–89,95–97] and here we seek to identify whether readily available[98–101] cyclotetraveratrylene (CTTV, **Figure 2.1B**) can undergo oxidation-induced actuation. Past studies have established that conformationally mobile CTTV at the neutral state prefers "sofa" conformation and not "boat" or "crown" conformations. Considering that the closed conformation of CTTV contains a pair of cofacially-arrayed aromatic rings well-suited for the efficient hole stabilization, in this work we question whether

CTTV would undergo oxidation-induced actuation from the (open) “sofa” to (closed) “boat” conformation.

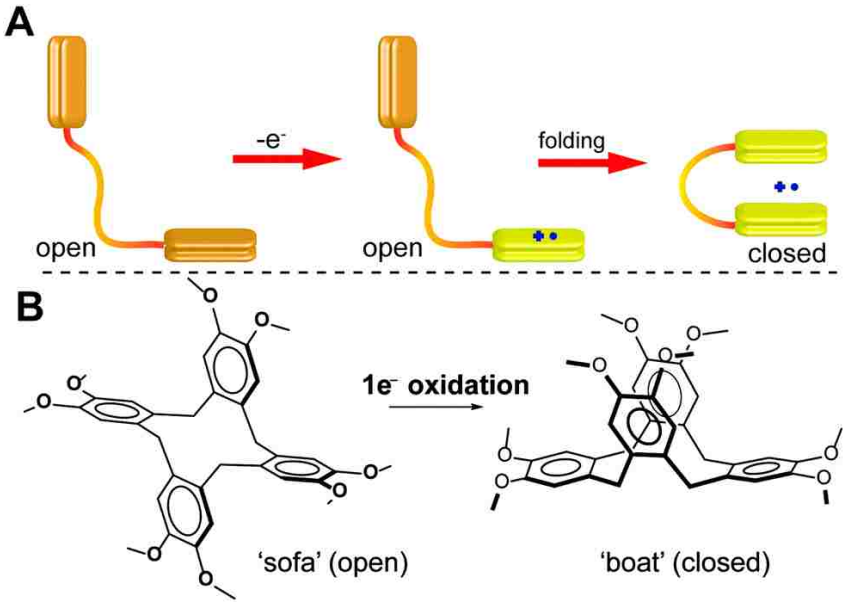

Figure 2.1 A. Schematic illustration of the electron-transfer-induced conformational transformation. B. Illustration of the oxidation-induced folding from (open) ‘sofa’ or (closed) ‘boat’ CTTV.

Accordingly, here we demonstrate with the aid of electrochemistry, generation of CTTV cation radical, and DFT calculations that in solution CTTV indeed undergoes (electro)chemical actuation as depicted in **Figure 2.1B**. Furthermore, we show that CTTV effectively binds chloranil (CA) and 2,3-dichloro-5,6-dicyano-p-benzoquinone (DDQ), forming electron donor-acceptor (EDA) complexes as shown via optical spectroscopy and X-ray crystallography. The latter showed that in the crystal structures of both EDA complexes, the CTTV molecule exists in open conformation, which allows a maximum number of

cofacial π-π contacts between the aromatic moieties of CTTV and the aromatic acceptors. These findings underscore the importance of local environment in promoting oxidation-induced actuation and contribute to the design of novel organic functional molecules based on oxidation-induced mechanical actuation.

Computational details: All electronic structure calculations were performed in Gaussian 09 package.[102] It is well known that accurate description of the electronic structure of the cation radicals of pi-conjugated and pi-stacked systems is challenging for many DFT functionals due to the self-interaction error that causes artificial hole delocalization and leads to underestimated oxidation potentials and incorrect nature of the excited states.[103–105] It was shown[106] that B1LYP[107] with 40% of the HF exchange provides a balanced description of the electronic structure of the poly-*p*-phenylene cation radicals. Accordingly, in this manuscript, we performed electronic structure calculations using B1LYP-40-D3/6-31G(d) level of theory. In order to account for dispersion interactions within B1LYP-40 functional we have utilized D3 version of Grimme's dispersion[108] parameters SR6=1.3780 and S8=1.2170. In recent studies we have shown[109,110] that such a modification provided a balanced description of the neutral and cation radical states of various pi-stacked systems. Solvent effects were included using the implicit integral equation formalism polarizable continuum model (IEF-PCM)[111] with dichloromethane solvent parameters (ε = 8.93). In all DFT calculations, ultrafine Lebedev's grid was used with 99 radial shells per atom and 590 angular points in each shell. In cation radical calculations, wave function stability test was performed to ensure absence of solutions with lower energy. Tight cutoffs on forces and atomic displacement were used to determine convergence in geometry optimization procedure. Harmonic

vibrational frequency calculations were performed for the optimized structures to confirm absence of imaginary frequencies. Free energies were computed within harmonic oscillator approximation for $T = 298.15$ K and $P = 1$ atm. NMR shielding tensors were computed with the Gauge-Independent Atomic Orbital (GIAO) method.[112]

Results and discussion: As first reported by White and Gesner, starting with veratryl alcohol in glacial acetic acid containing a few drops of concentrated sulfuric acid as catalyst, a mixture of cyclotriveratrylene (CTV, 68%) and CTTV (16%) can be generated by the cyclo-oligomerization reaction.[101] With the aim of selective production of CTTV, we employed (**Scheme 2.1**) methanesulfonic acid as catalyst and stirred the reaction mixture containing one equivalent of cyclotriveratrylene (CTV) and three equivalent of veratryl alcohol at room temperature for 3 hours, which afforded CTTV in excellent yield (>70%); see the Experimental section for full experimental details and complete characterization data.

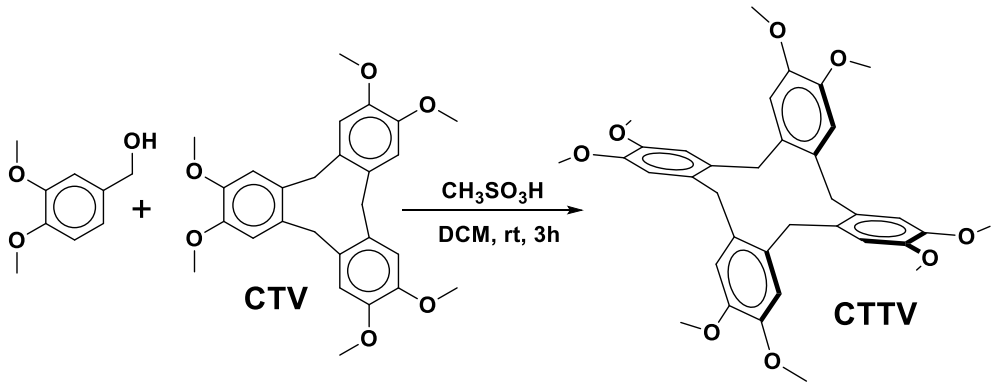

Scheme 2.1 Synthesis of cyclotetraveratrylene (CTTV).

Past studies using X-ray crystallography and variable temperature ^{1}H NMR (VT-NMR) have shown that CTTV and its derivatives prefer open conformation,

although the closed conformation may be energetically similar.[31,98,100,101,113–115] Here, in order to confirm these findings we performed VT-NMR experiment in CD_2Cl_2 solution. As shown in **Figure 2.2A** the NMR spectrum at 20 ˚C displays two broad signals at 6.60 and 3.72 ppm with the ratio of integration 1:4, respectively. Upon cooling to -80 ˚C, the aromatic signal separated into two equivalent sharp singlet signals at 6.82 and 6.22 ppm, while the peak from the methylene proton split into two doublets at 3.18 and 3.77 ppm. In addition, two sharp singlet signals at 3.48 and 3.85 were observed that were assigned to the methoxy groups. Simulation of the ^{1}H NMR spectra of open and closed conformations using DFT calculations confirmed that positions of the experimental peaks are consistent with the open conformation (**Figure 2.2B**). Thus, broadening of the signals at room temperature corresponds to the interchange between multiple equivalent conformers of open CTTV via pseudo rotation of the methylene carbons (**Figure 2.2A**). Note that temperature increase up to 60 °C did increases sharpness of the peaks without adding any new features (**Figure 2.9** in the Experimental section) suggesting that only one conformer of CTTV is present in solution.

In order to further confirm that open conformation is the most stable, we performed a conformational analysis of neutral CTTV using density functional theory (DFT) calculations. First, we note that the accurate description of the oxidation-induced actuation in such systems as CTTV presents a challenge for DFT.[116] Many standard density functionals do not include long-range dispersion

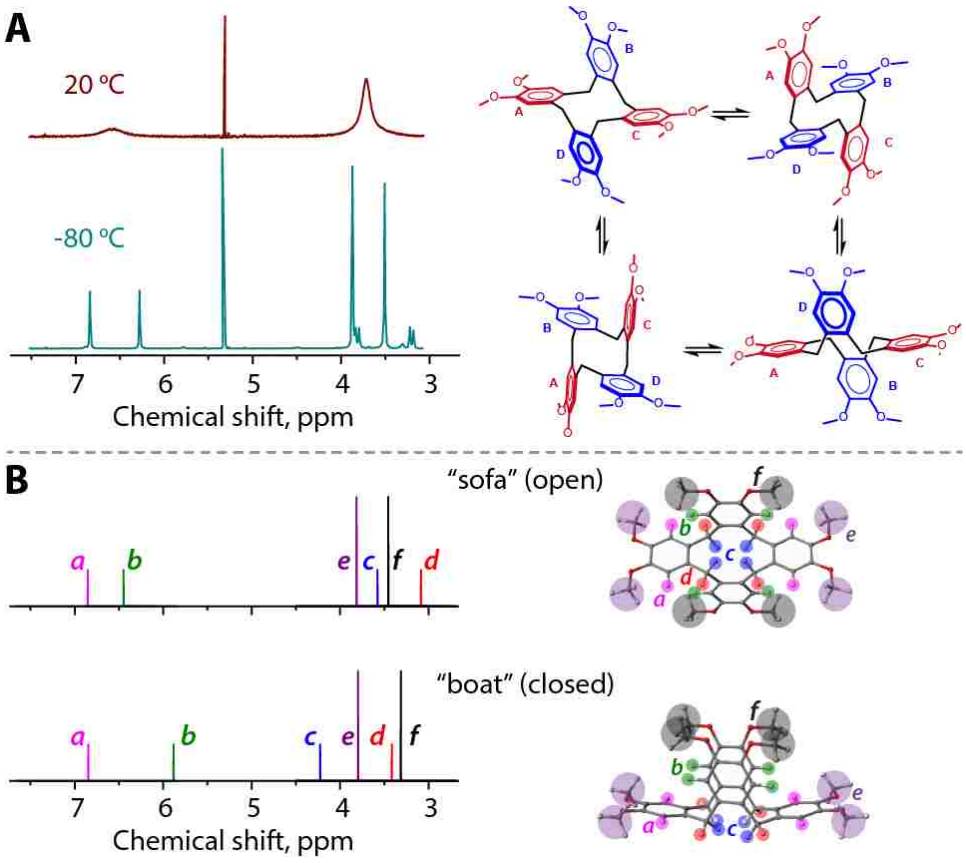

Figure 2.2 A. ^{1}H NMR spectra of CTTV at 20 and -80 ˚C. Representative interconverting structures of open CTTV are shown on the right. B. ^{1}H NMR spectra of open and closed CTTV calculated using B1LYP40-D3/6-31G(d)+PCM(CH_2Cl_2).

interactions and therefore total energy of the closed conformation of an actuator may be overestimated.[117] In addition, self-interaction error often leads to the underestimated oxidation potentials and artificially delocalized cation radical states.[118,119]

Recent benchmarking studies have demonstrated that standard B1LYP functional with 40% of Hartree-Fock exchange (i.e., B1LYP40) accurately reproduce oxidation potentials and the cation radical excitation energies of a variety of π-conjugated systems.[106,120] Furthermore, another recent study showed

that B1LYP40 accurately reproduces experimental binding energies of the van der Waals fluorene dimers, if the missing dispersion interactions are accounted for using the empirical Grimme's D3 term.[110] Therefore, in this work we employed B1LYP40-D3/6-31G(d) level of theory with the solvent effects accounted via polarizable continuum model (PCM) with CH_2Cl_2 parameters.

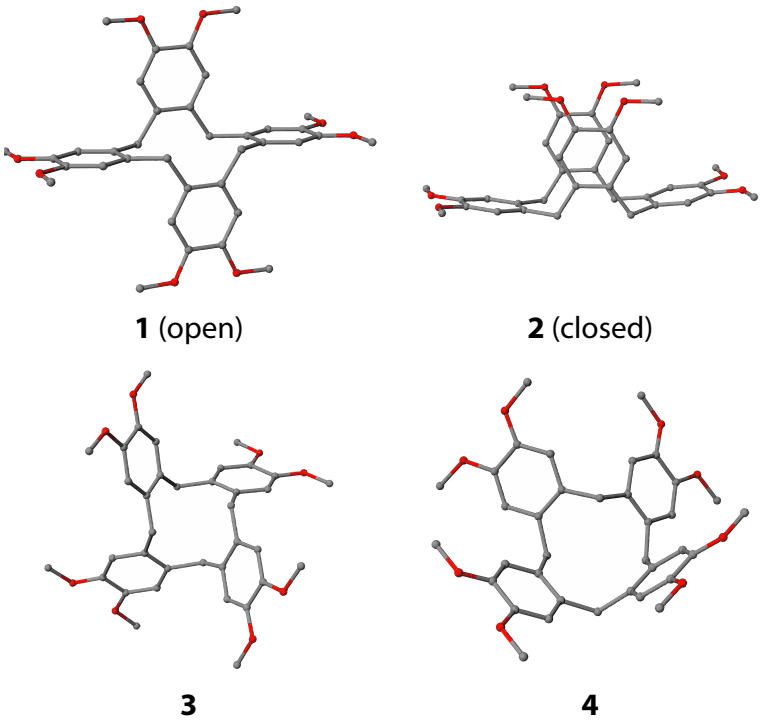

Figure 2.3 Conformations of CTTV calculated using B1LYP40-D3/6-31G(d).

Table 2.1 Relative free energies of CTTV conformers calculated using B1LYP40-D3/6-31G(d) and M062X/6-31G(d) in dichloromethane.

	B1LYP40-D3/6-31G(d)	M062X/6-31G(d)
1 (open)	0.00	0.00
2 (closed)	1.37	1.21
3	6.31	6.88
4	15.97	16.01

The calculations showed that among four different conformations, open CTTV is the lowest energy structure, lying 1.4 kcal/mol lower than the closed conformer (**Figure 2.3** and **Table 2.1**). While the energetic difference is small, this corresponds to 95.6% contribution of open CTTV at 22 ˚C according the Boltzmann distribution if entropic factor is included.

The electron donor strengths of CTTV and model monochromophoric compound 1,2-dimethoxy-4,5-dimethylbenzene (M) were evaluated by electrochemical oxidation at a platinum electrode as a 2.0×10^{-3} M solution in dichloromethane containing 0.1 M *n*-Bu_4NPF_6 as the supporting electrolyte. The cyclic voltammogram (CV) of model compound M showed (**Figure 2.4**) one reversible oxidation wave with the oxidation potential E_{ox} = 0.77 V vs Fc/Fc^+, while oxidation potential of CTTV was found to be 70 mV lower than M, i.e., E_{ox}[CTTV] = 0.70 V vs Fc/Fc^+, signifying that structural and conformational reorganization occurs leading to the stabilization of the cationic charge.

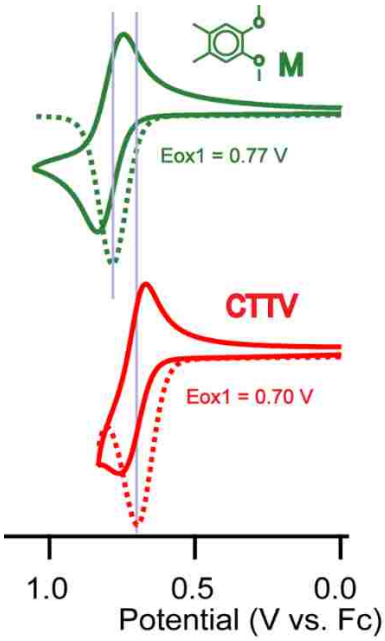

Figure 2.4 Cyclic voltammograms (CVs, solid lines) and square waves (SWs, dashed lines) of 2 mM CTTV (red color) and M (green color) in CH_2Cl_2 (0.1 M n-Bu_4NPF_6) at a scan rate 100 mV s^{-1}.

It has been established that at the cation radical state of a polyaromatic electron donor, charge-resonance stabilization is maximal when aromatic moieties adopt a perfect "sandwich-like" arrangement that allows for the maximal orbital overlap between the aromatic moieties.[93,94] Thus, many conformationally mobile actuators have been reported to undergo electromechanical actuation that is driven by the charge-resonance interactions. Yet, observed hole stabilization of 0.07 V in CTTV (i.e., $\Delta E_{ox} = E_{ox}[M] - E_{ox}[CTTV]$) is relatively small, especially considering that in *rigid* cofacially arrayed bichromophores hole stabilization may reach 0.35 V.[121,122] One has to note that although the enthalpy gain of a cofacial arrangement of two aromatic moieties may be indeed significant, the overall free energy gain depends also on the entropic contribution.[83] For example, a series of

veratrole- and acetal-based actuators showed a varied hole stabilization from ΔE_{ox} = 0.26 mV to 0.0 V, underscoring the important role of the linker connecting two chromophores (**Figure 2.5**).[87,89,95]

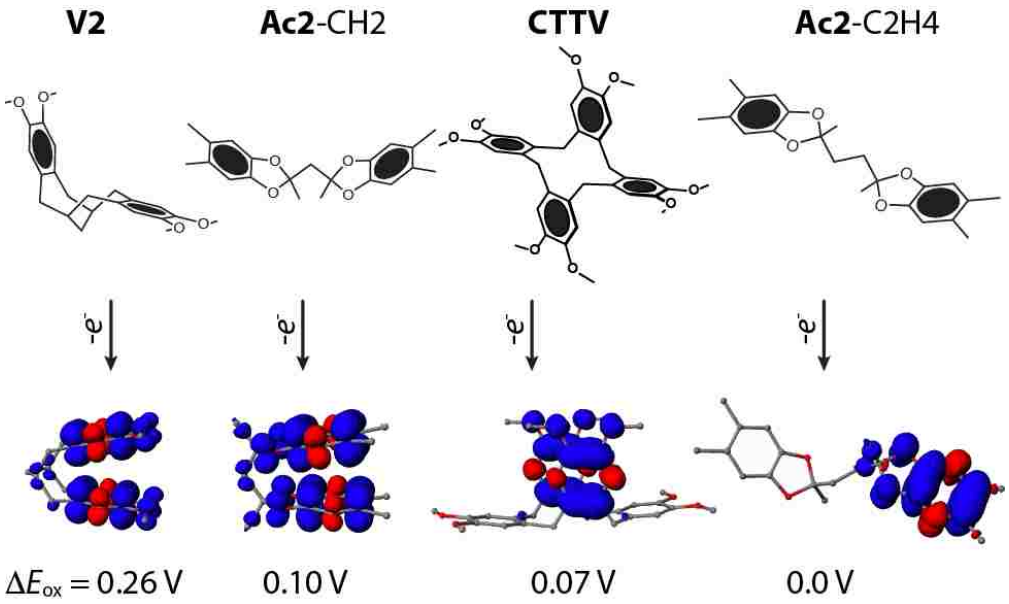

Figure 2.5 Examples of the actuators with varied hole stabilization (ΔEox) as indicated. Calculated [B1LYP40-D3/6-31G(d)+PCM(CH_2Cl_2)] spin-density plots show extent of hole delocalization in each case.

While actuators V2 and Ac2-CH_2 shown in **Figure 2.5** show a significant hole stabilization with the hole delocalization over both chromophores, compound Ac2-C_2H_4 does not display any stabilization with the hole localized on a single chromophore. In the case of CTTV, entropic penalty required to freeze (pseudo) rotation of the C-C bonds at four methylene groups upon its actuation, leads to a modest yet appreciable 70 mV stabilization with the hole delocalization over both chromophores. Finally, DFT calculations further confirmed that closed

conformation is the global minimum structure at the cation radical state that lies 5.6 kcal/mol lower than open $CTTV^{+\bullet}$ (**Table 2.2**).

Table 2.2 Relative free energies of $CTTV^{+\bullet}$ conformers calculated using B1LYP40-D3/6-31G(d) and M062X/6-31G(d) in dichloromethane.

	B1LYP40-D3/6-31G(d)	M062X/6-31G(d)
1 (open)	5.64	5.62
2 (closed)	0.00	0.00
3	12.57	18.82
4	20.37	21.31

In order to further support that CTTV undergoes oxidation-induced folding, we generated the cation radicals of CTTV via quantitative[123] redox titrations using stable cation-radical salt [$THEO^{+\bullet}SbCl_6^-$] (1,4,5,8-dimethano-1,2,3,4,5,6,7,8-octahydro-9,10-dimethoxyanthracene hexachloroantimonate; E_{red} = 0.67 V vs Fc/Fc^+, λ_{max} = 518, ε = 7300 M^{-1} cm^{-1}, as one-electron aromatic oxidants in dichloromethane.[121] The redox titration experiment was carried out by an incremental addition of sub-stoichiometric amounts of the electron donor (i.e., CTTV) to the solution of an oxidant cation radical (i.e., $THEO^{+\bullet}$). The one-electron oxidation of CTTV to $CTTV^{+\bullet}$ and reduction of $THEO^{+\bullet}$ to THEO can be described by an equilibrium shown in eq. 1.

$THEO^{+\bullet}$ + open CTTV ⇄ THEO + closed $CTTV^{+\bullet}$ (eq. 1)

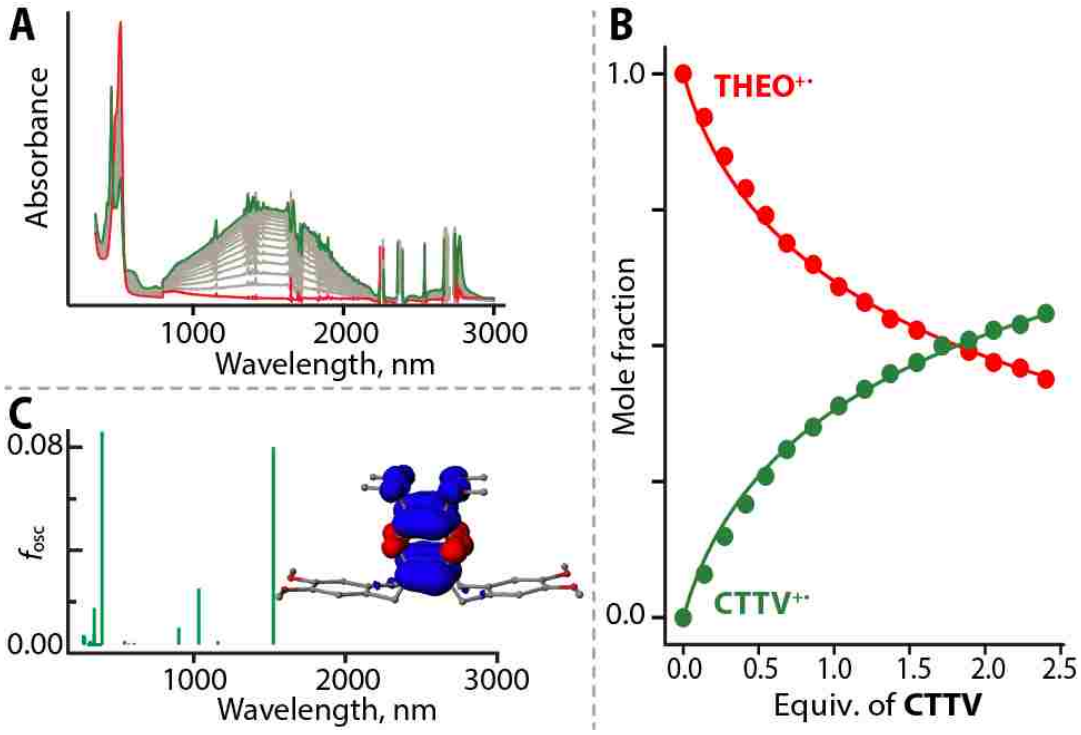

Figure 2.6 A: A: Spectral changes observed upon the reduction of 0.051 mM $THEO^{+\bullet}$ in CH_2Cl_2 (3 mL) with sub-stoichiometric addition of 1.49 mM solution of CTTV in CH_2Cl_2 at 22 ˚C. B: Plot of the mole fractions of $THEO^{+\bullet}$ (red) and $CTTV^{+\bullet}$ (green) against the added equivalents of neutral CTTV. Symbols represent experimental points, while the solid lines show best-fit to experimental points using $\Delta G = E_{ox}(CTTV) - E_{red}(THEO^{+\bullet}) = 25$ mV. C. Electronic transitions of closed $CTTV^{+\bullet}$ calculated using TD-B1LYP40-D3/6-31G(d)+PCM(CH_2Cl_2). Inset shows the isovalue plot of the spin-density distribution in $CTTV^{+\bullet}$ calculated at B1LYP40-D3/6-31G(d) level of theory.

Treatment of the orange-red solution of $THEO^{+\bullet}$ with increments of CTTV led to disappearance of the absorption bands of $THEO^{+\bullet}$ at 518 nm and concomitant growth of a new sharp band at 460 nm and a broad featureless band at ~1500 nm (**Figure 2.6A**). Numerical deconvolution[123] of the absorption spectrum at each increment produced mole fractions of $THEO^{+\bullet}$ and $CTTV^{+\bullet}$ against the added equivalents of CTTV (**Figure 2.6B**), confirming the redox reaction follows 1:1 stoichiometry as shown in eq. 1 without formation of CTTV dications or any

biproducts. Unfortunately, repeated attempts to generate crystal of $CTTV^{+\bullet}$ were unsuccessful due to the overnight decomposition of $CTTV^{+\bullet}$ even at -30 ˚C.

The presence of the intense absorption band at the near-IR region in $CTTV^{+\bullet}$ indicates extensive through-space hole delocalization, suggesting that $CTTV^{+\bullet}$ exists in the (cofacial) closed conformation. Indeed, a similar band at ~1500 nm has been previously reported in various other rigid veratrole-based cofacially-arrayed bichromophores.[83,87] Furthermore, TD-DFT calculations confirmed that closed $CTTV^{+\bullet}$ contains a strong transition at 1525 nm in full agreement with the experimental spectrum (**Figure 2.6C**).

As the isolation of the CTTV cation radical was not feasible, we questioned whether the partial oxidation upon interaction with an acceptor molecule might lead to the interconversion into a closed conformation. Thus, next we examined the electron donor-acceptor (EDA) complexes of CTTV with acceptors of varied strength, i.e., chloranil (CA, E_{red} = 0.02 V vs SCE)[124] and DDQ (E_{red} = 0.56 V vs SCE).[125,126] Mixing of CTTV with CA or DDQ in dichloromethane solvent produced a yellowish or brownish colored solution, respectively, indicative of the formation of the EDA complex. Indeed, the UV-vis absorption spectra of the CTTV~CA and CTTV~DDQ EDA complexes showed a charge-transfer band at λ_{CT} = 610 and 810 nm, respectively (**Figure 2.7**). The quantitative analysis of the binding of CA and DDQ with CTTV in solution was carried out by spectrophotometric analysis, with absorbance data treated according to the Benesi-Hildebrand procedure[127,128] to derive the values of association constants (K), extinction coefficient (ε_{CT}), and the "effective absorbance" ($K_{DA}\varepsilon_{CT}$) of the EDA complexes (**Table 2.3**). Interestingly, the CTTV~DDQ EDA complex displays a

high association constant K = 591 M^{-1}, which is about 40 times higher than that of CTTV~CA complex, and is consistent with the varied electron acceptor strength of DDQ and CA.

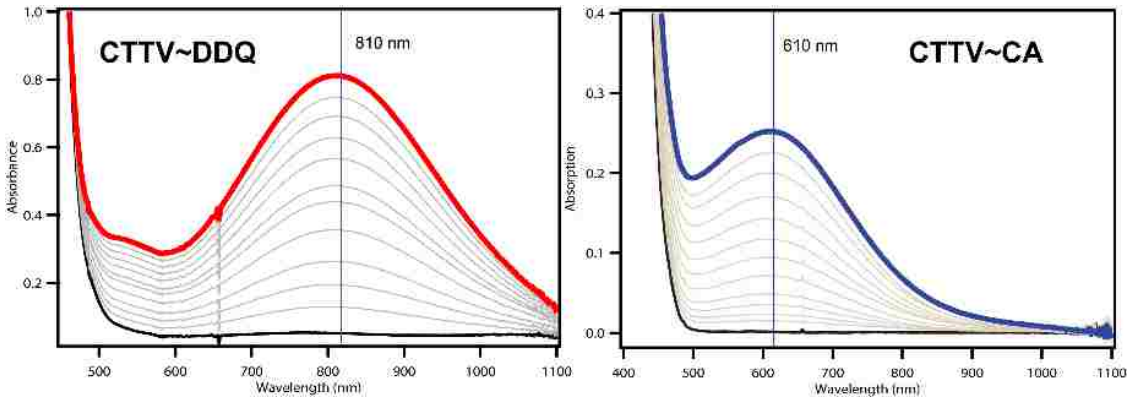

Figure 2.7 Left: Spectral changes recorded upon the incremental addition of CTTV (6.0×10^{-5} M) to DDQ (0.011 M) in dichloromethane. Right: Spectral changes recorded upon the incremental addition of CTTV (1.08×10^{-3} M) to CA (0.022 M) in dichloromethane.

Table 2.3 Compilation of wavelength of CT band, association constants, extinction coefficient and "effective absorbance".

Acceptor	λ_{CT} (nm)	K_{DA} (M^{-1})	ε_{CT} (M^{-1} cm^{-1})	$K_{DA}\varepsilon_{CT}$ ($\times10^3$)
DDQ	810	591	2066	1221
CA	610	15	347	5.205

Large quantities of the EDA complexes CTTV~DDQ/CTTV~CA can be easily prepared by mixing the CTTV with DDQ/CA in chloroform or dichloromethane at room temperature. After careful layering with hexane and a slow evaporation, X-ray quality single crystals were generated in good yield.

Availability of the EDA complexes of CTTV with varied acceptors allowed a detailed elucidation of the role of acceptor on the structure of the EDA complex.

First, we note that the relative arrangement between CTTV and acceptor is distinct in CTTV~DDQ and CTTV~CA crystal structures (**Figure 2.8**). In CTTV~DDQ crystal, CTTV and DDQ form one-dimensional arrays with 1:1 stoichiometry (**Figure 2.8A**). Noteworthy, the mean plane of DDQ is almost parallel to two adjacent veratrole planes of the two neighbouring CTTV molecules. The short distances between the DDQ mean plane and centroids of the veratrole rings of 3.17 and 3.13 Å reflect the strength of the donor-acceptor interactions. Importantly, the distances of C_{Ar}-O in the veratrole units that form contacts with DDQ are 0.8-1.1 pm shorter than those that are free from any contact, indicating an appreciable charge-transfer character in the formation of the EDA complexes.

Remarkably, the CTTV~CA complex exhibits completely different packing (**Figure 2.8B**). Analysis of the crystal structure shows that multiple CH-π interaction and π-π interactions are established in the full net of the crystal. The crystal structure shows that each CTTV molecule is surrounded by four CA molecules, i.e., each CA molecule interacts with two CTTV molecules, which corresponds to a 1:2 stoichiometry. The CA molecules are tilted by 20.9˚-14.2˚ towards to the veratrole rings due to the C-H…Cl hydrogen-bond and C-H-π interactions.

Finally, we note that open conformation of CTTV was found in both donor-acceptor complexes, as it allows a maximum number of cofacial π-π contacts between the veratroles of CTTV and the aromatic moiety of the acceptors.

According to Mulliken theory,[124] the redox potential of the acceptor directly affects the strength of the interaction in the charge-transfer complex,[113,117] thereby explaining the difference in the acceptor-to-donor stoichiometry in the crystal structures of CTTV~CA and CTTV~DDQ.

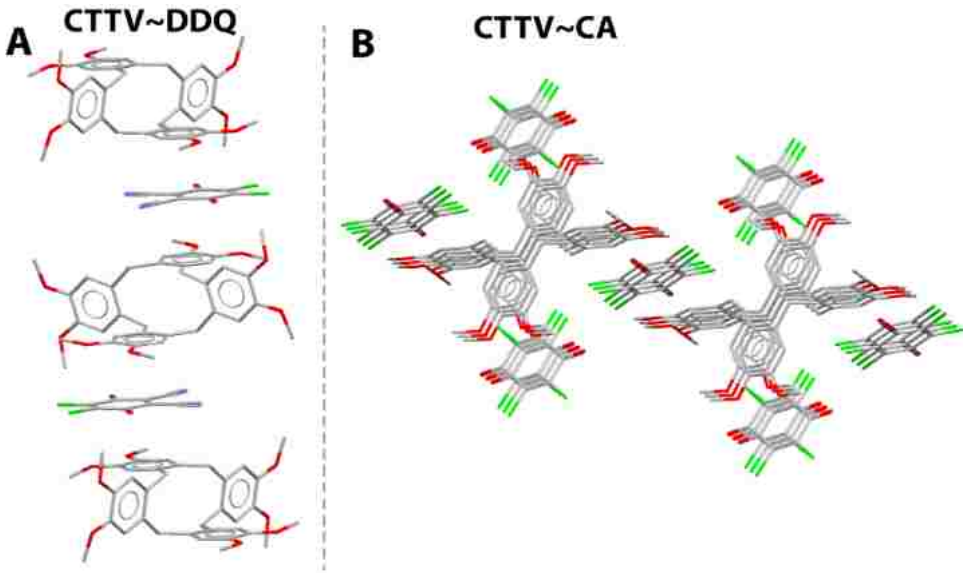

Figure 2.8 Packing diagrams of EDA complexes CTTV~DDQ (A) and CTTV~CA (B). (Thermal ellipsoids drawn at 50% probability, solvent molecules and hydrogen atoms removed for clarity).

Conclusions: Motivated by the interest in identification of novel redox-controlled actuators, in this manuscript, we sought to identify whether readily available CTTV molecule undergoes a conformational reorganization from (open) "sofa" into a (closed) "boat" conformation upon electron ejection. Synthesis of CTTV via an improved synthetic approach followed by electrochemical, spectroscopic and computational analyses showed that in the neutral state CTTV exists in the "sofa" conformation and upon oxidation undergoes interconversion into a "boat"

conformation where a pair of cofacially-arrayed veratrole rings effectively stabilizes cationic charge via charge-resonance. We further examined the electron donor-acceptor (EDA) complexes of CTTV with CA and DDQ using optical spectroscopy and X-ray crystallography. In the solid state, CTTV exists in a "sofa" conformation that is stabilized by the charge-transfer interaction with four and two acceptor molecules of CA and DDQ, respectively. We believe that these findings can be applied to the design and synthesis of novel organic functional molecules based on oxidation-induced mechanical actuation.

Acknowledgement: I thank Dr. Maxim V. Ivanov (University of Southern California) for DFT calculations and relevant computational works of this chapter.

Experimental

General methods and Synthesis

General methods: All reactions were performed under an argon atmosphere unless otherwise noted. All commercial reagents were used without further purification unless otherwise noted. Dichloromethane (Aldrich) was repeatedly stirred with fresh aliquots of concentrated sulfuric acid (~10 % by volume) until the acid layer remained colorless. After separation, CH_2Cl_2 layer was washed successively with water, 5% aqueous sodium bicarbonate, water, and saturated aqueous sodium chloride and dried over anhydrous calcium chloride. The CH_2Cl_2 was distilled twice from P_2O_5 under an argon atmosphere and stored in a Schlenk flask equipped with a Teflon valve fitted with Viton O-rings.

NMR spectra were recorded on Varian 400 MHz NMR spectrometers. UV-vis absorption spectra were collected with an Agilent 8453 diode array spectrometer, and infrared (IR) spectra were measured using a Nicolet Magna-IR 560 spectrometer. Electronic absorption (UV-Vis/NIR) measurements were made on a Cary 5000 instrument. Cyclic and square-wave voltammograms were measured under inert atmosphere with an epsilon EC potentiostat (iBAS) at a scan rate of 100 mV/s with 0.1 M $[NBu_4]PF_6$ electrolyte. The three-electrode cell consisted of an Ag/AgCl reference electrode, a platinum auxiliary electrode, and a glassy carbon working electrode.

Synthesis of cyclotetraveratrylene (CTTV)

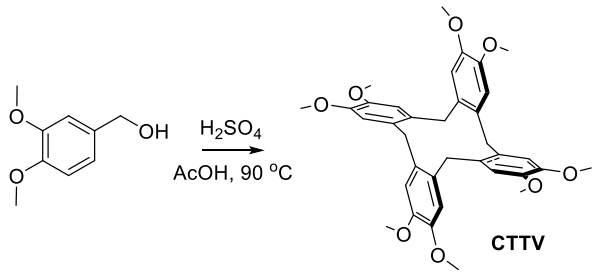

Method A[101]: A solution of 3,4-dimethoxy benzyl alcohol (1.68 g, 10 mmol) in glacial acetic acid (20 mL) containing five drops of concentrated sulfuric acid, After heated to 90 ºC for 15 minutes, large amount of precipitate formed in the solution. Solid crude product was collected by filtration and washed with large amount of water, which was further purified by many times recrystallization from chloroform/benzene and chloroform to give cyclotriveratrylene (CTV, 0.88 g, yield 58%) and cyclotetraveratrylene (CTTV, 0.18 g, yield 12%).

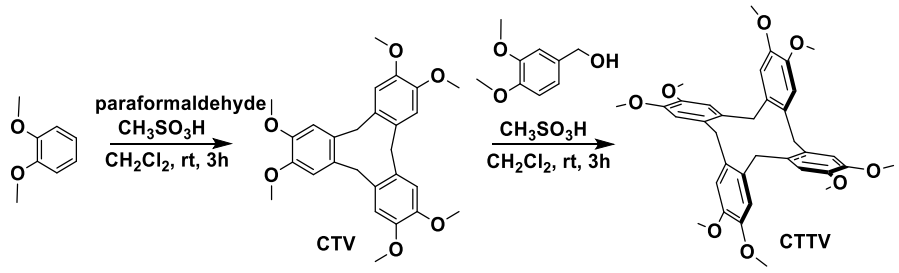

Method B: Veratrole (0.69g, 5 mmol) and paraformaldehyde (0.3g, 10 mmol) were dissolved into 9 ml of dichloromethane at room temperature. Then methanesulfonic acid (1 mL) was added drop wisely into reaction mixture. The color slowly changed to dark brown. After 3 hours stirring at room temperature, the reaction was quenched with addition of 40 ml of water. The mixture was filtered and solid residue was washed several times with water to give brownish color crude product, which was further washed with 20 ml of methanol to give white powder as pure cyclotriveratrylene (CTV, 0.63 g, yield 85%). ^{1}H NMR ($CDCl_3$ at 22 ˚C) δ: 3.57 (d, 3H), 3.84 (s, 18H), 4.78 (d, 3H), 6.83 (s, 6H).

Cyclotriveratrylene (0.54g, 1.2 mmol) was added into 18 ml of dichloromethane solution containing 2 ml of methanesulfonic acid. Then 3,4-dimethoxybenzyl alcohol (0.6g, 3.6 mmol) in 5 ml of dichloromethane solution was dropwisely added into the mixture and stirred for 3 hours at room temperature. After quenched with addition of 40 ml of water, the mixture was filtered and washed several times with water to give brownish crude product, which was further washed with 20 ml of methanol and easily recrystallized from chloroform to give colorless crystal as pure cyclotetraveratrylene (CTTV, 0.76 g, yield 70 %). ^{1}H NMR (CD_2Cl_2 at 22 ˚C) δ: 3.72 (broad, 32 H), 6.60 (broad, 8H). ^{1}H NMR (CD_2Cl_2 at -80 ˚C) δ: 3.18 (d, 4H), 3.48 (s, 12H), 3.77 (d, 4H), 3.85 (s, 12H), 6.22 (s, 4H), 6.82 (s, 4H). ^{1}H NMR ($CDCl_3$ at 22 ˚C) δ: 3.78 (broad, 32 H),

6.58 (broad, 8H). ^{13}C NMR ($CDCl_3$ at 22 ˚C) δ: 34.99, 54.08, 111.31 (broad), 115.67 (broad), 131.66 (broad), 147.30.

NMR Spectroscopy

^{1}H NMR spectrum of cyclotriveratrylene at 22°C in $CDCl_3$

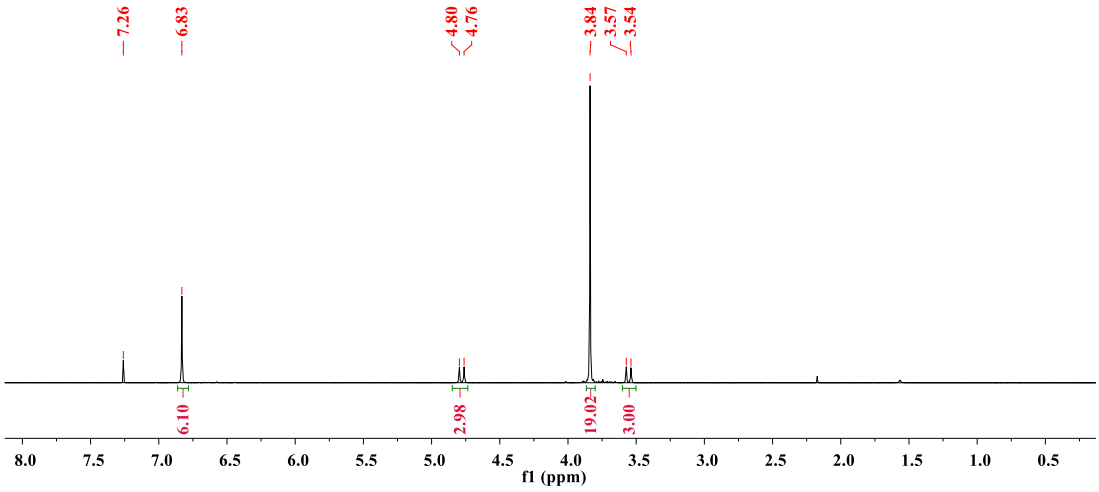

^{1}H NMR spectrum of CTTV at -80 °C in CD_2Cl_2

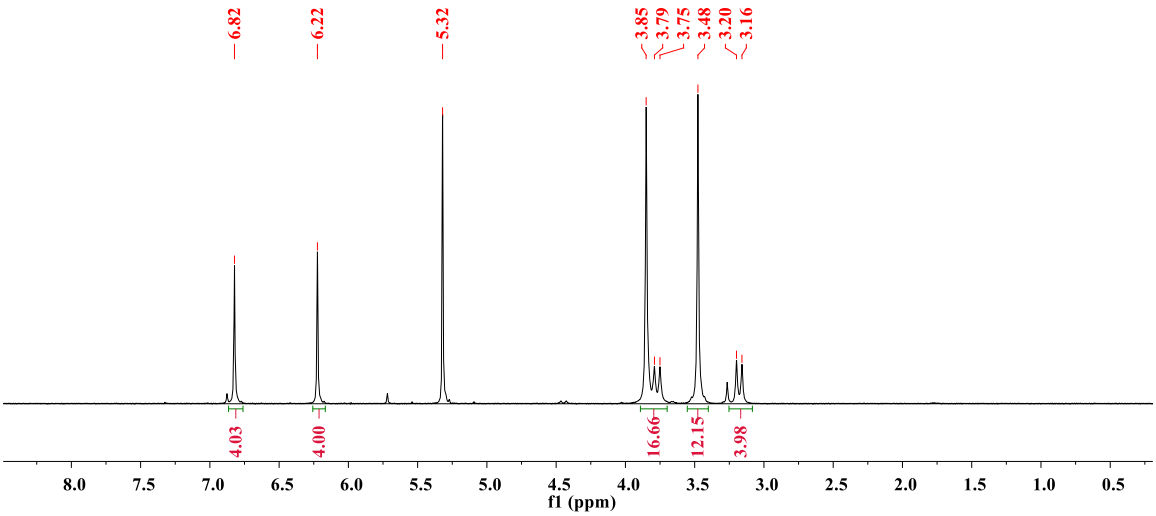

^{1}H NMR spectrum of CTTV at 20 °C in CD_2Cl_2

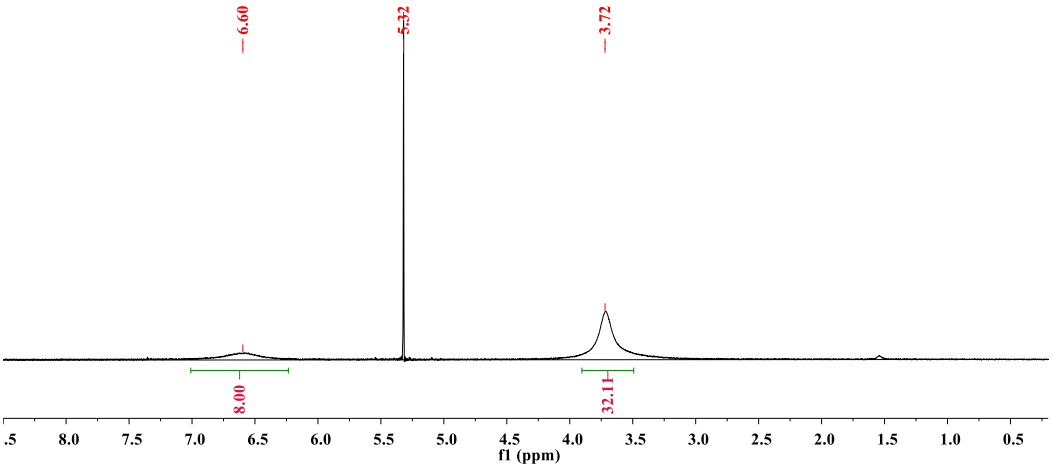

^{1}H NMR spectrum of CTTV at 20 °C in $CDCl_3$

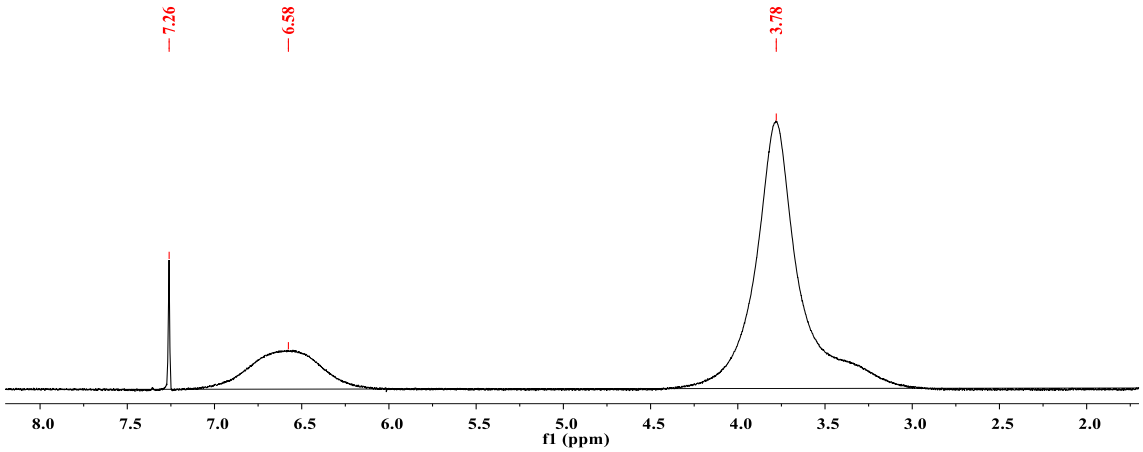

^{13}C NMR spectrum of CTTV at 20 °C in $CDCl_3$

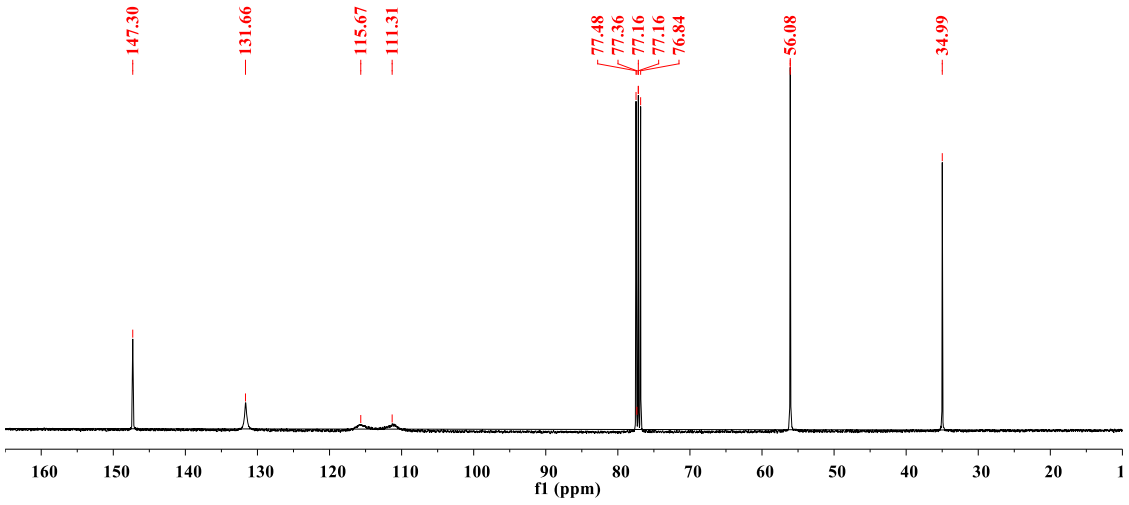

Variable temperature NMR data were recorded on Varian 400 MHz NMR spectrometers. Sample were prepared by dissolving 5 mg of CTTV in 0.5 mL of CD_2Cl_2 and $CDCl_3$ separately. The results were showed in **Figure 2.8** (in CD_2Cl_2 from 20 to -80 °C) and **Figure 2.9** (in $CDCl_3$ from 20 to 60 °C).

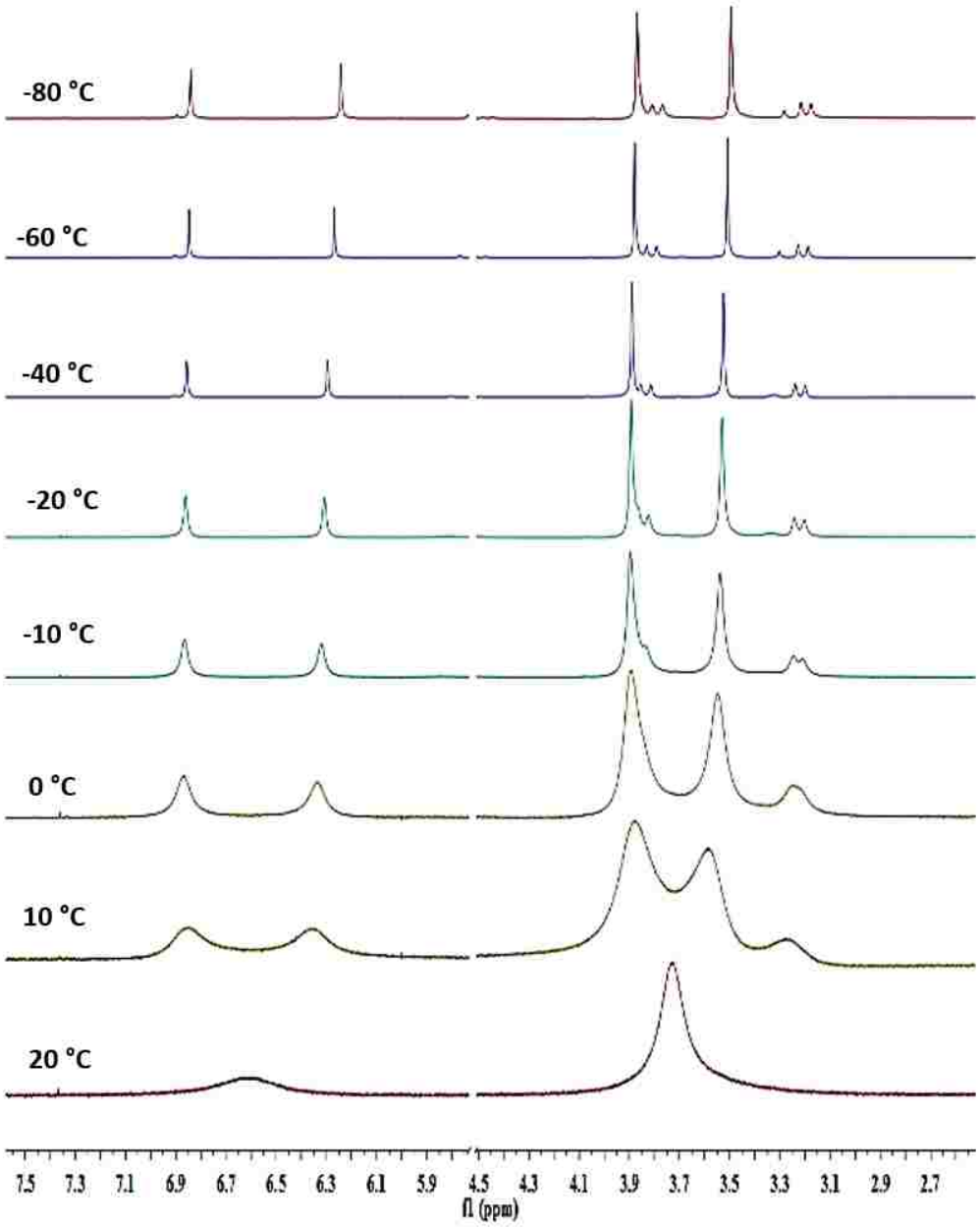

Figure 2.9 Variable temperature (VT) NMR of CTTV in CD_2Cl_2 in the range from 20 to -80 ºC. The activation energy for the interchange between four conformers (shown in **Figure 2.10** below) w as estimated to be 14.9 kcal mol^{-1}.

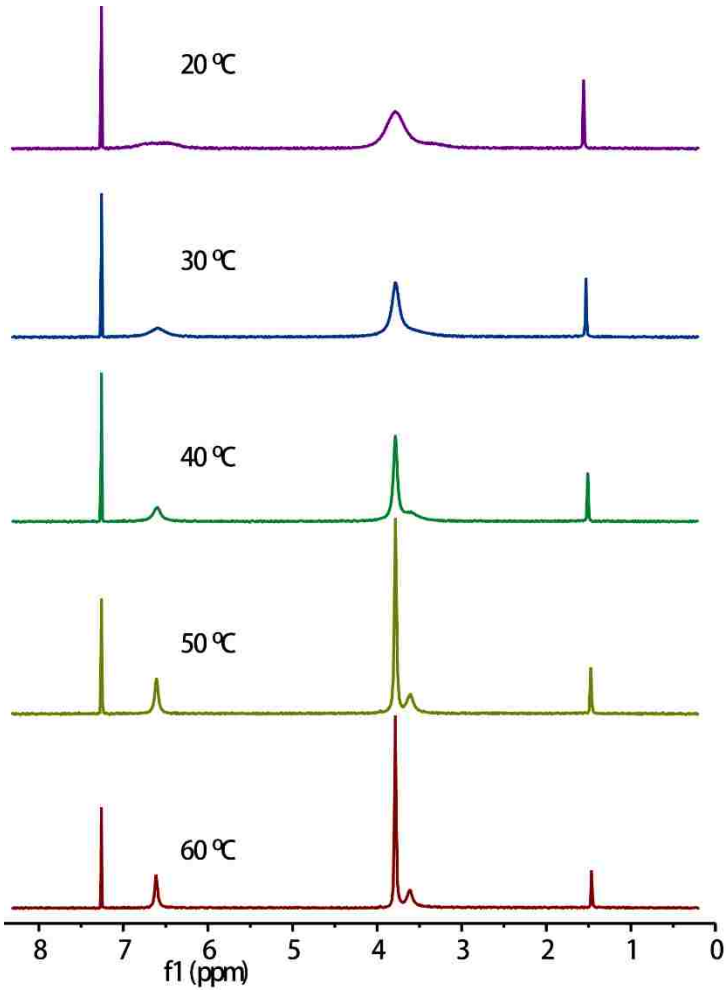

Figure 2.10 Variable temperature (VT) NMR of CTTV in $CDCl_3$ in the range from 20 to 60 ºC.

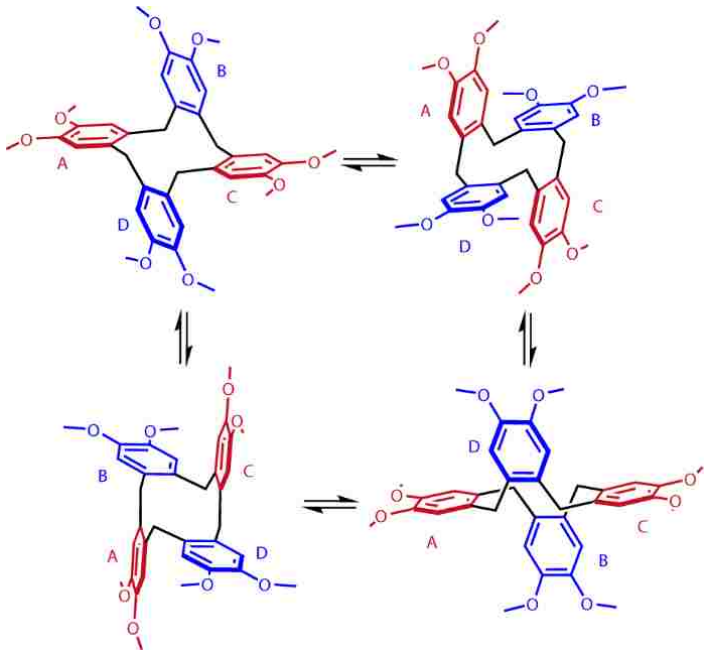

Figure 2.11 Four interconverted structures of open CTTV.

The activation energy was calculated[129] as $\Delta G = a\mathrm{T}_c[9.972 + \log(\frac{T_c}{\Delta v})]$, where a equals to 4.575×10^{-3} kcal/mol; Δv is the separation in Hz between the two signals at slow-exchange limit, Δv = 21 Hz between peaks at 6.26 and 6.32 ppm; T_c = 20 °C is coalescence temperature.

Electrochemistry characterization of CTTV and model complexes

Cyclic and square-wave voltammograms were measured under inert atmosphere with an epsilon EC potentiostat (iBAS) at a scan rate of 100 mV/s with 0.1 M $[NBu_4]PF_6$ electrolyte at -30 °C. The three electrode cell consisted of an Ag/AgCl reference electrode, a platinum auxiliary electrode, and a glassy carbon working electrode. Ferrocene was used as internal reference.

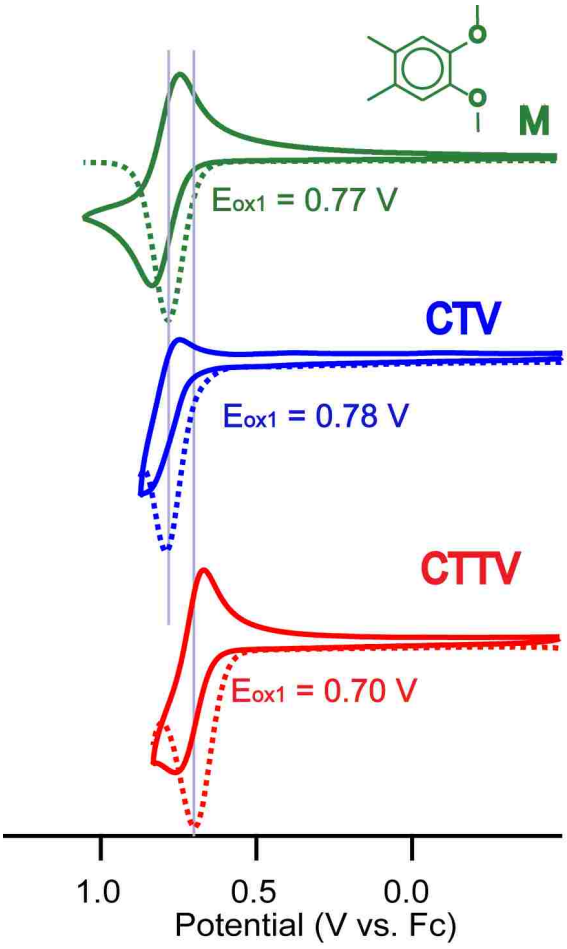

Figure 2.12 Cyclic voltammograms (CVs, solid lines) and square waves (SWs, dashed lines) of 2 mM M (top, green color), CTV (middle, blue color) and CTTV (bottom, red color) in CH_2Cl_2 (0.1 M n-Bu_4NPF_6) at a scan rate 100 mV s^{-1}.

Generation of $CTTV^{+\bullet}$ by redox titrations

Electronic absorption spectra of $CTTV^{+\bullet}$ in CH_2Cl_2 at 22 °C were obtained by quantitative redox titrations using robust aromatic oxidant, i.e. [$THEO^{+\bullet}SbCl_6^-$] (1,4,5,8-dimethano-1,2,3,4,5,6,7,8-octahydro-9,10-dimethoxyanthracene hexachloroantimonate; E_{red1} = 0.67 V vs Fc/Fc^+, λ_{max} = 518 nm, λ_{max} = 7300 cm^{-1} M^{-1}).[130]

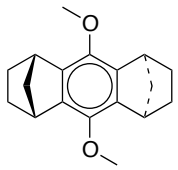

THEO

Figure 2.13 Chemical structures of aromatic oxidant THEO used in redox titrations.

The redox titration experiment was carried out by an incremental addition of CTTV to the solution of $THEO^{+\bullet}$ where the 1-e^- oxidation of CTTV and reduction of $THEO^{+\bullet}$ can be described by equilibrium equation:

$$THEO^{+\bullet} + CTTV \rightleftarrows THEO + CTTV^{+\bullet} \qquad \text{(eq. 1)}$$

Numerical deconvolution[131] of the absorption spectrum at each increment produced mole fractions of $THEO^{+\bullet}$ and $CTTV^{+\bullet}$ against the added equivalents of CTTV and confirmed a 1:1 stoichiometry of the redox reaction (Figure S6 below reproduced from Figure 5 in the main text). The experimental plots of mole fraction vs equivalent of added donor were fitted by varying $\Delta G_1 = E_{ox1}^{\boldsymbol{CTTV}} - E_{red}^{\mathbf{THEO^{+\bullet}}}$.

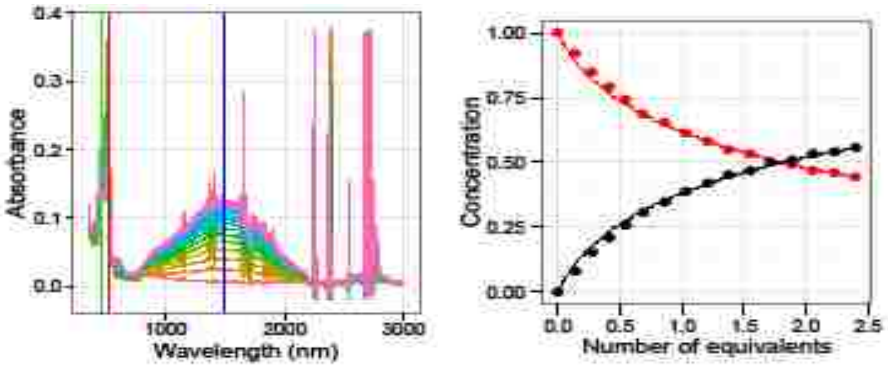

Figure 2.14 A: Spectral changes observed upon the reduction of 0.051 mM $THEO^{+\bullet}$ in CH_2Cl_2 (3 mL) of 1.49 mM solution of CTTV in CH_2Cl_2 at 22 °C. Inset: the isovalue plot of spin density distribution in $CTTV^{+\bullet}$. B: Plot of the mole fractions of $THEO^{+\bullet}$ (red) and $CTTV^{+\bullet}$ (black) against the added equivalents of neutral CTTV. Symbols represent experimental points, while the solid lines show best-fit to experimental points using $\Delta G = E_{ox}(CTTV) - E_{red}(THEO^{+\bullet}) = 25$ mV.[131]

Electron donor-acceptor (EDA) complexes of CTTV

The quantitative intermolecular association was evaluated in the form of the *K*DA and εCT values for the formation and visualization, respectively, of various tweezer/acceptor complexes; and the quantitative analysis of the spectrophotometric absorption changes was treated by the Benesi-Hilderbrand method using the eq. 2:[127]

$$\frac{[\mathrm{A}]}{\mathrm{ACT}} = \frac{1}{\varepsilon_{CT}} + \frac{1}{K_{DA}\varepsilon_{CT}}\frac{1}{[\mathrm{D}]} \quad \text{(eq. 2)}$$

In eq. 2, A_{CT} is the molar absorbance and ε_{CT} is the extinction coefficient of the charge transfer band at the monitoring wavelength. The concentration of the electron acceptor was kept at least 10 times greater than that of tweezer donors, and a plot of [A]/*A*CT versus the reciprocal donor concentration was found to be linear in all tweezer/acceptor complexation measurements. From the slope $[K_{DA}\varepsilon_{CT}]^{-1}$ and the intercept $[\varepsilon_{CT}]^{-1}$, the values of association constant (K_{DA}) and extinction coefficient (ε_{CT}) were readily calculated.

$$\mathbf{CA + CTTV \rightarrow CTTV{\sim}CA} \quad \text{(eq. 3)}$$

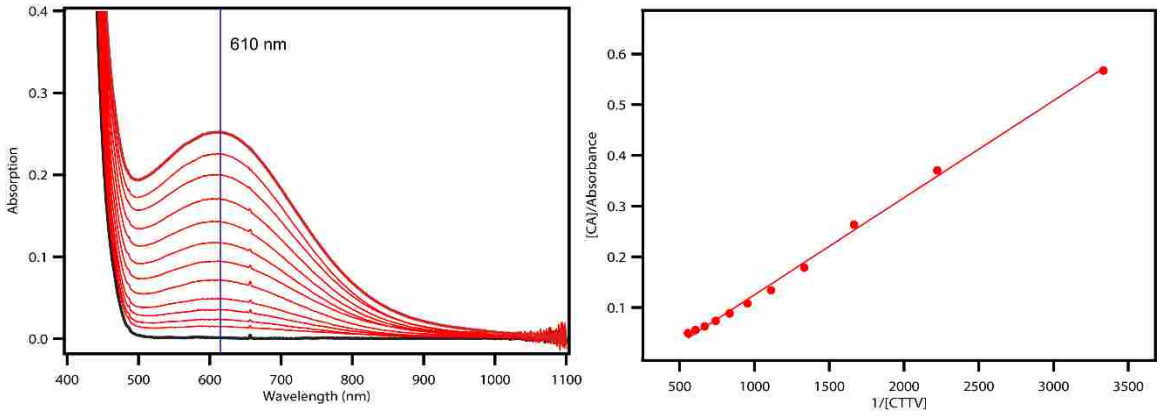

Figure 2.15 Spectral changes attendant upon the incremental addition of CTTV (1.08×10^{-3} M) to chloranil (0.022 M) in DCM (left) and Benesi-Hildebrand plot (right). K_{DA} = 15 M^{-1}, ε_{CT} = 347 M^{-1} cm^{-1}.

$$\mathbf{DDQ + CTTV \rightarrow CTTV{\sim}DDQ} \quad \text{(eq. 4)}$$

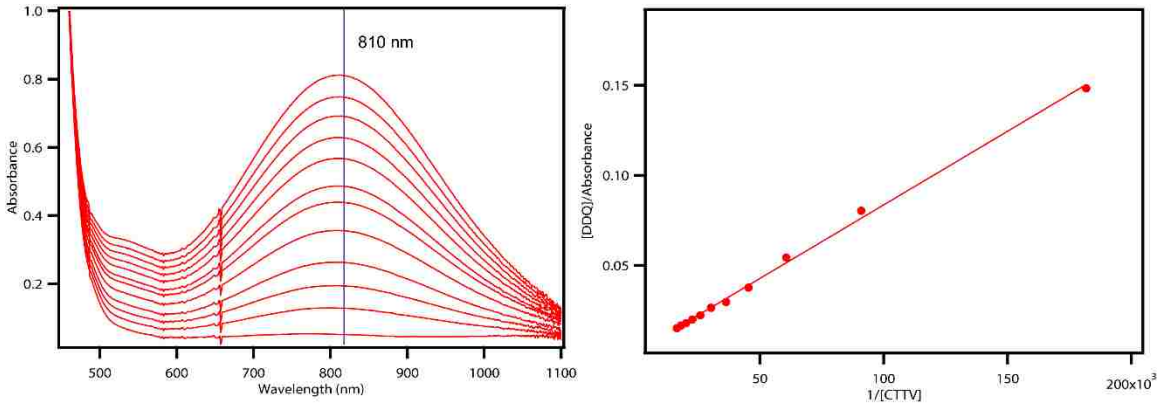

Figure 2.16 Spectral changes attendant upon the incremental addition of CTTV (6.0×10^{-5} M) to DDQ (0.011 M) in DCM (left) and Benesi-Hildebrand plot (right). K_{DA} = 591 M^{-1}, ε_{CT} = 2066 M^{-1} cm^{-1}.

Table 2.4 Summary of X-ray crystallographic data of CTTV.

	CTTV~DDQ	CTTV~CA
Empirical formula	$C_{49.55}H_{48.65}Cl_{11.68}N_2O_{10}$	$C_{50}H_{44}Cl_{12}O_{12}$
Formula weight	1246.2	1262.25
Temperature/K	100.15	100(2)
Crystal system	triclinic	triclinic
Space group	P-1	P-1
a/Å	10.0667(4)	9.0593(2)
b/Å	16.1954(7)	12.1761(2)
c/Å	19.0021(8)	12.5506(2)
α/°	111.109(4)	74.4930(10)
β/°	94.141(4)	89.5790(10)
γ/°	100.255(4)	84.4840(10)
Volume/Å^3	2812.4(2)	1327.60(4)
Z	2	1
ρ_{calc}g/cm^3	1.472	1.579
μ/mm^{-1}	5.743	6.256
F(000)	1277	644
Crystal size/mm^3	0.286 × 0.103 × 0.017	0.26 × 0.16 × 0.10
Radiation	CuKα (λ = 1.54184)	CuKα (λ = 1.54178)
2Θ range for data collection/°	9.028 to 141.55	7.32 to 134.32
Index ranges	$-12 \le h \le 12$, $-19 \le k \le 19$, $-23 \le l \le 23$	$-10 \le h \le 10$, $-13 \le k \le 14$, $0 \le l \le 14$
Reflections collected	52221	11087
Independent reflections	10686 [Rint = 0.0954, Rsigma = 0.0660]	4379 [Rint = 0.0134, Rsigma = 0.0133]
Data/restraints/parameters	10686/129/760	4379/0/423
Goodness-of-fit on F^2	0.955	1.069
Final R indexes [I>=2σ (I)]	R1 = 0.0664, wR2 = 0.1840	R1 = 0.0245, wR2 = 0.0633
Final R indexes [all data]	R1 = 0.0995, wR2 = 0.2048	R1 = 0.0252, wR2 = 0.0637
Largest diff. peak/hole / e Å^{-3}	2.13/-0.49	0.24/-0.29

Chapter 3

META (1,3) METHYLENE-BRIDGED MACROCYCLIC ARENES: CALIX[4]ARENES CONFROMATIONAL CHANGE FROM SOLUTION TO CRYSTAL AND FORM SINGLE CRYSTAL TO SINGLE CRYSTAL TRANSFORMAITON

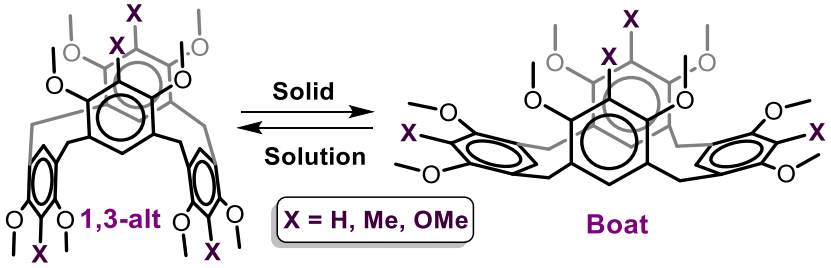

The conformations of macrocycle molecules have significant effect on their interactions with other species as guest. Herein, the alkoxy substituted calix[4]arenes (R4, T4 and P4) were synthesized and their conformations have been studied both experimentally and computationally. The results revealed that for the methoxy substituted species of ^{Me}R4 and ^{Me}P4 the crystal packing forces can change the conformer from 13-alternate in solution to boat in solid state (crystal). However, increasing the size of substituent to ethoxy (^{Et}R4) or propoxy (^{Pr}R4) prevent this phenomenon and the conformation in solution and solid is same (1,3-alternate). However, for the alkoxy substituted toluene (T4) the length of substituent is not significant and both methoxy (^{Me}T4) and propoxy (^{Pr}T4) substituents showing the conformational change upon the crystallization. Interestingly, the crystal structure of ^{Pr}T4 indicated thermal single-crystal to single-crystal transformation which include the 180° rotation of two propoxy substituents and slipping of whole molecule upon each other.

Introduction: Since the first report of calix[4]arene, these molecules showed a broad spectrum of applications in the host-guest and supramolecular chemistry.[132–136] Moreover, in spite of the long history of this molecules, around a century, even recently several novel substituted calix[4]arenes are reported.[137] The calix[4]arenes can ideally show four different conformers (**Figure 3.1**). Surveying the literature indicate that the substituents on the aromatic ring have significant effects on the conformation, electronic properties and the host-guest interactions of this family of arene-based macrocyclic molecules.[138–140]

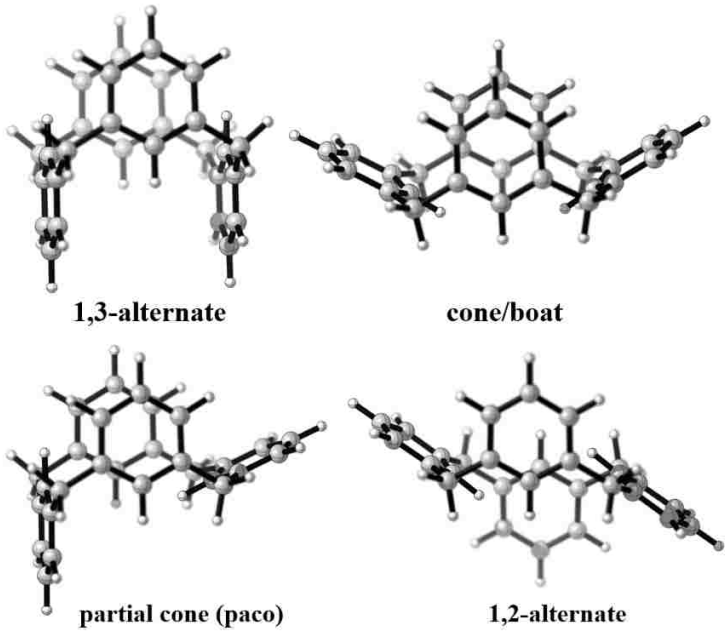

Figure 3.1 Four possible conformations of calix[4]arenes; the position of all aromatic protons can be occupied with different substituents (e.g., alkoxy, hydroxyl, methyl, etc.).

To the contrary of the hydroxyl substituted calix[4]arenes which the intra-hydrogen bonding governs the most stable conformer (crown)[137,141], some other substituents can show conformational flexibility in the solution.[142] Konishi and co-

workers reported the 1,3-alternate conformer for the methoxy resorcino[4]arenes (^{Me}R4) based on the NMR spectra.[143] Moreover, their results indicated that increasing the size of the alkyl group do not change the aromatic protons chemical shift, which imply on the same conformer for different alkyl groups in the solution.[143] In agreement with the NMR data, the crystal structure of *iso*-propyl substituted calix[4]arene showed the 1,3-alternate conformer in the solid state.[144] However, later the Leonhardt et al., reported the crystal structure of ^{Me}R4 which showed the boat conformer.[145]

In addition to ^{Me}R4, in the 2002, Iwanek et al., reported the synthesis and complexation of methoxypyragallo[4]arene (^{Me}P4, using 1,2,3-trimethoxybenzene) with different alkali metals. They reported the crown conformer for the un-ligated and ligated ^{Me}P4 with Na^+ and K^+ metals based on the semi-empirical calculations.[146] Recently, Neri and co-workers replaced the middle methoxy group with methyl group (2,6-dimethoxytoluene, ^{Me}T4).[147] In both ^{Me}P4 and ^{Me}T4 molecules the aromatic protons appeared as a sharp singlet peak around 6.2 ppm which indicates the presence of same conformer for them. Though, the reported crystal structure of ^{Me}T4 revealed the boat conformer for this molecule in the solid state.[147]

Surveying the reported conformations of ^{Me}R4, ^{Me}P4 and ^{Me}T4 raise this question that which conformer, boat or 1,3-alt, is the lowest energy conformer for methoxy substituted calixarenes. Herein, in order to answer this question, we synthesized several different substituted calixarenes (^{Me}R4, ^{Et}R4, ^{Pr}R4, ^{Pr}T4 and ^{Me}P4) and scrutinized their conformations both experimentally and computationally. The results indicated that for the methoxy substituted calixarenes (^{Me}R4, ^{Me}T4 and ^{Me}P4) the conformational change occurs upon the crystallization. The most stable conformer in the solution is 1,3-alternate,

however, in the solid state the boat conformer is more stable. Though, increasing the size of the alkyl group to ethyl or propyl prevent this conformational change for R4 system. To the contrary of R4, this conformational change occurs for both methoxy and propoxy substituted T4. Notably, the ^{Pr}T4 single crystal structure revealed the thermal phase transformation with significant conformational variation. To the best of knowledge, this is the first comprehensive experimental and computational study on the solvent and crystal packing influences on the conformational adjustment of calixarenes. These phenomena which occur due to the solvation/crystallization and thermal phase transformation can help us to have a deeper insight about this family of macrocyclic molecules. Moreover, the results can open a new gate for the future investigations regarding the application of macrocyclic molecules as the solid state molecular switch.[148,149]

Computational details: All density functional (DFT) calculations were carried out using Gaussian 09 software package.[102] The geometries were fully optimized using five different DFT functionals (B3LYP, CAM-B3LYP, M06-2X, PBE0 and ωB97XD).[150–154] Double-ζ basis sets 6-31G* and Def2-SVP are used for most of the calculations.[155] However, in order to have better insight about the basis set effects, some of the calculations were repeated using higher basis sets. Moreover, to include the dispersion corrections, the D3BJ empirical factors are used for three of our selected functionals (B3LYP, CAM-B3LYP and PBE0).[156] In order to simulate the solvation effects, two implicit solvation models (SMD and PCM) were utilized for all of the calculations and the results are compared.[111,157] The NMR calculations were carried out using B3LYP-D3BJ functional using Gauge-Independent Atomic Orbital (GIAO) method

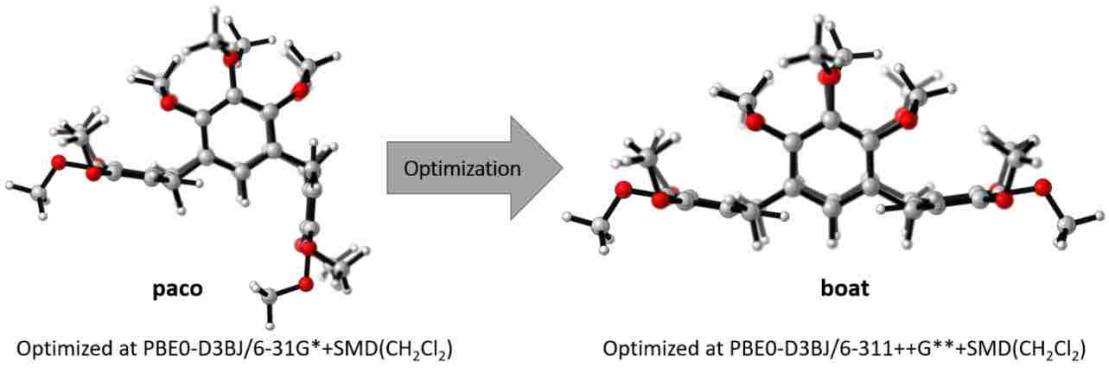

Figure 3.2 Effect of basis set size on the partial cone (paco) conformer; reoptimizing paco conformer with higher basis set change the structure to more stable boat conformer. It should be noted that reoptimizing the paco conformer using the optimized geometry form PBE0-D3BJ/6-31G*+SMD(CH_2Cl_2) employing M062X/6-31G*+SMD(CH_2Cl_2) level of theory change the structure to boat conformer too.

and 6-31G* basis set.[158] As depicted in **Figure 3.1**, there are four possible conformers for calix[4]arene molecules (boat or cone, 1,3-alt, 1,2-alt and paco). Our calculations indicated that the last two conformers are not stable, and they will be converted to other conformers during the optimization. However, for ^{Me}P4, the partial-cone (paco) was stable using some DFT functionals (e.g. PBE0) and double-ζ basis sets. But, it will be optimized to the boat structure using M06-2X functional or triple-ζ basis set (e.g. 6-311++G(d,p), **Figure 3.2**). Therefore, we focused on two boat and 1,3-alternate conformers. In order to verify the conformational flexibility of investigated calixarenes, the molecular dynamic calculations were performed using MM3 force field as implemented in the TINKER software package at 300 K. [159–162]

Results and discussion: The alkoxy substituted calix[4]arenes were synthesized using methanesolfunic acid ($MeSO_3H$) as the catalyst for the condensation of 1,3-dimethoxybenze, and 1,2,3-trimethoxybenzene with paraformaldehyde (**Scheme 3.1**).

This Bronsted acid showed promising results for the synthesis of several macrocyclic systems including Pillarenes, Calixarens and CTTV.[29,142,163] The methoxy substituted resorcino[4]arene (^{Me}R4) showed poor solubility in chloroform. Therefore, in order to improve the solubility and also investigate the effects of the substituents size on the conformations, we synthesized the 1,3-diethoxybenzene and 1,3-dipropoxybenzene and condensation reactions have been carried out under the same condition to yield the ^{Et}R4 and ^{Pr}R4 (see the Experimental section for more details). It seems that the condensation of 2,6-dimethoxytoluene with paraformaldehyde is not feasible using Bronsted acids (e.g., $MeSO_3H$ or CF_3COOH); therefore, we synthesized the ^{Pr}T4 molecule using Lewis acid ($BF_3 \cdot Et_2O$).[147] All structures are confirmed by NMR and MALDI-TOF mass spectroscopies. Moreover, the crystal structures of ^{Et}R4, ^{Pr}R4, ^{Pr}T4 and ^{Me}P4 are reported for the first time by our group. The crystal structures of ^{Me}R4 and ^{Me}T4 have been reported previously.[145,147]

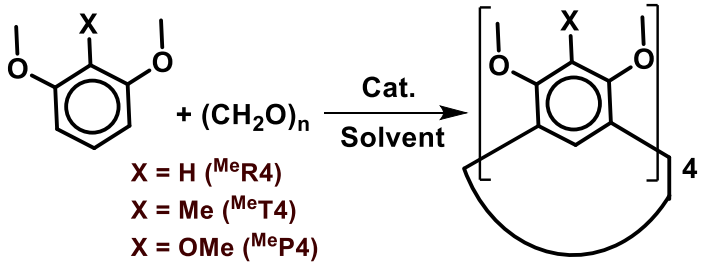

Scheme 3.1 The general synthesis method of ^{Me}R4, ^{Me}T4 and ^{Me}P4.

As aforementioned, the crystal structure of resorcino[4]arene (^{Me}R4) showed the boat conformer as the most stable structure.[145] However, the NMR data suggested that in the solution the 1,3-alternate is preferred. In order to overcome the poor solubility of

^{Me}P4, ^{Pr}P4 is synthesized. The ^{1}H NMR of both molecules are depicted in the **Figure 3.3**. The aromatic protons showed two sharp peaks for both molecules, 6.19 and 6.42 ppm for ^{Me}P4 and 6.27 and 6.37 ppm for ^{Pr}R4. Also, the bridge CH_2 group showed very close chemical shift 3.69 and 3.73 ppm for ^{Me}P4 and ^{Pr}R4, respectively. Identical ^{1}H NMR data imply on the presence of similar conformational structure for both ^{Me}R4 and ^{Pr}R4 calix[4]arenes. But, to the contrary of same NMR spectra, the crystal structure of ^{Pr}R4 showed twisted 1,3-alternate (^{twist}1,3-alt) conformer which is different with the reported crystal structure of ^{Me}R4 which has shown the boat conformer. Therefore, in order to clarify the most stable structure of ^{Me}R4 and also evaluate the effects of solvents, these three conformers (boat, 1,3-alt and ^{twist}1,3-alt) were investigated computationally.

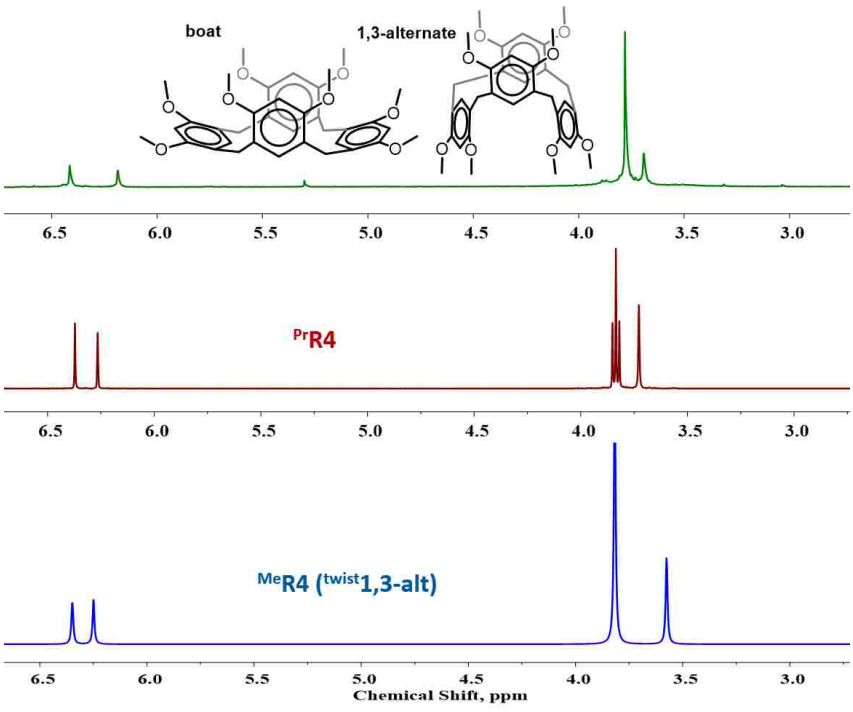

Figure 3.3 ^{1}H NMR spectra of ^{Me}R4 (green) and ^{Pr}R4 (red) at 20 °C in $CDCl_3$ and calculated ^{1}H NMR spectra (blue) of 1,3-alternate conformer of ^{Me}P4 using B3LYP-D3BJ/6-31G(d)+SMD(CH_2Cl_2).

The results of DFT calculations are listed in the **Table 3.1**. Regardless of the functional or basis set, the boat conformer is more stable. Moreover, the ^{twist}1,3-alt which match with the crystal structure of ^{Pr}R4 is more stable than the regular 1,3-alt conformer. Among the examined functionals, the M06-2X showed the lowest energy differences (around 1 kcal/mol) between the boat and ^{twist}1,3-alt conformers. Therefore, the optimizations were carried out using higher basis set (6-311++G(d,p) and Def2-TZVPP using SMD(CH_2Cl_2)). The results reveled that increasing the size of the basis set will increase the energy gap to 1.3 and 1.4 kcal/mol for Pople and Ahlrichs triple-ζ basis sets, respectively.

Table 3.1 The relative free energies (ΔG, kcal/mol) of different conformers of ^{Me}R4 using SMD and PCM (values in the parenthesis) solvation models (CH_2Cl_2).

	B3LYP	CAM-B3LYP	M062X	PBE0	ωB97XD
6-31G*					
boat	0.0 [0.0]	0.0 [0.0]	0.0 [0.0]	0.0 [0.0]	0.0 [0.0]
1,3-alt	5.2 [3.1]	4.9 [4.1]	8.7 [8.3]	5.6 [3.8]	4.9 [5.0]
^{twist}1,3-alt	3.4 [4.3]	3.4 [2.8]	1.2 [1.3]	2.6 [2.1]	2.1 [2.7]
Def2-SVP					
boat	0.0 [0.0]	0.0 [0.0]	0.0 [0.0]	0.0 [0.0]	0.0 [0.0]
1,3-alt	6.0 [1.7]	4.9 [3.4]	7.8 [5.7]	5.0 [5.2]	6.2 [4.7]
^{twist}1,3-alt	4.1 [4.8]	3.5 [3.7]	0.6 [0.2]	2.9 [3.6]	2.9 [4.6]

To the contrary of relative free energies, the calculated ^{1}H NMR spectrum of ^{twist}1,3-alt conformer is in very good agreement with the experimental data (**Figure 3.3**). The calculated ^{1}H NMR chemical shift for the aromatic protons is 6.34 and 6.25 ppm which are very close to the experimental result, 6.42 and 6.19 ppm. Also, the predicted ^{1}H NMR of bridge CH_2 groups (3.56 ppm) and non-aromatic CH_3 groups (3.93 ppm) are

in very good agreement with the experimental data (3.69 and 3.78 ppm, respectively). However, the calculated ^{1}H NMR of the less stable conformer (1,3-alt) showed more deviation from the experimental data. The chemical shifts of aromatic protons are 6.60 and 5.90 ppm. These data and also the relative energies (**Table 3.1**) indicating the very low probability of the existence of this conformer in the solution. Also, the boat conformer should show four different aromatic peaks which disagrees with the experimental outcomes. Evaluating the experimental vs. computational data suggesting that the present implicit solvation models are not able to properly simulate the solvation effects on the conformational stability of ^{Me}R4. Therefore, the explicit solvent ($CHCl_3$) effects were simulated using the ONIOM method by employing 171 $CHCl_3$ molecules.[164] The ^{Me}R4 and solvent molecules were optimized using M06-2X/6-31G(d) and UFF molecular mechanic force field, respectively (**Figure 3.4**).[165] The results revealed that the ^{twist}1,3-alt conformer is around 6.7 kcal/mol more stable than the boat conformer. The results of the ONIOM method and also the crystal structure of ^{Pr}R4 indicating that the twisted 1,3-alternate is the most stable structure of ^{Me}R4 in solution. However, the crystal packing forces push the methoxy substituted molecule toward the other conformer (boat). Moreover, the same conformer of ^{Et}R4 (according to NMR and single x-ray crystal structure, see the Experimental section) suggesting that this conformational change is only feasible for methoxy substituted R4 species.

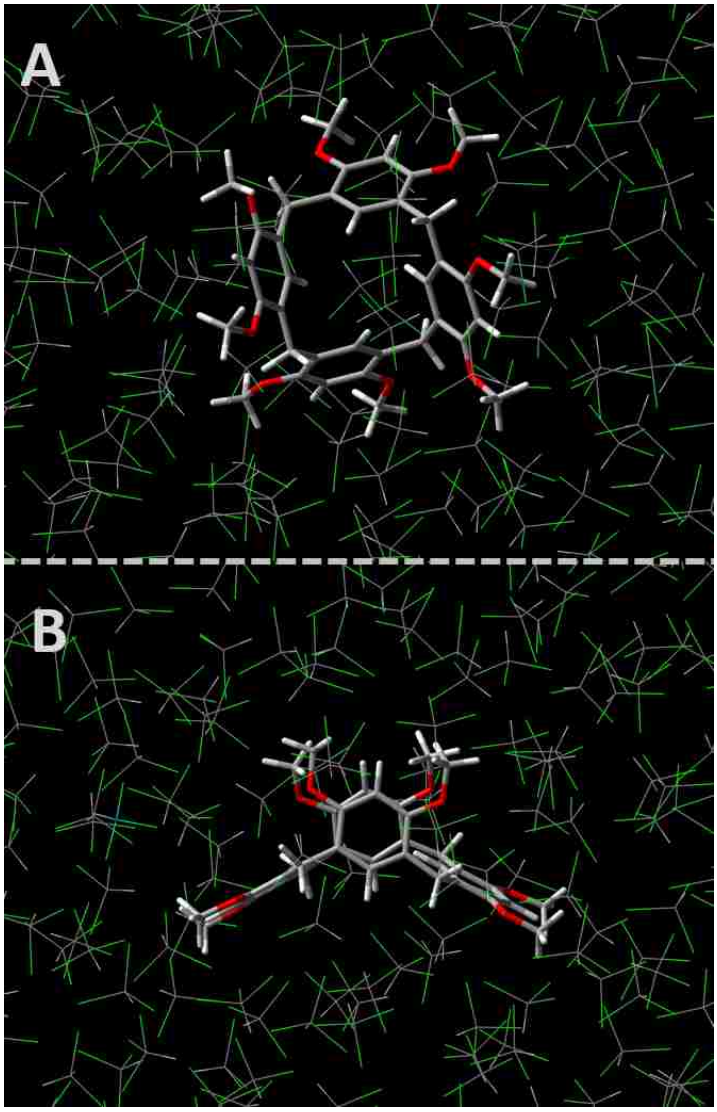

Figure 3.4 The optimized structures of ^{twist}1,3-alt (A) and boat (B) conformers of ^{Me}R4 using ONIOM(M06-2X/6-31G*:UFF) method.

The ^{Me}T4 molecule (X = Me, see **Scheme 3.1**) showed similar condition as the ^{Me}R4. The ^{1}H NMR data of ^{Me}T4 showed one sharp singlet peak at 6.19 ppm in $CDCl_3$.[147] Very much alike to methoxy substituted, the ^{Pr}T4 showed identical chemical shift (6.18 ppm) for the aromatic protons (see the Experimental section). Moreover, the variable temperature ^{1}H NMR of ^{Pr}T4 (from 20 °C to -70 °C in CD_2Cl_2) showed negligible upfield

shift from 6.19 at 20 °C to 6.04 at -70 °C, which imply on the presence of same conformation at the investigated temperature range. This conformer should have same environment for all aromatic protons of these molecules which imply on the only possible conformation which following this condition (1,3-alt, see **Figure 3.1**). To the contrary of ^{1}H NMR, the single crystal structure of both ^{Me}T4 and ^{Pr}T4 showed the boat conformer. Therefore, the relative free energies of ^{Me}T4 conformers (boat, ^{twist}1,3-alt and 1,3-alt) were evaluated using DFT methods.

The calculated relative free energies of the ^{Me}T4 are listed in the **Table 3.2**. The boat conformer has shown to be the most stable structure at the investigated level of theories. Also, it seems that the employed basis sets and implicit solvation models do not alter the relative energies significantly. In contrast to the implicit solvation models (SMD and PCM), simulating the solvation effects using 171 explicit chloroform molecules (ONIOM(M06-2X/6-31G(d):UFF)) revealed that the ^{twist}1,3-alt conformer is around the 3.1 kcal/mol more stable than the boat conformer which agrees with the experimental data. To the contrary of twisted structure, simulating the solvation effects explicitly increased the instability of regular 1,3-alternate conformer to around 14.4 kcal/mol. Therefore, the results revealed that the ^{twist}1,3-alt is the most stable conformer in the solution and crystal packing forces (intermolecular dipole-dipole, steric and hydrogen bonding interactions) are possible reasons for conformational changes form solution to crystal state.[166–168]

Table 3.2 The relative free energies (ΔG, kcal/mol) of different conformers of ^{Me}T4 using SMD and PCM (values in the parenthesis) solvation models (CH_2Cl_2).

	B3LYP	CAM-B3LYP	M062X	PBE0	ωB97XD
6-31G*					
boat	0.0 [0.0]	0.0 [0.0]	0.0 [0.0]	0.0 [0.0]	0.0 [0.0]
1,3-alt	2.0 [4.1]	3.6 [3.8]	8.1 [6.0]	4.9 [3.1]	3.6 [5.5]
^{twist}1,3-alt	4.3 [4.5]	3.9 [5.2]	3.7 [1.2]	2.7 [2.8]	2.5 [2.1]
Def2-SVP					
boat	0.0 [0.0]	0.0 [0.0]	0.0 [0.0]	0.0 [0.0]	0.0 [0.0]
1,3-alt	3.4 [2.4]	4.3 [3.6]	5.0 [6.8]	2.6 [3.8]	5.3 [4.3]
^{twist}1,3-alt	2.5 [6.2]	4.7 [3.7]	1.5 [3.4]	2.8 [2.8]	4.5 [3.2]

In order to evaluate the effects of the alkoxy chain length on the single crystal structure packing, the crystal structure of ^{Pr}T4 is obtained by slow evaporation of chloroform/methanol solution. Opposite to the observed condition for R4 system, the single crystal of ^{Pr}T4 showed boat conformer, resembling ^{Me}T4, which means that the alkyl chain length cannot prevent the conformational change of T4 species form solution (1,3-alt) to solid state (boat). Interestingly, the crystal structure of ^{Pr}T4 showed dramatic thermal conformational change in the solid state. Three possible single crystal structures are obtained. **Figure 3.5** illustrating two of them at the 250 K and 100 K before and after the phase transition, respectively. The crystals undergo a phase transition at ~240 K and break down mechanically on sharp cooling. The parameters for the third structure which obtained at 210 K are shown in the experimental section. In general, all of the acquired single crystal structures for ^{Pr}T4 molecule adopt a boat conformation, but a different one from the previously reported for methoxy substituent (^{Me}T4).[147]

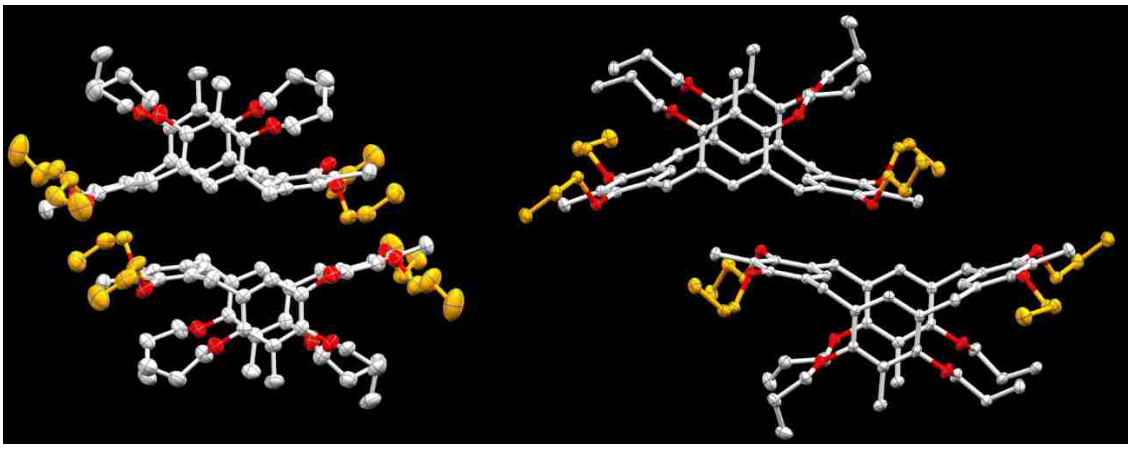

Figure 3.5 The crystal structures of ^{Pr}T4 at 250 K (left) and 100 K (right) with 50% probability; the hydrogens are omitted for more clarity and outlying (non-cofacial benzenes) propyl groups are shown in golden.

In the crystals, the molecules are associated pairwise with their flat sides which formed by the outlying rings to form centrosymmetrically overlapping. However, the overall overlap is markedly different at low and high temperature. At low temperature only one benzene ring overlaps with its inversion analog forming a homo couple. At the higher temperature, different rings overlap, forming two hetero couples. However, the rings in these couples are additionally shifted across the long axes of the molecules, as oppose to the overlap observed at low temperature. In both cases, there is no actual stacking interaction and the molecules mostly interact over weak C-H…pi contacts. The cofacial benzene rings are almost parallel to each other with dihedral angle between their mean planes just 4.3°; this value is around 8.6° in the 100 K structure. Moreover, the roughly equal plane-centroid distance (~4.9 Å) is observed for crystals at low and high temperatures. However, the outlying benzene rings are oriented differently. Whereas in the 250 K structure, one of the rings has an outlying pseudo-exo orientation, the opposite ring is endo-oriented. This pattern changed after phase transformation at low temperature

and both rings are shown pseudo-exo orientation. There is no cleft between these rings, and their planes are essentially parallel, but not co-planar. The another major different between low and high temperature structures is the different orientation of non-conjugated propoxy groups (OPr); in the high-temperature, the OPr substituents at one of the outlying benzene rings are exo-oriented and at the another one is endo-oriented. Whereas at low temperature all propoxy groups are endo-oriented. In contrast to the 180° rotation of two OPr groups of non-cofacial benzene rings, the OPr groups at the cofacial benzene rings showed similar alternating endo-exo orientations before and after the phase transformation. The third molecular structure which obtained immediately after the phase transition (210 K) is almost totally disordered. Basically, it represents a superposition of 80% conformer of observed structure at 100K and 20% of observed pre-transition structure at 250K (see SI).

The last analogous investigated molecule is the methoxypyragallo[4]arene (^{Me}P4, X = OMe, see **Scheme 3.1**). The ^{1}H NMR of ^{Me}P4 in $CDCl_3$ is illustrated in the **Figure 3.6**. The ^{1}H NMR in different solvents and ^{13}C NMR spectra are provided in the Experimental section. As depicted in the **Figure 3.6**, the ^{1}H NMR of ^{Me}P4 showed one sharp singlet peak for the aromatic proton in $CDCl_3$ (6.20 ppm). This spectrum is consistent in the other solvents (DMSO-D_6, Aceton-D_6 and CD_3CN) which indicate that the polarity of the solvent cannot change the conformer.[169] Moreover, the variable temperature ^{1}H NMR (form -50 °C to 100 °C using $CDCl_3$ and DMSO-D_6 solvent, respectively) study did not show any broadening or emerging of new peaks which implies on the single stable conformer of ^{Me}P4 in the investigated solvents and temperature range. Similar to the R4 and T4 cases, this conformer should have same environment for the

aromatic protons which imply that the only possible conformer is 1,3-alternate (see **Figure 3.1**).

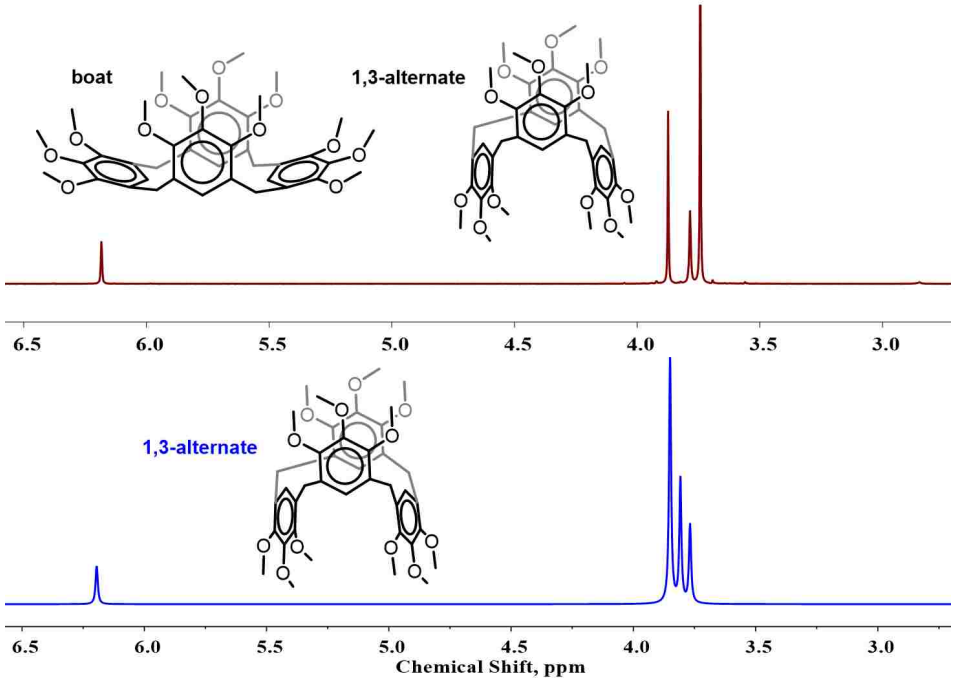

Figure 3.6 ^{1}H NMR spectra of ^{Me}P4 at 20 °C in $CDCl_3$ (red) and calculated ^{1}H NMR spectra (blue) of 1,3-alternate conformer of ^{Me}P4 using B3LYP-D3BJ/6-31G(d)+SMD(CH_2Cl_2).

However, growing the crystal structure using slow evaporation of ^{Me}P4 in DCM/CH_3CN, yielding another conformer (boat). Therefore, in order to evaluate the stability of these two conformers, comprehensive computational calculations were carried out. As listed in the **Table 3.3**, all selected DFT methods indicated the boat conformer as the most stable structure. However, their energies are not in close range (1.9 to 6.6 kcal/mol). Also, the PCM solvation model, in comparison to SMD, indicated higher energy differences between these two conformers. Moreover, we examined the effects of

different atomic radii (Bondi, Pauling, UA0, UAHF, UAKS) using PBE0-B3BJ/6-31G*+PCM(CH_2Cl_2). However, all of them indicated almost similar energy gap between boat and 1,3-alt conformers. In contrast to R4 and T4, we were not able to optimize the twisted 1,3-alternate conformer for this molecule.

Table 3.3 The relative free energies (ΔG, kcal/mol) of different conformers of ^{Me}P4 using SMD and PCM (values in the parenthesis) solvation models (CH_2Cl_2).

	B3LYP	CAM-B3LYP	M062X	PBE0	ωB97XD
6-31G*					
boat	0.0 [0.0]	0.0 [0.0]	0.0 [0.0]	0.0 [0.0]	0.0 [0.0]
1,3-alt	2.7 [4.4]	2.7 [5.1]	5.3 [6.6]	2.8 [4.2]	4.7 [3.2]
Def2-SVP					
boat	0.0 [0.0]	0.0 [0.0]	0.0 [0.0]	0.0 [0.0]	0.0 [0.0]
1,3-alt	1.9 [4.8]	3.4 [4.8]	4.5 [5.6]	3.2 [5.1]	1.9 [3.7]

In opposition to the calculated free energy differences using DFT, comparing the calculated ^{1}H NMR with the experimental results showing the 1,3-alternate conformer as the corresponding structure in solvent (**Figure 3.6**). The calculated ^{1}H NMR chemical shift for the aromatic proton is 6.26 ppm which is in good agreement to the experimental result (6.20 ppm). The calculated ^{1}H NMR chemical shifts for aromatic protons of boat conformer showing two different values (6.57 and 6.18 ppm) which are not in agreement with the experimental results. Evaluating the experimental vs. computational data suggesting that the presents implicit solvation models are not able to properly simulate the solvation effects on the conformational stability of ^{Me}P4. In order to prove our data with more accuracy, the solvation effects are simulated using the ONIOM method. The results revealed that the 1,3-alt is around 3.1 kcal/mol more stable than the boat conformer in this solvent. This value means that the explicit solvation model can reverse

the relative free energy around 8 kcal/mol in favor of 1,3-alt conformer (**Figure 3.7**). Comparing the implicit solvation models results with the QM/MM and experimental NMR data showing the implicit solvation models are not reliable for accurate conformational investigation of these species. Thus, we believe that the inclusion of the explicit solvent is vital for obtaining more reliable computational evaluation of relative stability of calixarenes conformers.

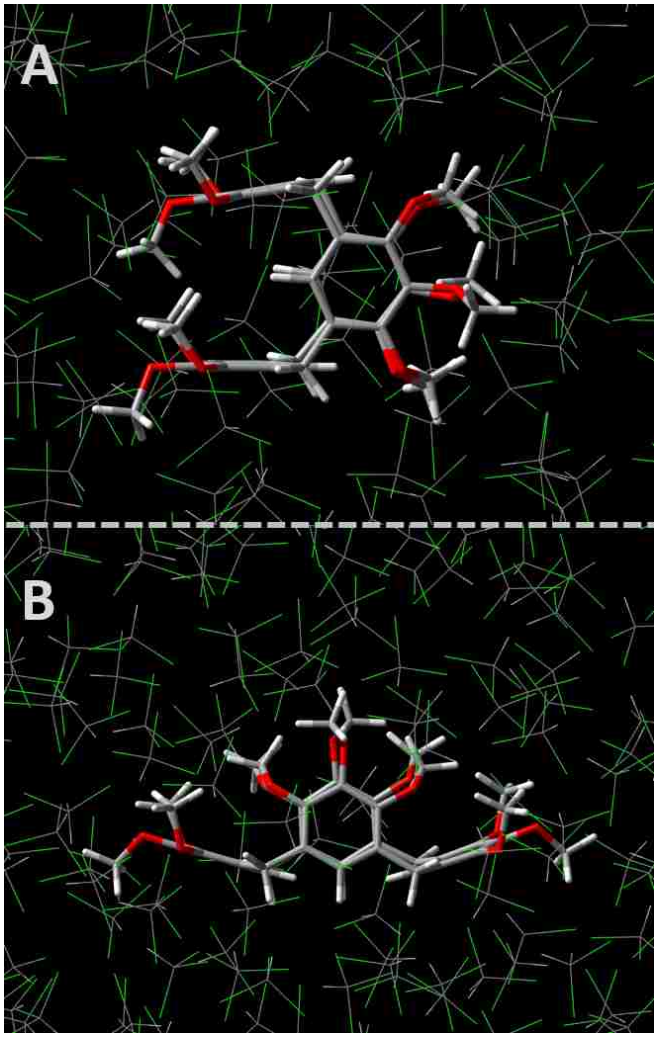

Figure 3.7 The optimized structures of 1,3-alt (A) and boat (B) conformers of ^{Me}P4 using ONIOM(M06-2X/6-31G*:UFF) method.

Conclusion: Several alkoxy substituted calix[4]arenes were synthesized and their conformational variation are studied both experimentally and computationally. The results (NMR and ONIOM) revealed that in all methoxy substituted molecules (^{Me}P4, ^{Me}T4 and ^{Me}R4) the 1,3-alternate is the most stable structure in solution. Moreover, the results indicated that the present implicit solvation models cannot simulate the real solvation effects properly. All employed methods indicated the boat conformer as the most stable structure in the solution which is in direct contrast with the experimental data. To the contrary of implicit solvation models, simulating the solvent effects using ONIOM calculations can represent the correct conformer in the solution media. Due to the crystal packing forces, these molecules prefer to crystalize in the boat confirmation. Though, increasing the size of the substituent (e.g., ^{Et}R4 or ^{Pr}R4) can prevent this conformational change. However, this effect has not been observed for the ^{Pr}T4 system. Interestingly, the ^{Pr}T4 system showed the single-crystal to single-crystal transformation upon the temperature variation. The results can help us to have better insight about the macrocyclic molecules, especially calix[4]arenes, conformational properties and how the intera and intermolecular, calix[4]arene-calix[4]arene and calix[4]arene-solvent, can have significant role in the observed conformer in the solution or solid phases. Moreover, the results raised a new challenge for the implicit solvation models to refining/optimizing their parameters for more accurate simulation of solvent media for supramolecular chemistry.

Experimental

General methods and synthesis

All reactions for the synthesis of calixarenes were performed under argon atmosphere unless otherwise noted. NMR spectra were recorded on Varian 300 and 400 MHz NMR spectrometers. Mass spectra were recorded on Bruker Daltonics MALDI-TOF mass spectrometer.

The 1,3-dialkylbenzene (alkyl = Ethyl, Propyl) were synthesized using the Resorcinol and alkyl bromide (2.2 eq) in the DMF as the solvent and KOH (2.2 eq) as the base. The reaction stirred for 30 h at 65 °C and 30 °C for propyl and ethyl, respectively. The reaction cooled down to room temperature and water was added to the solution. The organic product has been extracted using DCM. The solvent has been evaporated under low pressure to obtain a brownish oil. The product (colorless oil) has been purified using the flash column using pure hexanes. The purity of the product has been confirmed using the ^{1}H-NMR and ^{13}C-NMR (see the NMR section). The yield for Ethyl and Propyl was 55% and 83%, respectively.

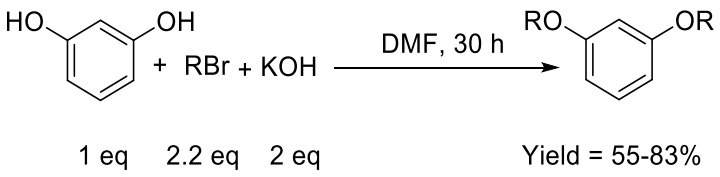

The 2,6-diproxytoluene was synthesized using the 2-methyresorcinol and 1-Bromopropane (2.2 eq) in the DMF as the solvent and KOH (2.2 eq) as the base. The reaction stirred for 30 h at 65 °C. The reaction cooled down to room temperature and water was added to the solution. The organic product has been extracted using DCM. The

solvent has been evaporated under low pressure to obtain a brownish oil. The product (colorless oil) has been purified using the flash column using pure hexanes. The purity of the product, yield 80%, has been confirmed using the ^{1}H-NMR and ^{13}C-NMR (see the NMR section).

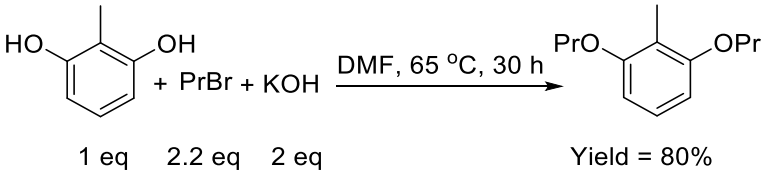

^{Me}R4, ^{Et}R4 and ^{Pr}R4 synthesis: To a solution of 1,3-dialkylbenzene (5 mmol, R = Methyl, Ethyl and Propyl) in dichloromethane (DCM, 30 ml), paraformaldehyde was added (0.3 g, 10 mmol, 2.0 eq) under the Argon atmosphere. Then, the methanesulfonic acid (0.1 ml, 0.15 mmol) was added at one portion. The mixture was stirred at the room temperature for 12 h. The reaction has been quenched by adding saturated sodium bicarbonate solution (30 ml) to the Schlenk flask and letting it stir vigorously for 30 min. The organic layer has been separated using the separatory funnel. The DCM has been evaporated under the vacuum. The solid has been washed with methanol (20 ml * 3 times) and then washed one time with acetone (20 ml). For ^{Me}R4 the product has been washed with boiling ethyl acetate. The pure products have been confirmed using the ^{1}H-NMR, ^{13}C-NMR and MALDI-TOF spectroscopy techniques (yield = 73-83%).

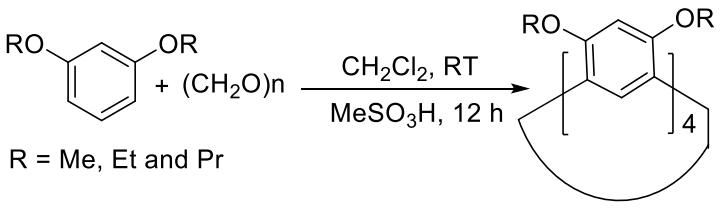

^{Me}R4: mass 0.61 g, yield 80%; MALDI Mass (calculated: 600.27; experimental: 599.13); ^{1}H-NMR ($CDCl_3$ at 20 °C, collected over 8 h) δ: 3.69 (s, 8H), 3.78 (s, 24H), 6.19 (s, 4H), 6.41 (s, 4H).

^{Et}R4: mass 0.65 g, yield 73%; MALDI Mass (calculated: 712.40; experimental: 712.10); ^{1}H-NMR ($CDCl_3$ at 20 °C) δ: 1.31 (t, 24H), 3.71 (s, 8H), 3.94 (q, 16H), 6.25 (s, 4H), 6.38 (s, 4H); ^{13}C-NMR ($CDCl_3$ at 20 °C) δ: 15.20, 28.18, 64.48, 98.20, 121.81, 131.09, 155.71.

^{Pr}R4: mass 0.85 g, yield 83%; MALDI Mass (calculated: 824.52; experimental: 824.45); ^{1}H-NMR ($CDCl_3$ at 20 °C) δ: 0.97 (t, 24H), 1.72 (sext, 16H), 3.73 (s, 8H), 3.84 (t, 16H), 6.27 (s, 4H), 6.37 (s, 4H); ^{13}C-NMR ($CDCl_3$ at 20 °C) δ: 10.75, 22.98, 28.12, 70.37, 97.87, 121.65, 131.06, 155.79.

^{Pr}T4 synthesis: To a solution of 2,6-dipropoxytoluene (5 mmol) in dichloromethane (DCM, 30 ml), paraformaldehyde was added (0.3 g, 10 mmol, 2.0 eq) under the Argon atmosphere. The reaction cooled down using the ice bath. Then, the BF3.Et2O (1 ml, 15 mmol) was added at one portion. The mixture was stirred over the night (0 °C → RT). The reaction has been quenched by adding saturated sodium bicarbonate solution (30 ml) to the Schlenk flask and letting it stir vigorously for 30 min. The organic layer has been separated using the separation funnel. The DCM has been evaporated under the vacuum. The pure product has been purified using the flash column (Hexane/Ethyl acetate = 100/30). The purity of the product has been confirmed using the ^{1}H-NMR, ^{13}C-NMR and MALDI-TOF spectroscopy techniques (yield = 85%). The MALDI-TOF spectrum is collected by dissolving the pure product in potassium acetate solution in DCM.

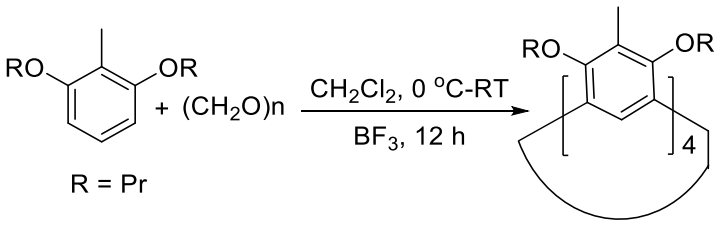

^{Pr}T4: mass 0.94 g, yield 85%; MALDI Mass (calculated: 880.59; experimental: 880.76); ^{1}H-NMR ($CDCl_3$ at 20 °C) δ: 0.99 (t, 24H), 1.72 (sext, 16H), 2.15 (s, 12H), 3.63 (t, 16H), 3.83 (s, 8H), 6.18 (s, 4H); ^{13}C-NMR ($CDCl_3$ at 20 °C) δ: 10.13, 10.72, 23.69, 29.52, 74.31, 123.73, 128.94, 154.88.

^{Me}P4 synthesis: To a solution of 1,2,3-trimethoxybenzene (5 mmol) in dichloromethane (DCM, 30 ml), paraformaldehyde was added (0.3 g, 10 mmol, 2.0 eq) under the Argon atmosphere. Then, the methanesulfonic acid (0.1 ml, 0.15 mmol) was added at one portion. The mixture was stirred at the room temperature for 12 h. The reaction has been quenched by adding saturated sodium bicarbonate solution (30 ml) to the Schlenk flask and letting it stir vigorously for 30 min. The organic layer has been separated using the separatory funnel. The DCM has been evaporated under the vacuum. The product has been purified using column (Hexane/Ethyl acetate = 100/5). The pure products have been confirmed using the ^{1}H-NMR, ^{13}C-NMR and MALDI-TOF spectroscopy techniques (yield = 22%).

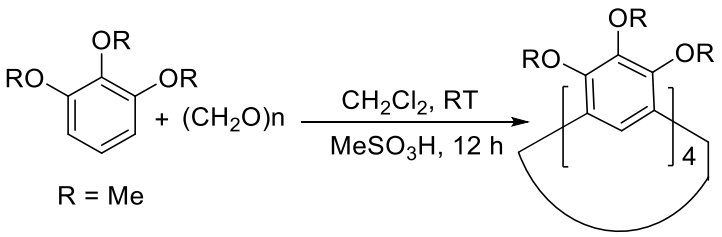

^{Me}P4: mass 0.20 g, yield 22%; MALDI Mass (calculated: 720.31; experimental: 720.68); ^{1}H-NMR ($CDCl_3$ at 20 °C) δ: 3.75 (s, 24H), 3.79 (s, 8H), 3.88 (s, 12H), 6.20 (s, 4H); ^{13}C-NMR ($CDCl_3$ at 20 °C) δ: 29.20, 60.66, 60.70, 125.12, 129.33, 146.19, 150.06.

^{1}H- and ^{13}C-NMR spectra of calixarenes and reactants.

^{1}H NMR spectrum ^{Pr}T4 ($CDCl_3$, 20 °C)

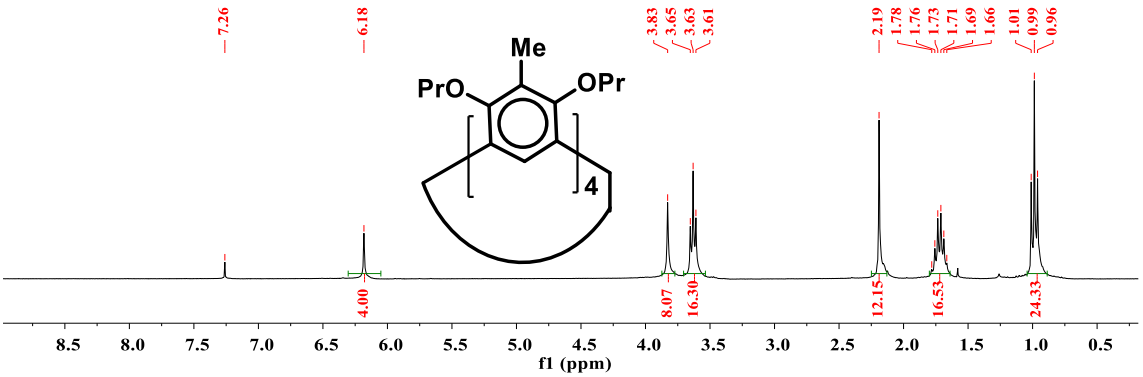

^{1}H NMR spectrum ^{Pr}T4 (Acetone-D_6, 20 °C)

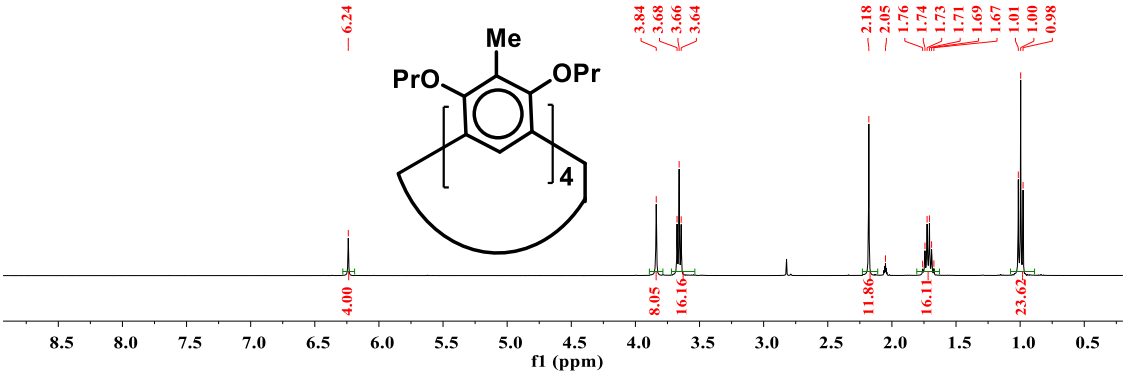

^{13}C NMR spectrum of $^{Pr}T4$ ($CDCl_3$, 20 °C)

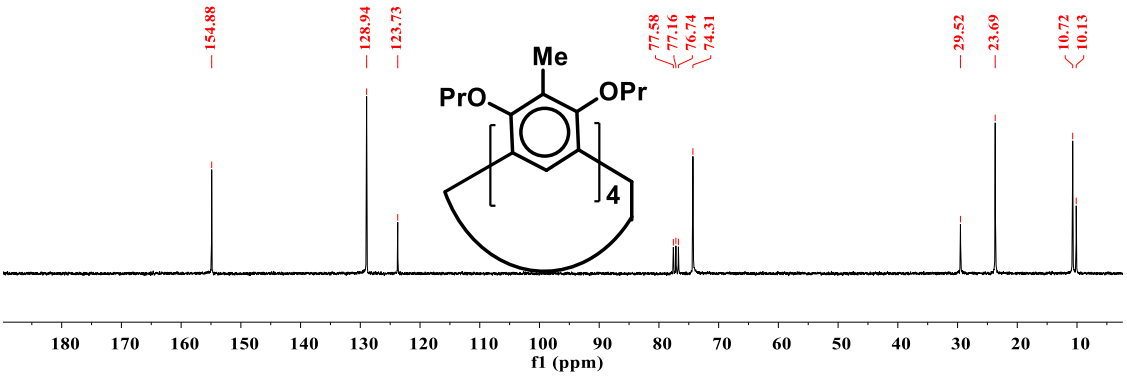

Variable temperature ^1H NMR spectra of $^{Pr}T4$ (CD_2Cl_2, 20 °C to -70 °C)

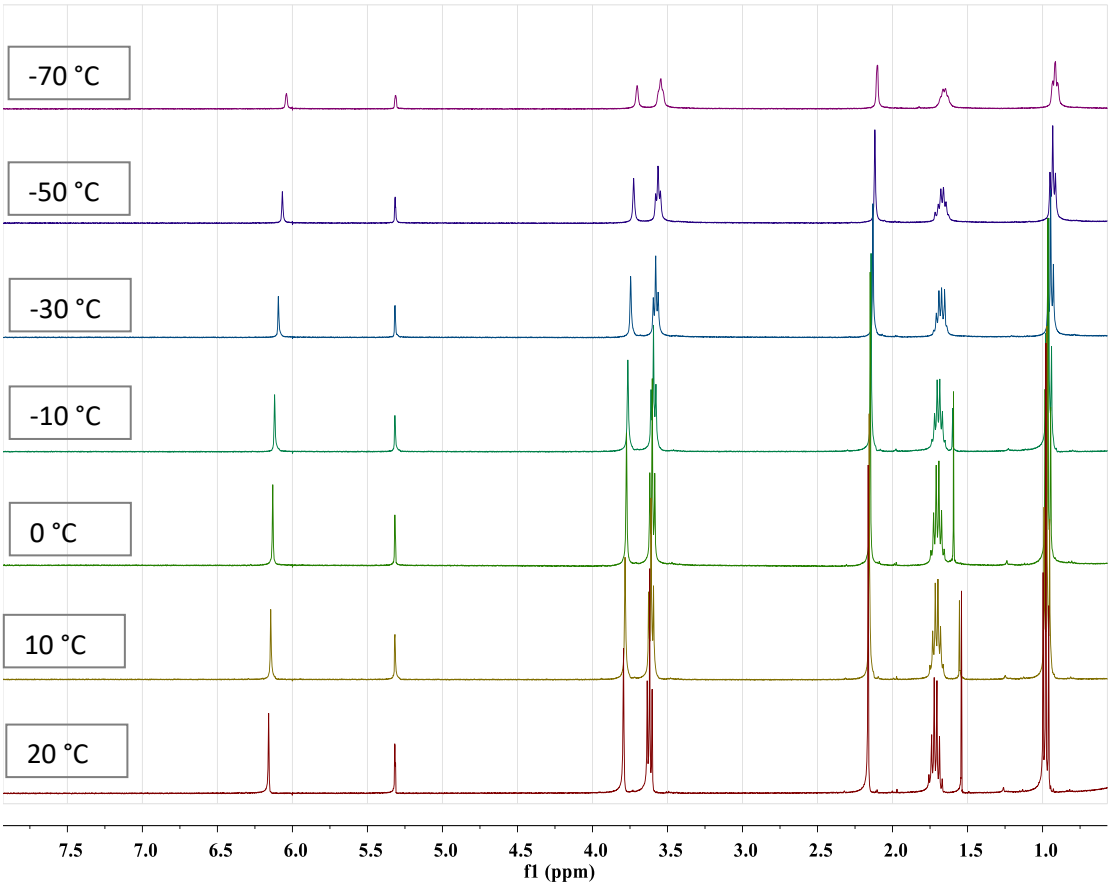

^{1}H NMR spectrum ^{Me}P4 ($CDCl_3$, 20 °C)

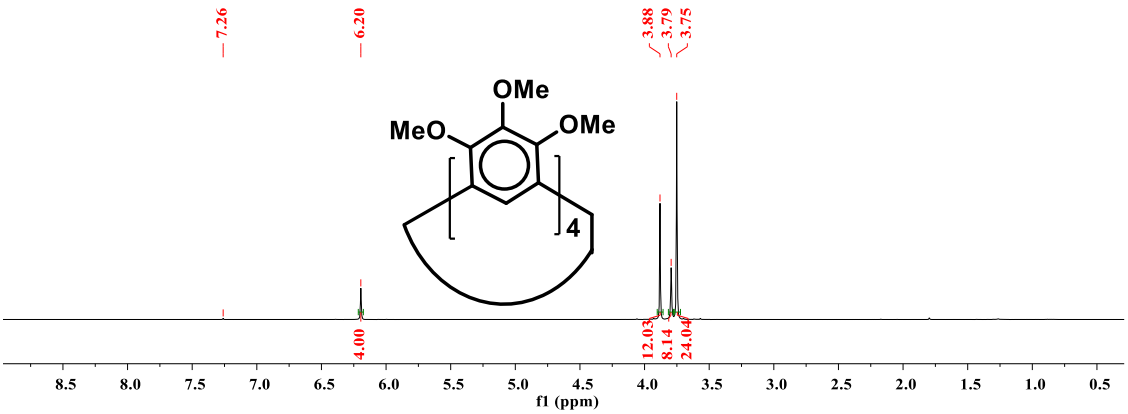

Variable temperature ^{1}H NMR spectra of ^{Me}P4 ($CDCl_3$, -20 °C to -50 °C)

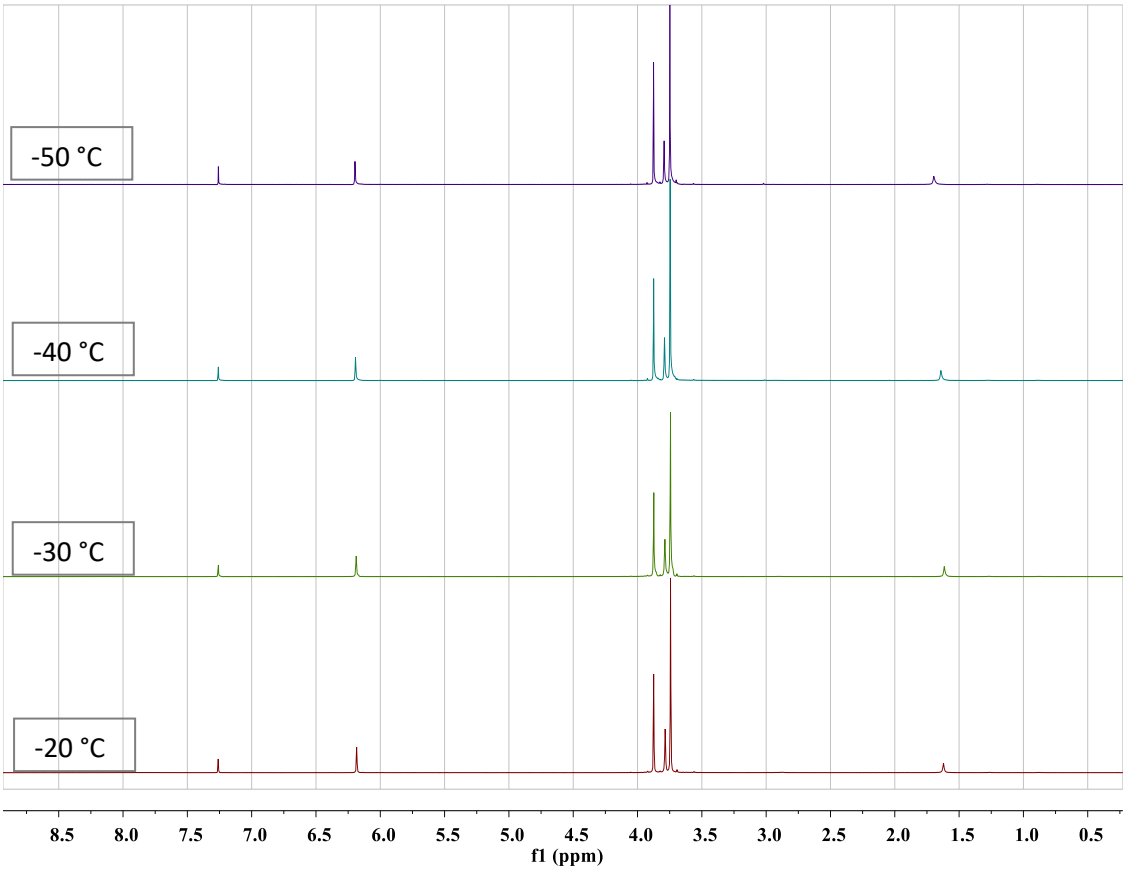

^{1}H NMR spectrum ^{Me}P4 (DMSO-D$_6$, 100 °C)

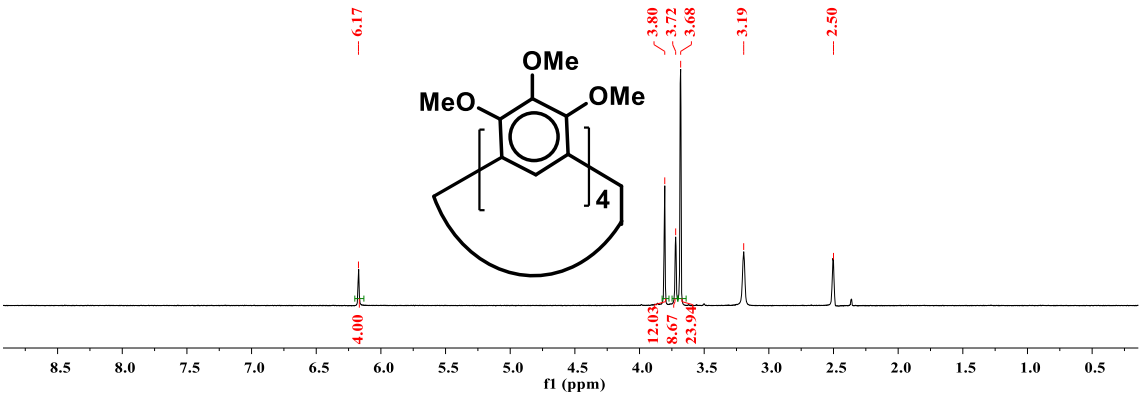

Variable temperature ^{1}H NMR spectra of ^{Me}P4 (DMSO-D$_6$, 20 °C to 100 °C)

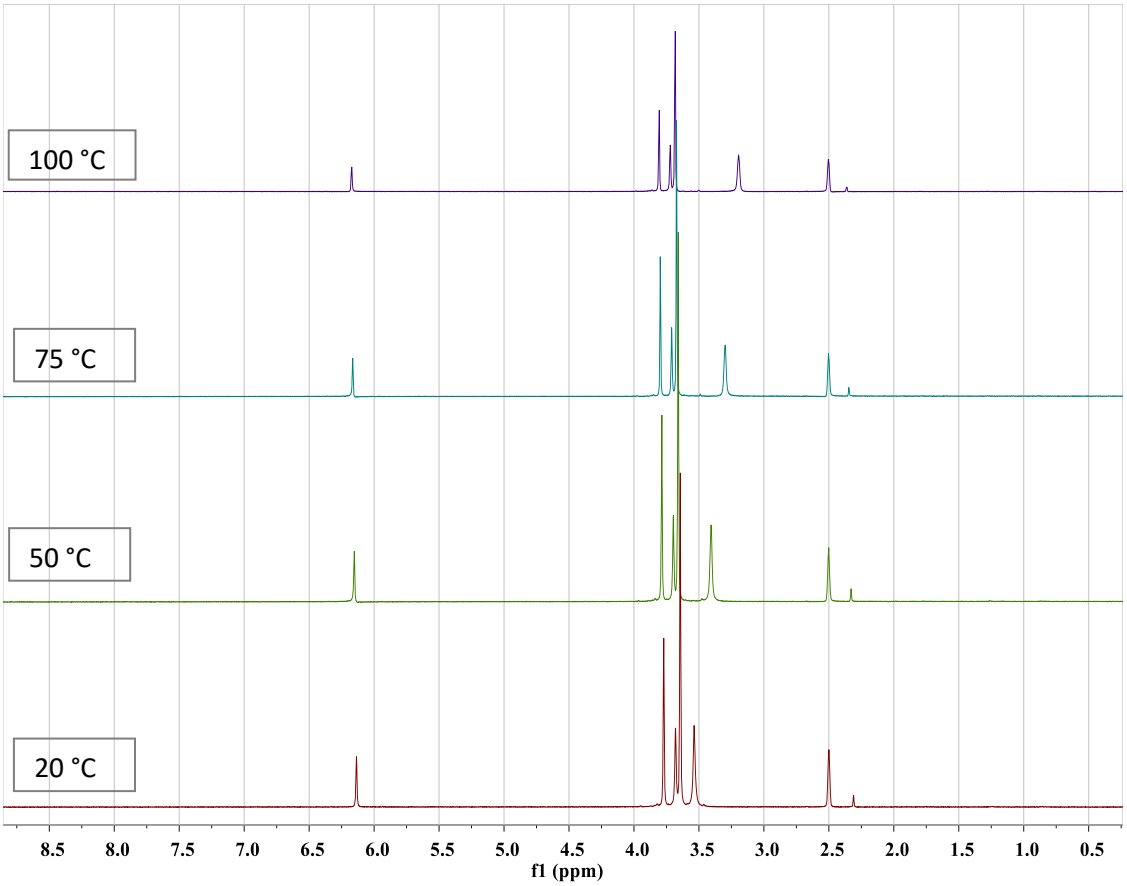

^{1}H NMR spectrum ^{Me}P4 (CD_3CN, 20 °C)

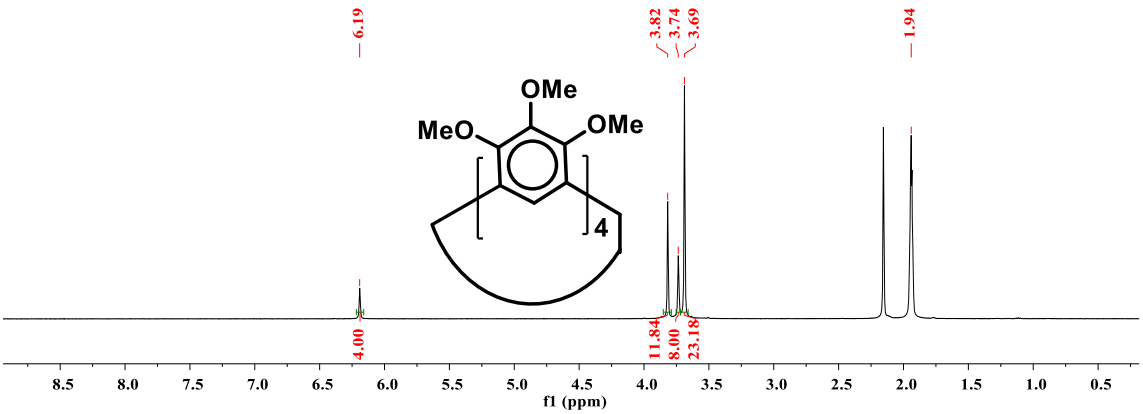

^{1}H NMR spectrum ^{Me}P4 (Acetone-D_6, 20 °C)

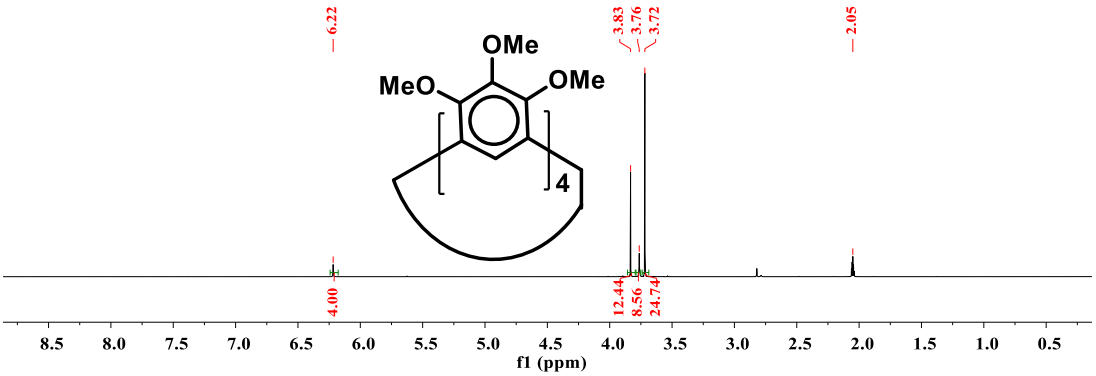

^{13}C NMR spectrum of $^{Me}P4$ ($CDCl_3$, 20 °C)

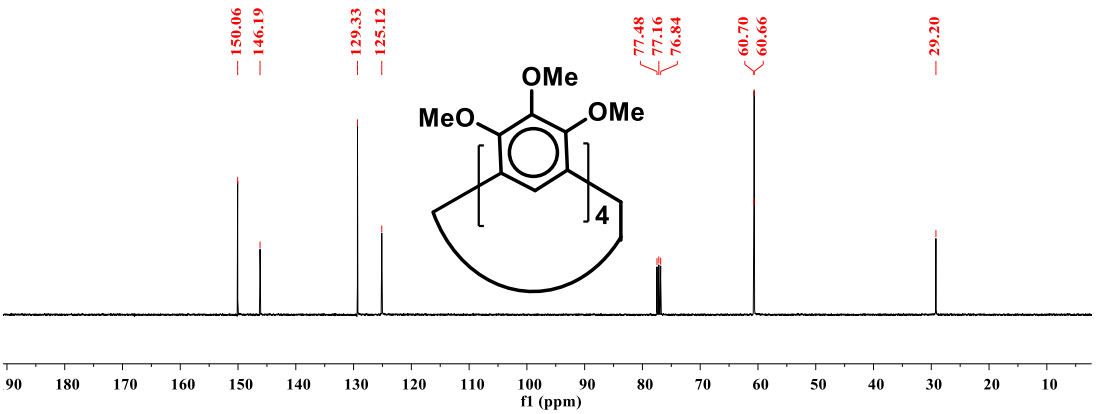

^{1}H NMR spectrum $^{Pr}R4$ ($CDCl_3$, 20 °C)

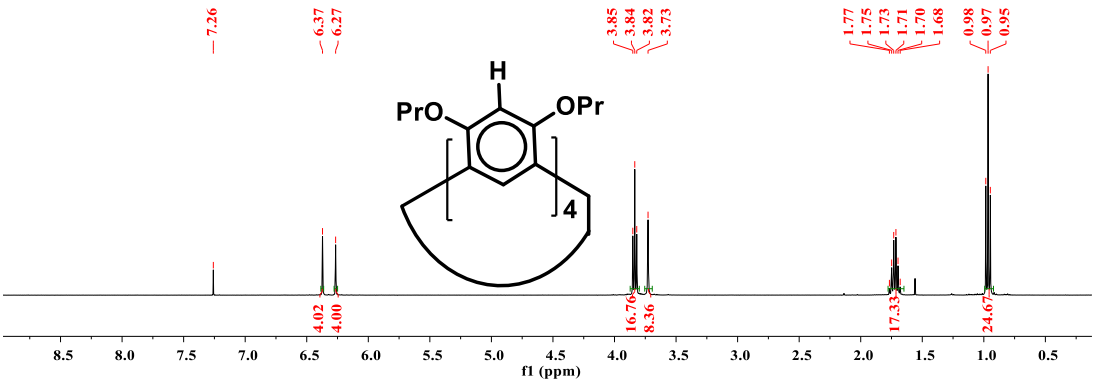

^{13}C NMR spectrum of $^{Pr}R4$ ($CDCl_3$, 20 °C)

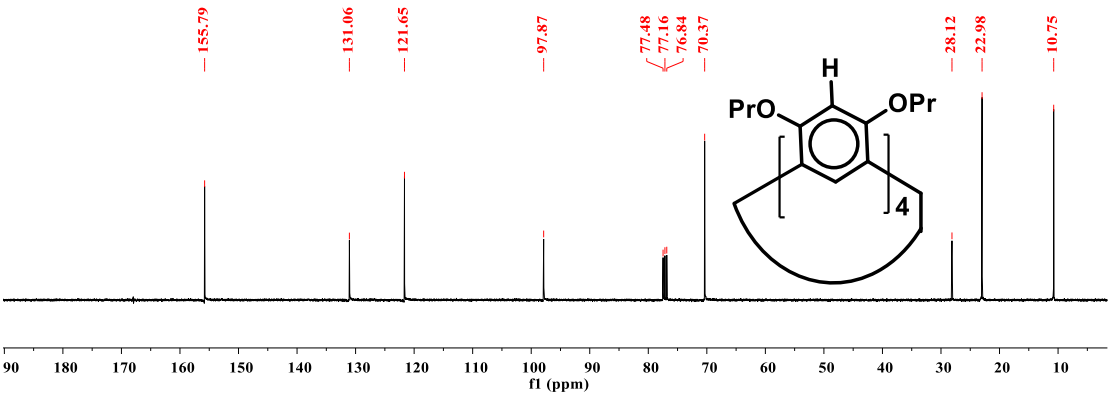

^{1}H NMR spectrum $^{Et}R4$ ($CDCl_3$, 20 °C)

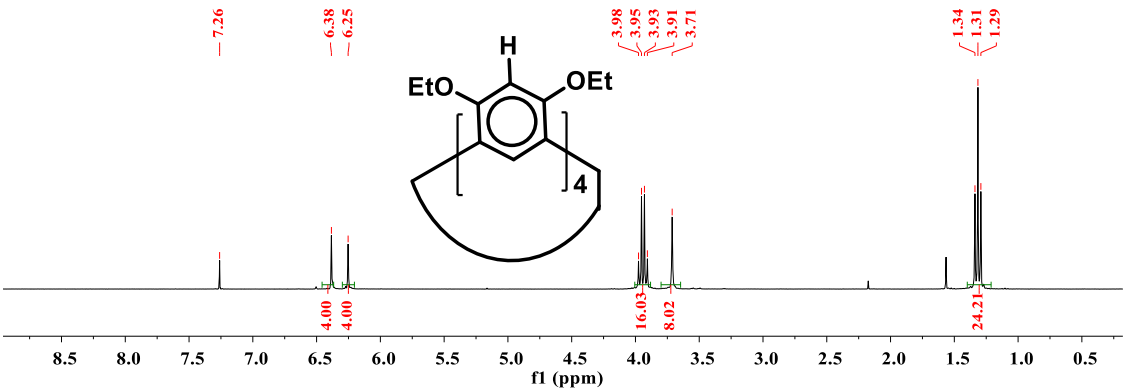

^{13}C NMR spectrum of $^{Et}R4$ ($CDCl_3$, 20 °C)

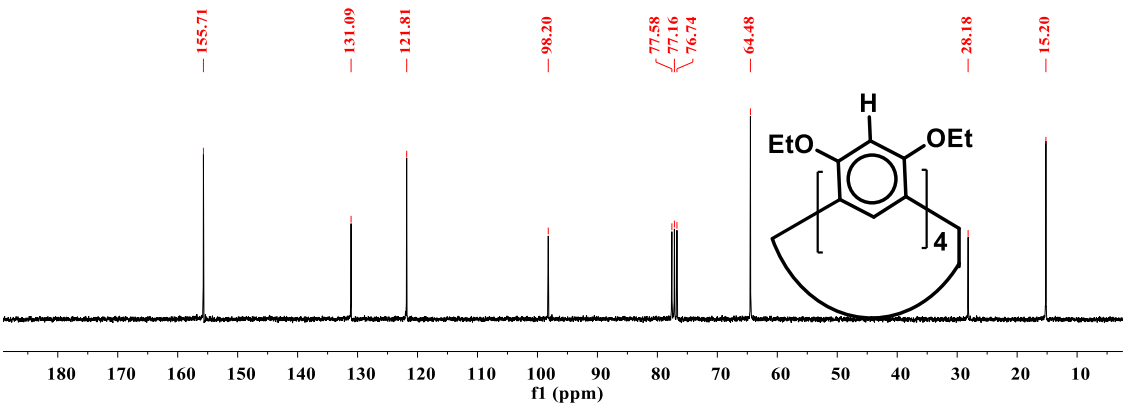

^{1}H NMR spectrum $^{Me}R4$ ($CDCl_3$, 20 °C)

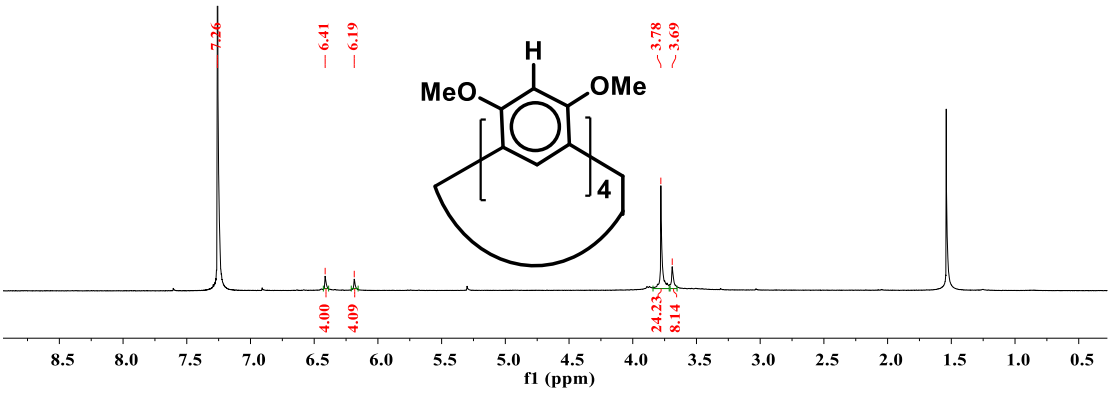

^{1}H NMR spectrum of 1,2,3-trimethoxybenzene ($CDCl_3$, 20 °C)

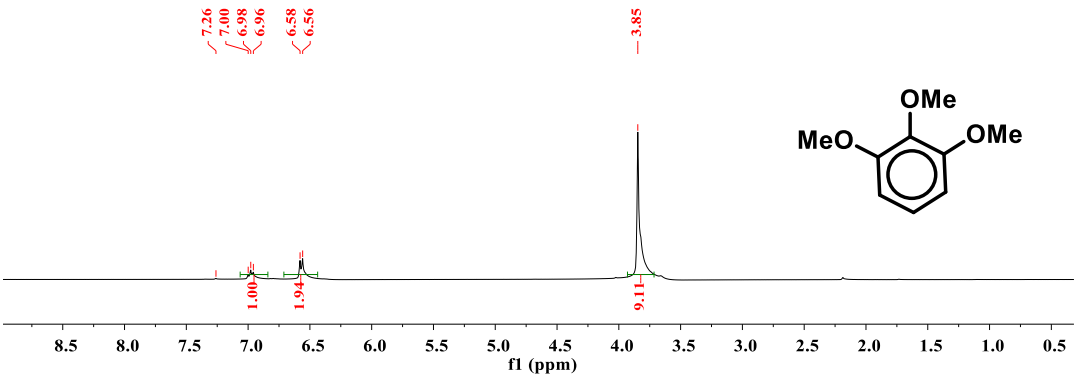

^{13}C NMR spectrum of 1,2,3-trimethoxybenzene ($CDCl_3$, 20 °C)

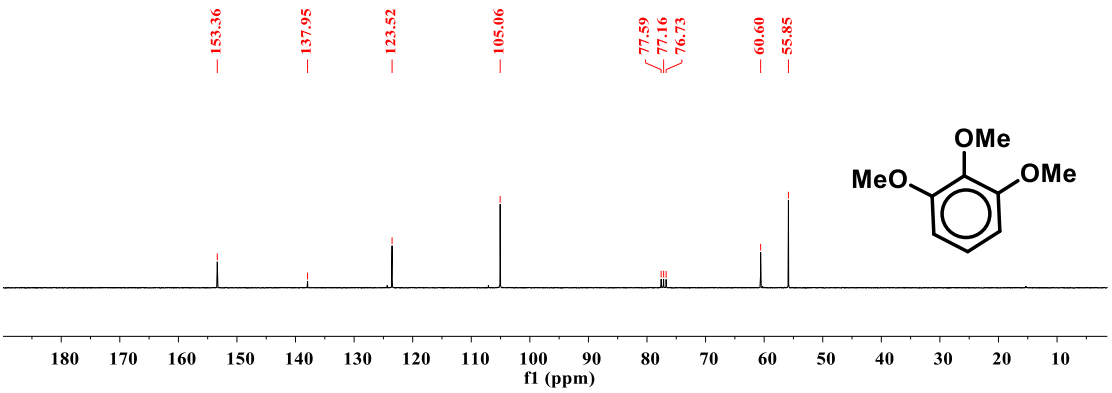

^{1}H NMR spectrum of 1,3-diproxybenzene ($CDCl_3$, 20 °C)

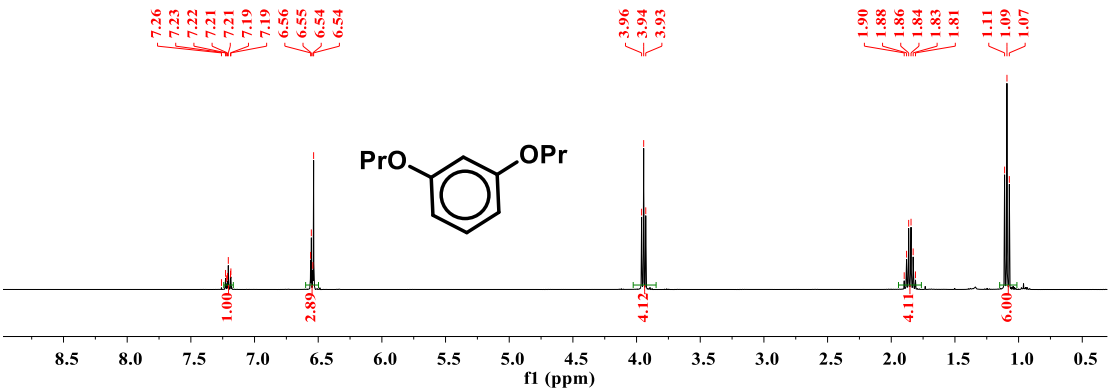

^{13}C NMR spectrum of 1,3-diproxybenzene ($CDCl_3$, 20 °C)

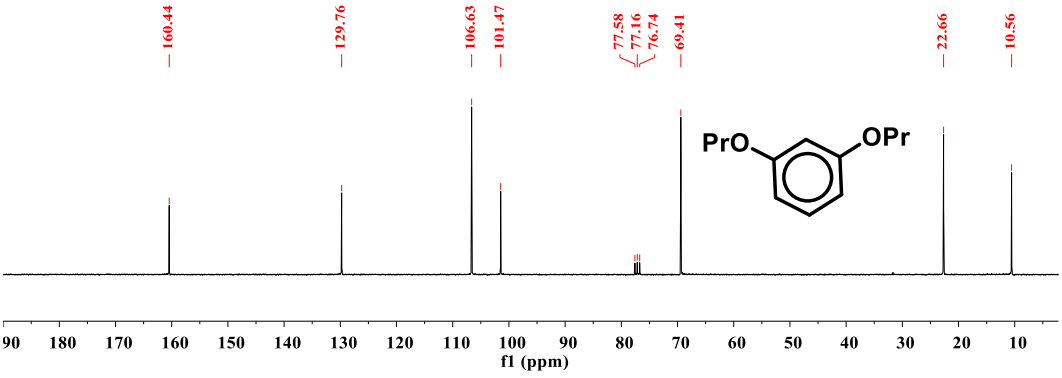

^{1}H NMR spectrum of 1,3-diethoxybenzene ($CDCl_3$, 20 °C)

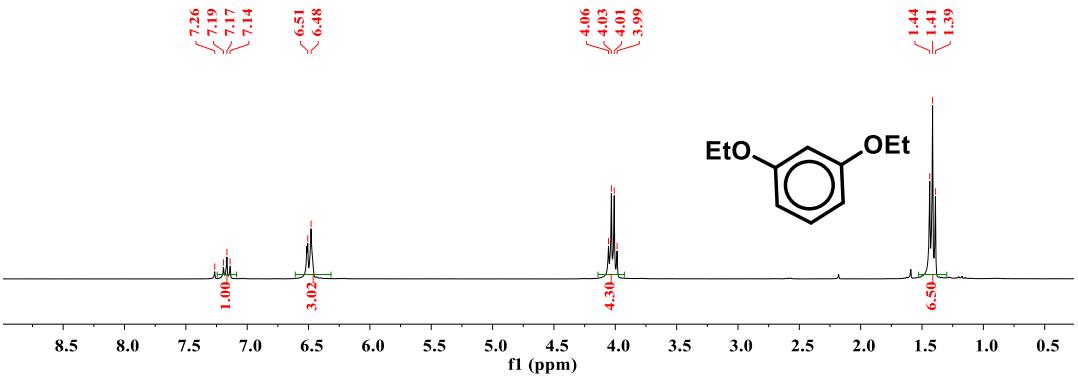

^{13}C NMR spectrum of 1,3-diethoxybenzene ($CDCl_3$, 20 °C)

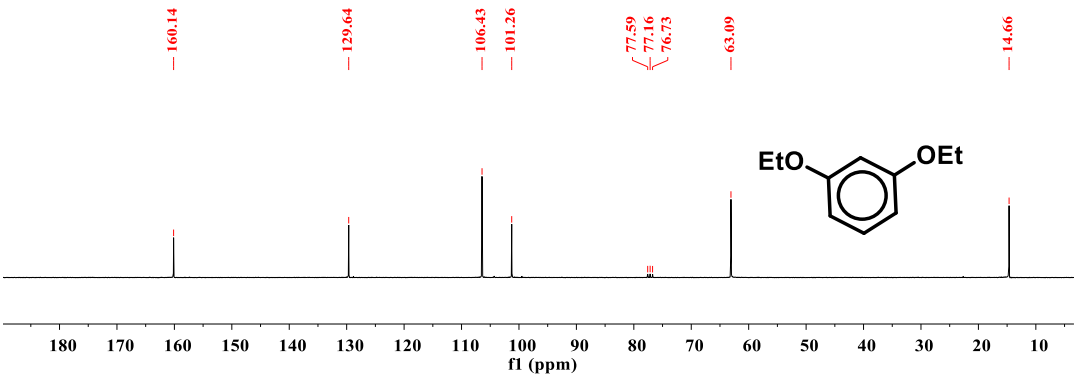

^{1}H NMR spectrum of 1,3-dimethoxybenzene ($CDCl_3$, 20 °C)

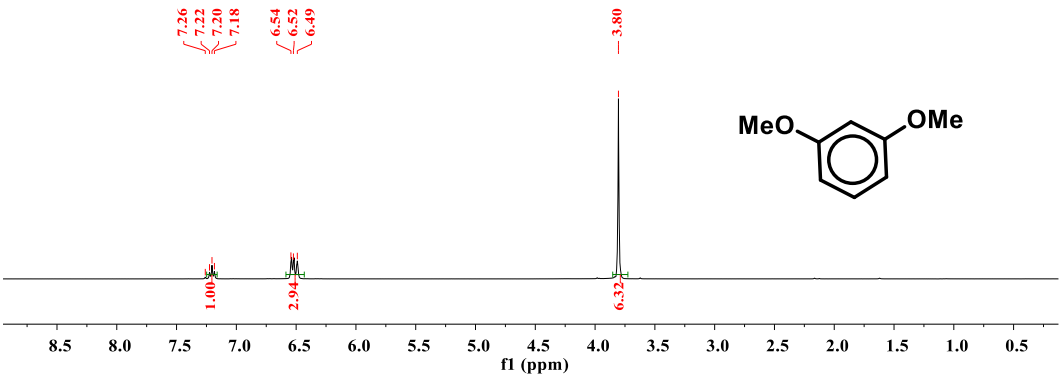

^{13}C NMR spectrum of 1,3-dimethoxybenzene ($CDCl_3$, 20 °C)

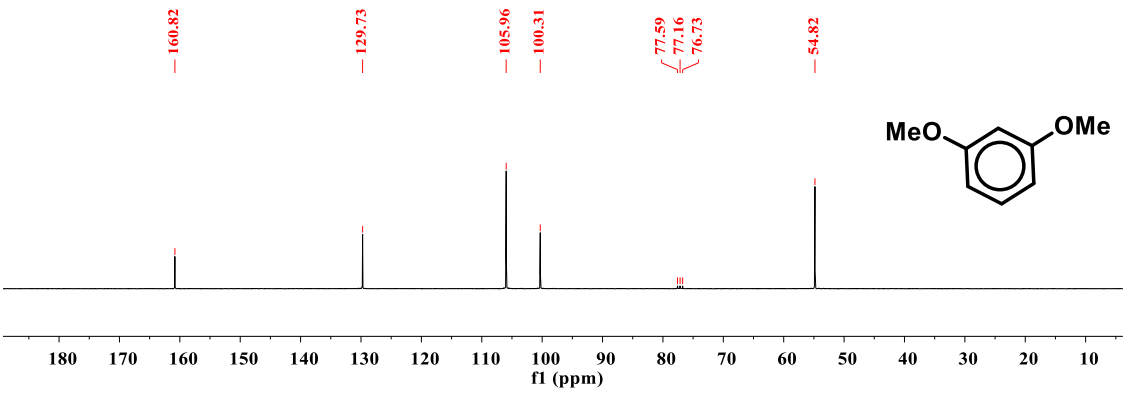

^{1}H NMR spectrum of 2,6-diproxytoluene ($CDCl_3$, 20 °C)

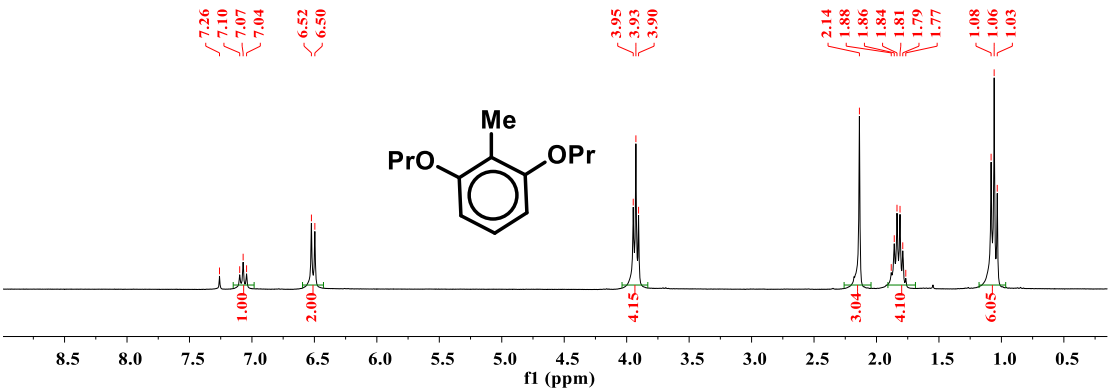

^{13}C NMR spectrum of 2,6-diproxytoluene ($CDCl_3$, 20 °C)

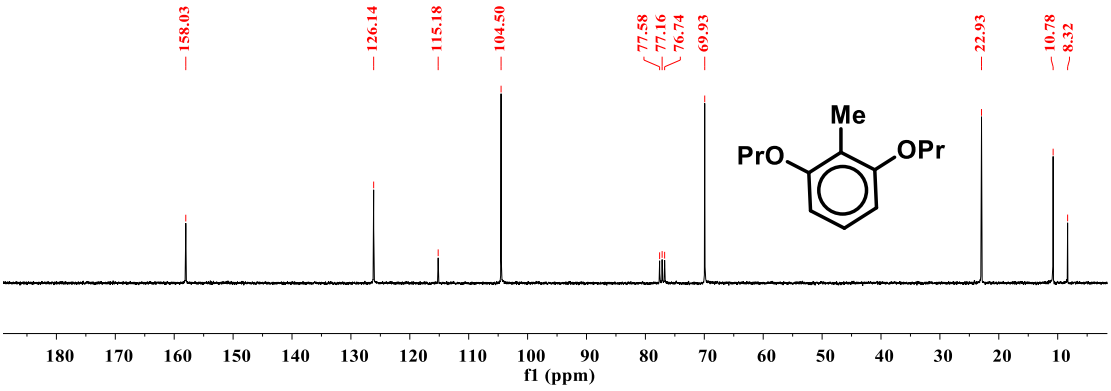

MALDI-TOF data

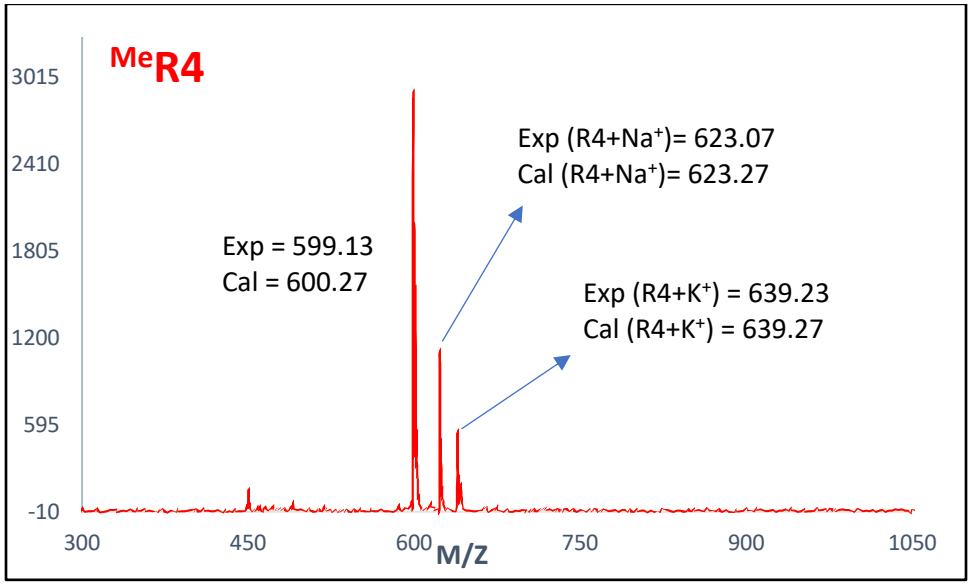

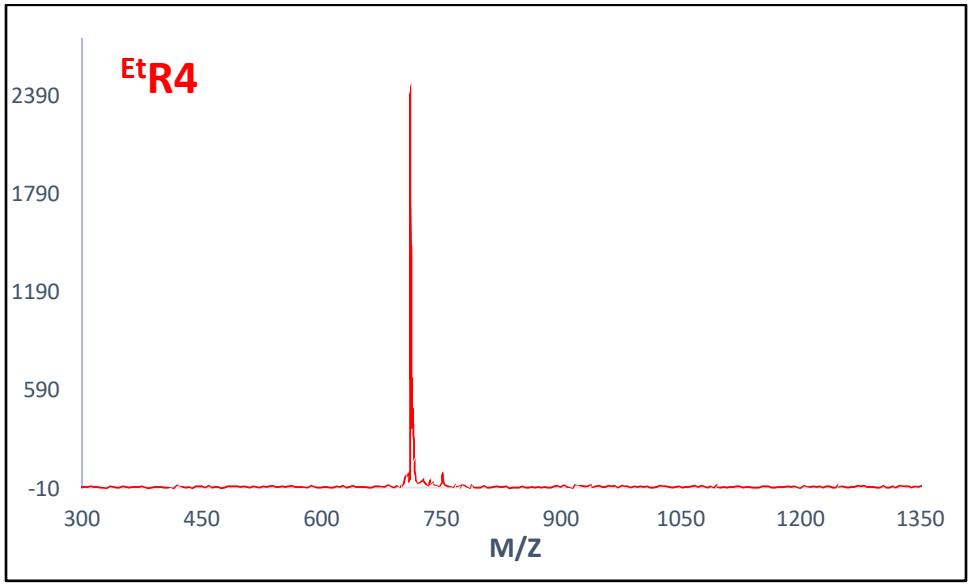

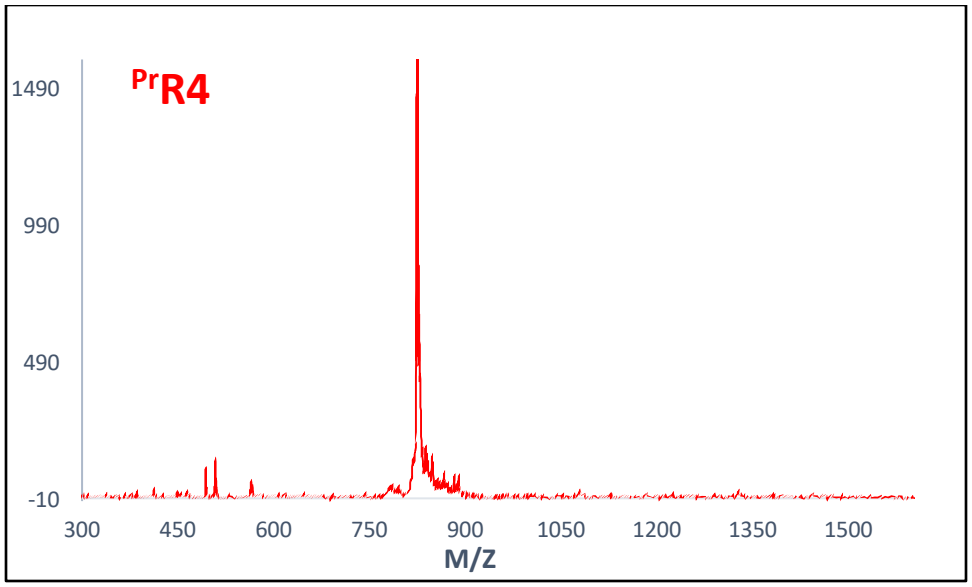
PrR4
1490
990
490
-10
300
450
600
750
900
1050
1200
1350
1500
M/Z

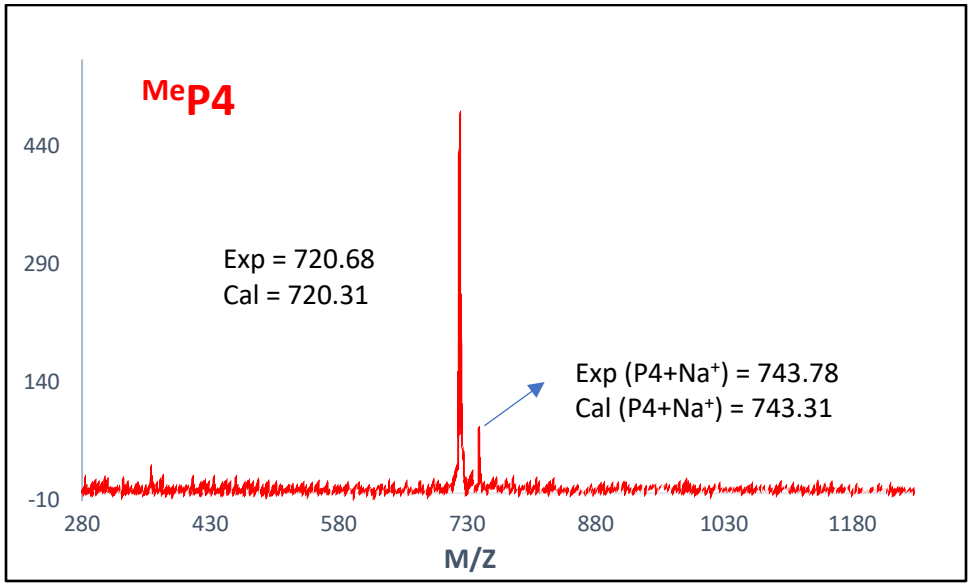
MeP4
440
290
140
-10
Exp = 720.68
Cal = 720.31
Exp (P4+Na+) = 743.78
Cal (P4+Na+) = 743.31
280
430
580
730
880
1030
1180
M/Z

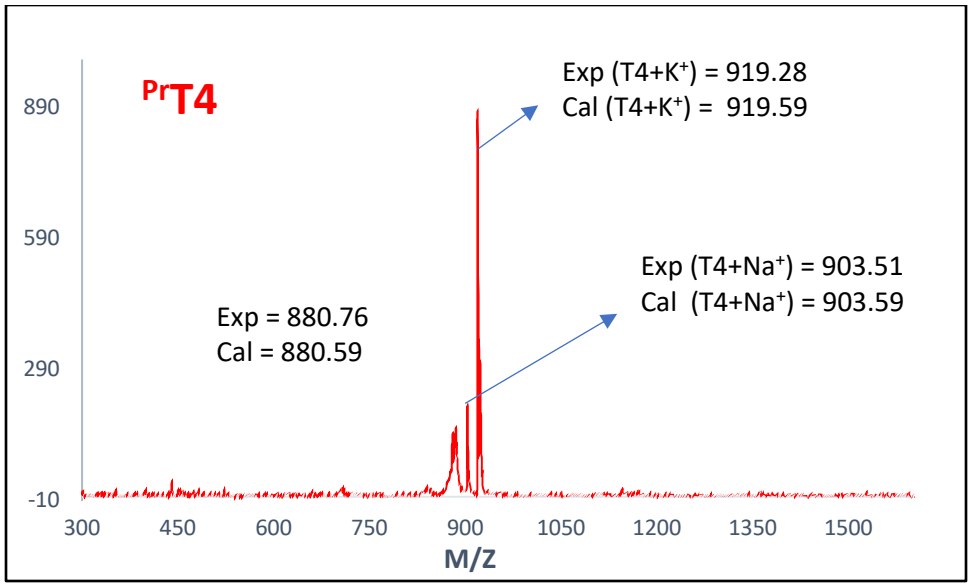
PrT4
Exp (T4+K+) = 919.28
Cal (T4+K+) = 919.59
Exp (T4+Na+) = 903.51
Cal (T4+Na+) = 903.59
Exp = 880.76
Cal = 880.59
890
590
290
-10
300
450
600
750
900
1050
1200
1350
1500
M/Z

Table 3.4 Summary of X-ray crystallographic data collection of ^{Et}R4 and ^{Pr}R4.

Identification code	kad1h (^{Et}R4)	kad1f (^{Pr}R4)
Empirical formula	$C_{45}H_{62}O_{10}$	$C_{52}H_{72}O_8$
Formula weight	762.94	825.09
Temperature/K	100.05 (10)	100.15
Crystal system	triclinic	monoclinic
Space group	P-1	$P2_1/n$
a/Å	12.1752(4)	15.0375(6)
b/Å	12.5842(3)	13.5431(5)
c/Å	15.2418(4)	23.7954(10)
α/°	104.549(2)	90
β/°	97.243(2)	99.490(4)
γ/°	106.190(2)	90
Volume/Å^3	2121.90(11)	4779.7(3)
4Z	2	4
ρ_{calc}g1.47/cm^3	1.194	1.147
μ/mm^{-1}	0.672	0.599
F(000)	824.0	1792.0
Crystal size/mm^3	0.42 × 0.03 × 0.03	0.584 × 0.239 × 0.118
Radiation	CuKα (λ = 1.54184)	CuKα (λ = 1.54184)
2Θ range for data collection/°	7.67 to 141.504	7.534 to 145.558
Index ranges	-14 ≤ h ≤ 14,-15 ≤ k ≤15,-18≤l≤ 18	-13≤h≤ 18, -16≤k≤ 16, -29 ≤l ≤ 28
Reflections collected	37900	42676
Independent reflections	8046 [R_{int}=0.0516, R_{sigma}= 0.0275]	9102 [R_{int} =0.0558, R_{sigma}=0.0307]
Data/restraints/parameters	8046/0/477	9102/0/560
Goodness-of-fit on F^2	1.028	1.095
Final R indexes [I>=2σ(I)]	R_1 = 0.0543, wR_2 = 0.1485	R_1 = 0.0580, wR_2 = 0.1642
Final R indexes [all data]	R_1 = 0.0600, wR_2 = 0.1559	R_1 = 0.0756, wR_2 = 0.1892
Largest diff. peak/hole / e Å^{-3}	0.96/-0.38	0.46/-0.34

Table 3.5 Summary of X-ray crystallographic data collection of ^{Me}P4 and ^{Pr}T4 (100 K, kad1ix).

Identification code	raj29m4 (^{Me}P4)	kad1ix (^{Pr}T4)
Empirical formula	$C_{40}H_{48}O_{12}$	$C_{56}H_{80}O_8$
Formula weight	720.78	881.20
Temperature/K	100.15	99.8(4)
Crystal system	Triclinic	triclinic
Space group	P-1	P-1
a/Å	9.16095(18)	12.9716(3)
b/Å	17.9495(3)	13.0379(3)
c/Å	22.5941(3)	14.9706(3)
α/°	103.8575(14)	95.6026(16)
β/°	95.1560(14)	92.8626(16)
γ/°	97.6996(15)	94.0129(16)
Volume/Å^3	3545.76(11)	2509.49(9)
Z	4	2
ρ_{calc}g/cm^3	1.350	1.166
μ/mm^{-1}	0.821	0.599
F(000)	1536.0	960.0
Crystal size/mm^3	0.358 × 0.254 × 0.166	0.332 × 0.233 × 0.093
Radiation	CuKα (λ = 1.54184)	CuKα (λ = 1.54184)
2Θ range for data collection/°	9.822 to 141.334	6.832 to 141.226
Index ranges	-11≤ h≤ 11, -21 ≤k≤ 21, -27≤ l≤ 27	-15 ≤ h≤ 15, -15≤k≤15, -18≤ l≤ 18
Reflections collected	60090	45942
Independent reflections	13284[R_{int}=0.0924, R_{sigma}=0.0449]	9537[R_{int}=0.0262,R_{sigma}=0.0171]
Data/restraints/parameters	13284/0/961	9537/0/589
Goodness-of-fit on F^2	1.030	1.037
Final R indexes [I>=2σ(I)]	R_1 = 0.0884, wR_2 = 0.2378	R_1 = 0.0359, wR_2 = 0.0935
Final R indexes [all data]	R_1 = 0.0942, wR_2 = 0.2457	R_1 = 0.0411, wR_2 = 0.0981
Largest diff. peak/hole / e Å^{-3}	1.03/-0.53	0.45/-0.24

Table 3.6 Summary of X-ray crystallographic data collection of ^{Pr}T4 (250 K, kad1j) and ^{Pr}T4 (210 K, kad1i).

Identification code	kad1j (^{Pr}T4)	kad1i (^{Pr}T4)
Empirical formula	$C_{56}H_{80}O_8$	$C_{56}H_{80}O_8$
Formula weight	881.20	881.20
Temperature/K	250.00(14)	210.05(10)
Crystal system	triclinic	triclinic
Space group	P-1	P-1
a/Å	12.6612(4)	13.0566(3)
b/Å	14.1198(3)	13.1211(3)
c/Å	15.7544(4)	15.1852(3)
α/°	104.714(2)	92.7541(18)
β/°	96.728(2)	96.9186(18)
γ/°	99.499(2)	94.0236(18)
Volume/Å^3	2649.12(12)	2571.97(10)
Z	2	2
ρ_{calc}g/cm^3	1.105	1.138
μ/mm^{-1}	0.568	0.585
F(000)	960.0	960.0
Crystal size/mm^3	0.463 × 0.398 × 0.177	0.372 × 0.238 × 0.093
Radiation	CuKα (λ = 1.54184)	CuKα (λ = 1.54184)
2Θ range for data collection/°	7.18 to 141.192	6.84 to 141.194
Index ranges	-15≤h≤15, -17≤ k≤17, -19≤ l≤17	-15≤h≤15, -16≤ k≤ 15, -18≤l≤18
Reflections collected	48412	46925
Independent reflections	10031[R_{int}=0.0194, R_{sigma}=0.0116]	9768 [R_{int}=0.0241, R_{sigma}=0.0143]
Data/restraints/parameters	10031/6/636	9768/139/692
Goodness-of-fit on F^2	1.065	1.044
Final R indexes [I>=2σ(I)]	R_1 = 0.0748, wR_2 = 0.2460	R_1 = 0.0581, wR_2 = 0.1717
Final R indexes [all daa]	R_1 = 0.0844, wR_2 = 0.2636	R_1 = 0.0666, wR_2 = 0.1837
Largest diff. peak/hole / e Å^{-3}	0.40/-0.22	0.57/-0.35

Chapter 4

PARA (1,4) METHYLENE-BRIDGED MACROCYCLIC ARENES: HIGHLY SELECTIVE SYNTHESIS OF PILLAR[*n*]ARENE (*n* = 5, 6)

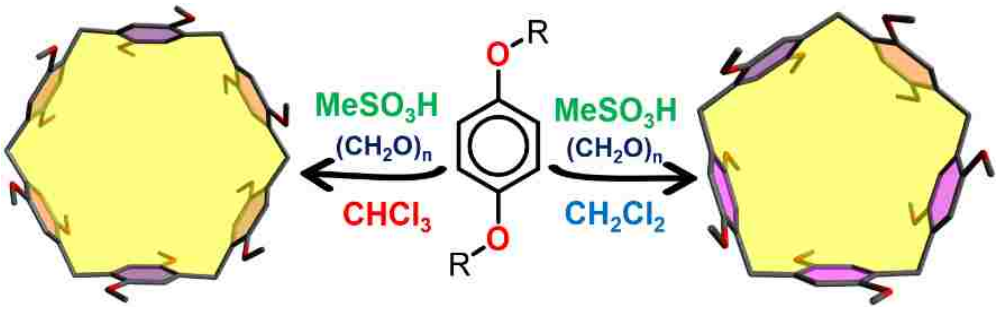

An efficient and highly selective synthetic method toward the preparation of pillar[n]arenes (n=5, 6) is reported, based upon a high solvent-dependent selectivity found in the condensation reaction between 1,4-dialkyloxybenzene and paraformaldehyde, involving methanesulfonic acid as catalyst. Pillar[6]arene (P6) is obtained as the major product when using chloroform as solvent, while in dichloromethane pillar[5]arene (P5) is the dominant product. Accordingly, a series of P5 and P6 have been selectively synthesized with excellent yield.

Introduction: In recent years, Ogoshi et al. and Cao et al. have discovered a novel supramolecular family,[65,170] pillar[n]arene, with a tubular and rigid macrocyclic structure, which has been applied in molecular recognition, asymmetric synthesis and polymer materials.[171,172,181–188,173–180] The development of pillar[n]arene (n=5-15) with different cavity sizes has significantly extended this field, affording an expanded variety of host-guest interactions dependent on the size of the pillarene cavities.[68,189] Recently, Rathore and coworkers have found that the cation radical of dimethoxy-pillar[5]arene can self-assemble in two-dimensional (2–D) arrays while maintaining both intra- and intermolecular electronic coupling (**Figure 4.1**), suggesting that pillarenes are a promising material toward achieving long-range charge transfer.[190] In this work, we thus focus on pillar[n]arene (n=5,6). Compared with pillar[5]arene, pillar[6]arene has a more symmetrical structure, hexagonal, which more easily leads to self-assembly and the formation of 2–D structures with long-distance charge transfer properties. However, selective synthesis of pillar[n]arenes is usually difficult, because the formation of these macrocycles occurs through a kinetically controlled cyclization process. Therefore, it is desirable to develop a more efficient synthetic method for the preparation of specific pillar[n]arenes, such as a pillar[6]arene.

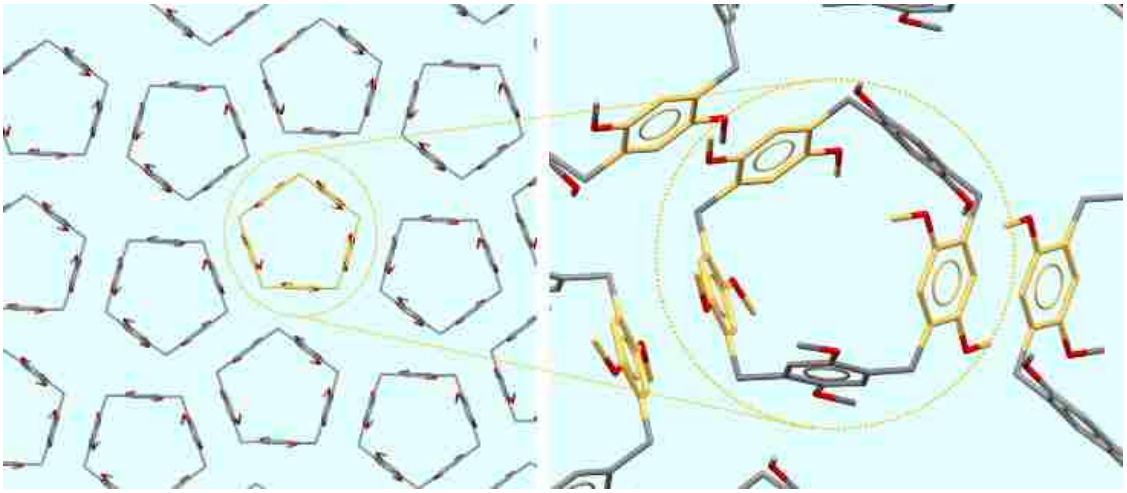

Figure 4.1 Two-dimensional arrangement of pillarene molecules in [$^{Me}P5^{1.5+}(SbCl_6)_{1.5}$, left] and a close-up view of three intermolecular dimeric contacts ~3.3 Å of phenyl rings (right).[190]

The pillar[6]arene was firstly synthesized by Cao and coworker at 2009.[1] In the literature, two primary methods to synthesize pillar[6]arene (P6) have been reported. The first involves the direct synthesis of P6 from 1,4-dialkyloxybenzene and paraformaldehyde using a Lewis/Bronsted acid as catalyst.[191,192] However, the yield of P6 by this method usually does not exceed 40%, and thermodynamically stable P5 is the major product. Several research groups studied the effects of solvents, catalysts, and additives on the efficiency of P6 synthesis using this approach.[191–194] An alternative method involves self-condensation of the intermediate 2,5-alkoxybenzyl alcohol or bis(alkoxymethyl)-1,4-dialkoxybenzene using a Lewis/Bronsted acid as catalyst.[170,194] The synthesis of these intermediates usually requires multiple steps, which make this method time-consuming and afford low overall yield.[195] In order to overcome these mentioned drawbacks, recently, templated reactions have begun to be widely considered in the synthesis of P6. For example, Fabris, Scarso and coworkers reported the synthesis

of P6 using the cation template,[196] while Ogoshi and coworker reported the use of chlorocyclohexane as solvent template to afford highly selective synthesis of P6.[69] However, this method is limited due to solubility issues, i.e., simple chain-like substitute P6 cannot be produced in this condition with high yield and selectivity. Therefore, the synthesis of more applicable chain-linked P6 with higher yield and selectivity is an ongoing goal.

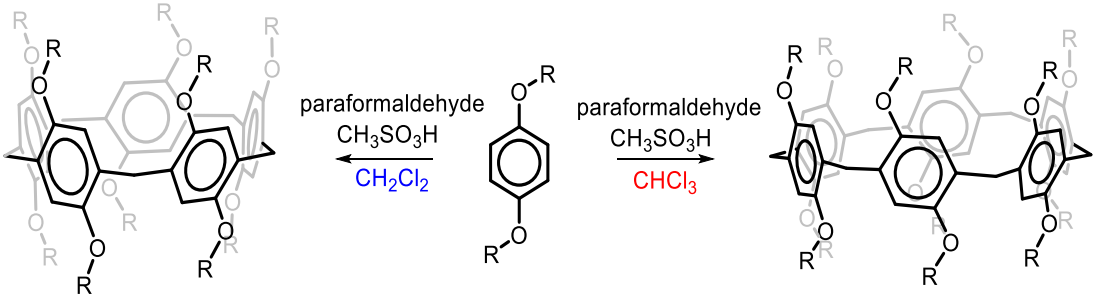

Figure 4.2 Solvent dependent synthesis of P5 and P6 involving CH_3SO_3H as catalyst.

More recently, our group has demonstrated that methanesulfonic acid is an efficient catalyst for preparation of macrocycle molecules.[29] Accordingly, a series of macrocyclic molecules (e.g., cyclotriveratrylene (CTV), cyclotetraveratrylene (CTTV) and dodecamethoxycalix[4]arene) have been generated with high yield. Motivated by these results, we explored whether methanesulfonic acid can serve as an efficient catalyst to improve the yield/selectivity of pillarene synthesis.

To address those question, herein, we report the using of methanesulfonic acid as a catalyst for solvent-dependent synthesis of P5 and P6 (**Figure 4.2**). Products P6 and P5 can be selectively obtained by applying chloroform and dichloromethane as the solvent,

respectively. It should be noted that the yield and selectivity of P6 are remarkable in comparison with previous reports. Using this method, we have successfully synthesized gram-scale quantities of both compounds. Furthermore, the binding energy between solvent molecules (dichloromethane or chloroform) as guest and host P5/P6 were calculated using DFT methods. The results reveal that dichloromethane and chloroform are suitable template for the selective synthesis of P5 and P6, respectively. The details of these findings are discussed herein.

Computational details: All of the calculations were carried out using the Gaussian 09 software package.[102] Two B3LYP and PBE0 functionals of density functional theory (DFT) have been used for all optimizations and frequency calculations.[152,197] In order to include the dispersion effects for both functionals, the empirical dispersion factors of Grimme and co-workers (D3) are employed.[198] The 6-31G* basis set has been used for full optimizations and frequency calculations. Also, in order to have more accurate evaluation of complexation free energies, the higher basis set 6-31+G(d,p) has been used for single point calculations. The implicit solvation effects (CH_2Cl_2) have been considered employing the polarizable continuum model (PCM) using the default radii (UFF) in all single point calculations (**Figure 4.6** in the Experimental section).[111] Moreover, the complexation energies of P6 has been calculated with M06-D3 functional which indicated same trend for CH_2Cl_2 (-1.2 kcal.mol^{-1}) and $CHCl_3$ (-3.1 kcal.mol^{-1}).[151]

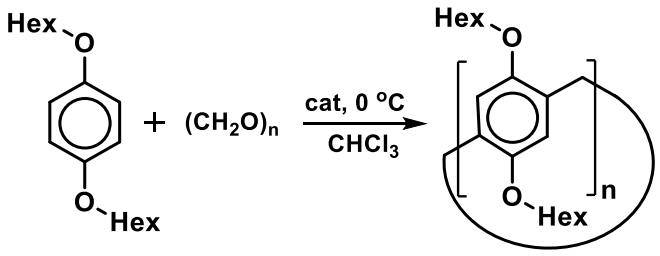

Scheme 4.1 The condensation-cyclization of 1,4-dihexoxybenzene with paraformaldehyde using different catalysts.

Results and discussion: At first, a variety of candidate catalysts including various Bronsted and Lewis acids were screened for the condensation-cyclization reaction between 1,4-dihexoxybenzene and paraformaldehyde under the same condition (**Scheme 4.1**). All of the reactions were carried out under an Argon atmosphere in $CHCl_3$ solvent at 0 °C; after stirring for 2 hours, the reaction mixture was quenched by adding 10% sodium carbonate solution. The results are summarized in **Table 4.1**.

We investigated three Lewis acid catalysts (entries 1-3). Among them, BF_3•Et_2O indicated the lowest selectivity which agrees with the previous data.[65,192] While $FeCl_3$ as catalyst can only achieve 32% and 19% yields for ^{Hex}P6 and ^{Hex}P5, respectively.[192] The major product of ^{Hex}P5 was obtained in $AlCl_3$ as catalyst with 43% yield. Entries 4-9 in **Table 4.1** summarize the results of several Bronsted acids as catalyst. The weak acids, such as acetic acid (CH_3COOH) and phosphoric acid (H_3PO_4), did not show any ability to catalyze the reaction, and the starting material (1,4-dihexoxybenzene) was fully recovered. The trifluoroacetic acid catalyst generated P5 with 15% yield under reflux condition,[67] however, neither ^{Hex}P5 nor ^{Hex}P6 was observed under our experiment condition at 0 °C, which indicates a high temperature sensitivity (described further in the

following section, see **Table 4.2**). However, both sulfuric acid (H_2SO_4) and methanesulfonic acid ($MeSO_3H$) exhibited good catalytic effects for selective synthesis of ^{Hex}P6. The methanesulfonic acid showed the best yield and selectivity with 80% of ^{Hex}P6 and 5% of ^{Hex}P5. The more powerful and more expensive candidate (trifluoromethanesulfonic acid, TfOH) displayed lower yield and selectivity than methanesulfonic acid. Comparing these series of experiments, methanesulfonic acid showed the best catalyzing capability toward the synthesis of ^{Hex}P6.

Table 4.1 The catalyst screen in the synthesis of ^{Hex}P5 and ^{Hex}P6.

Entry	cat.	%yield	
		^{Hex}P5	^{Hex}P6
1	BF_3•Et_2O	23 (20)	18 (15)[a]
2	$FeCl_3$	19 (28)	32 (45)[b]
3	$AlCl_3$	43	15
4	CH_3COOH	0	0
5	H_3PO_4	0	0
6	CF_3CO_2H	0 (15)[c]	0
7	H_2SO_4	7	48
8	$MeSO_3H$	5	80
9	TfOH	8	63
10	none	0	0

a. rt, R = Et, 20 min, Ref. 68; b. rt, 3 h, Ref. 192; c. R = Me, reflux, 2 h, Ref. 67.

To further optimize the reaction conditions, several other factors including the amount of catalyst, reaction temperature, reaction time, and solvent effect were examined. The results are listed in **Table 4.2**. Entries 1-4 illustrate the temperature effect

on the reaction. At low temperature (e.g. -10 °C) the reaction happens slowly, while excellent catalytic effect is observed at 0-20 °C, with the highest yield at 20 °C. At higher temperatures (e.g. 40 °C), a large amount of insoluble polymerized product was obtained (see entry 4). These results are in contrast with the results of the trifluoracetic acid, which needs high temperature (refluxing) to accomplish the reaction (see **Table 4.1** and Ref. 34). The effect of the amount of catalyst is shown in entries 5-7 in **Table 4.2**. An Excess amount of catalyst is preferred in this reaction, while only negligible product was detected with less than 1.0 eq. of catalyst. Entries 8-11, where reaction time was varied, indicate that the reaction was completed in 2 hours, and increasing the time up to 24 hours did not affect the yield and selectivity dramatically.

As aforementioned, solvent can play an important role in the synthesis of pillarene. Therefore, several different solvents are studied and the results are listed in entries 12-17 of **Table 4.2**. We found that toluene and acetonitrile lead to poor selectivity and low yield. However, high selectivity of ^{Hex}P6 can be obtained in chlorocyclohexane (ClCy, yield 56%) and chloroform ($CHCl_3$, yield 83%) solvents. On the other hand, ^{Hex}P5 as major product was observed in 1,2-dichloroethane (DCE yield 64%) and dichloromethane (DCM yield 71%). While the selectivity of the reaction was significantly reduced in the 1:1 mixture of CH_2Cl_2/$CHCl_3$, the overall yield remained high (~73%, entry 17).

Table 4.2 Temperature, reaction time and solvent effects on the yield and selectivity for ^{Hex}P5 and ^{Hex}P6 synthesis.

entry	solvent	temp (°C)	cat. (equiv)	time (h)	%yield	
					^{Hex}P5	^{Hex}P6
1	$CHCl_3$	-10	3.0	2	0	0
2	$CHCl_3$	0	3.0	2	5	80
3	$CHCl_3$	20	3.0	2	6	83
4	$CHCl_3$	40	3.0	2	ND[a]	ND[a]
5	$CHCl_3$	20	0.2	2	0	2
6	$CHCl_3$	20	0.5	2	0	5
7	$CHCl_3$	20	1.0	2	0	12
8	$CHCl_3$	20	3.0	10[b]	0	5
9	$CHCl_3$	20	3.0	30[b]	0	35
10	$CHCl_3$	20	3.0	1	3	60
11	$CHCl_3$	20	3.0	24	6	79
12	DCM	20	3.0	2	71	8
13	DCE	20	3.0	2	64	13(trace)[c]
14	Toluene	20	3.0	2	23	15
15	MeCN	20	3.0	2	10	18
16	ClCy	20	3.0	2	4	56
17	CH_2Cl_2/ $CHCl_3$[d]	20	3.0	2	46	27

a. Product not determined; b. in minutes; c. H_2SO_4, rt, R = Et, Ref. 193; d. ratio of volume = 1:1.

Based upon the results presented above, the reaction can be accomplished within two hours by employing large excess (3 equiv) of methanesulfonic acid at 20 °C (optimized condition). More importantly, the selectivity can be easily controlled by involving different solvent, dichloromethane for P5 and chloroform for P6. Based on this novel method, we extended the substrate with different length of alkoxy substituent

benzene as a starting material (ethoxy, propoxy, n-butyoxy, i-butyoxy and cyclohexylmethoxy). Accordingly, a series of P5 and P6 were synthesized straightforwardly and yields are listed in **Table 4.3**. It should be noted that substituted P6 were synthesized in 73-83% yields in the chloroform. Meanwhile, substituted P5 can be obtained by employing dichloromethane as solvent with relatively high yield 65-73%. All those P6 and P5 were characterized with ^{1}H- and ^{13}C-NMR, and MALDI-TOF mass spectroscopy techniques. Additionally, ^{Hex}P5 and ^{Cy}P5 structures were characterized with X-ray crystallography for the first time.

Table 4.3 Yields of P5 and P6 with different substitute (R) groups.

entry	R	%yield in $CHCl_3$		%yield in CH_2Cl_2	
		P5	P6	P5	P6
1	Ethyl	8	73	65	14
2	n-Propyl	6	76	72	8
3	n-Butyl	5	82	71	10
4	iso-Butyl	4	80	67	7
5	Hexyl	6	83	71	8
6	CH_2Cy	3	78	73	11

Crystals of ^{Hex}P5 and ^{Cy}P5 were grown separately by slow evaporation of a solution of P5 in a dichloromethane/acetonitrile mixture. As shown in **Figure 4.3**, both ^{Hex}P5 and ^{Cy}P5 crystals represents a pentagonal-cylindrical geometry and a racemic mixture of the enantiomers. As illustrated in **Figure 4.3A**, most of n-hexyl groups of ^{Hex}P5 have a staggered extended conformation, few of them are bent and close the openings of the cylinder. The guest molecules (e.g. solvents) can form C-H...π and

hydrogen-bond interactions with the host P5 molecule (**Figure 4.5** in the Experimental section). The crystal has some π-π overlapping in the layers with average distance ~4.3 Å.[199] However, the contacts between the layers are exclusively of van-der-Waals nature. **Figure 4.3B** represents the structure of ^{Cy}P5, the most distinct feature is the bulky cyclohexylmethyl group prevent the formation of π-π interaction between two ^{cy}P5 molecules. The closest distance between phenyl ether rings is 8.8 Å. The average distance between two phenyl rings is ~9.6 Å. It should be noted that in both crystals, two solvent molecules are trapped inside the cavity (**Figure 4.5** in the Experimental section).

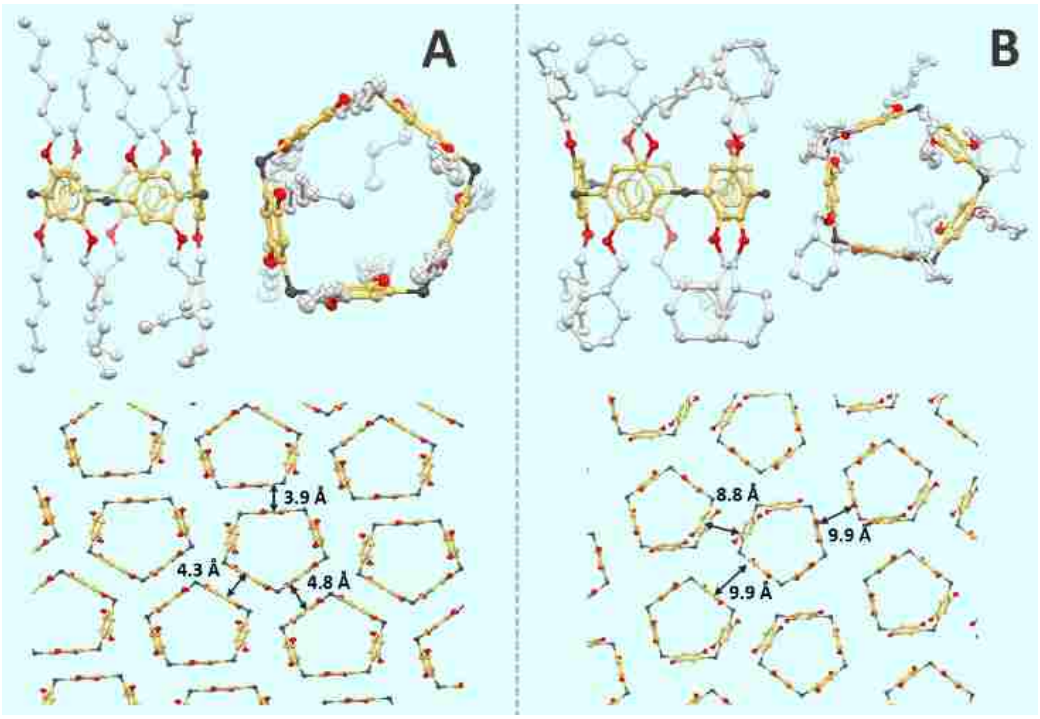

Figure 4.3 Side-view, top-view and packing of the crystal structures of ^{Hex}P5 (A), ^{Cy}P5 (B). Hydrogens and solvent molecules were omitted for clarity; oxygen atoms are red, phenyl rings are gold, alky group are bright gray and bridge carbon are dark gray; all alkyl group are omitted in the packing mode.

To obtain further insight about the interaction of solvent molecules with P5 or P6, the complexation energies between guest molecules, dichloromethane and chloroform, and host pillar[n]arene (5 and 6) were simulated using DFT method (B3LYP-D3/6-31+G(d,p)/PCM(CH_2Cl_2)//B3LYP-D3/6-31G*). The calculations revealed a stronger interaction of dichloromethane with P5 (complexation free energy -5.1 kcal.mol^{-1}) in comparison to chloroform (-1.7 kcal.mol^{-1}). Meanwhile, the binding energy of chloroform with P6 is -4.0 kcal mol^{-1}, which indicating a better interaction than dichloromethane as guest (binding energy of -0.9 kcal mol^{-1}). Therefore, the templating effect of $CH_2Cl/CHCl_3$ for selective synthesis of P5/P6 can be attributed to the stronger complexation with these solvents. Moreover, as depicted in **Figure 4.4**, the geometrical orientation of $CHCl_3$ inside the hexagonal structure of P6 can be another factor in controlling the selectivity. Calculations using a PBE0-D3 functional showed the same trend as the B3LYP-D3 calculations (**Figure 4.6** in the Experimental section).

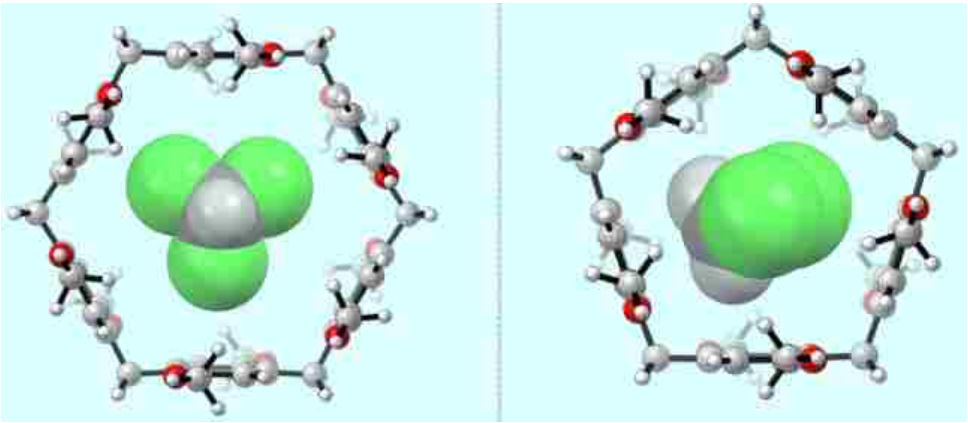

Figure 4.4 Top views of the optimized complexation structures of P6⊃$CHCl_3$ (left) and P5⊃CH_2Cl_2 (right).

Conclusion: In summary, an efficient and highly selective synthetic method with the aim of improving the efficiency and selectivity of pillar[n]arene (n=5,6) has been developed. By involving methanesulfonic acid as catalyst, the condensation reaction between 1,4-dialkyloxybenzene and paraformaldehyde displayed high solvent-dependency. Pillar[5]arene (P5) is major product in dichloromethane, while in chloroform pillar[6]arene (P6) is the dominant product. Accordingly, a series of P5 and P6 have been selectively synthesized with high yield. Furthermore, with the aid of DFT calculations, the solvent template effect can be rationalized. This method can thus significantly improve the synthesis efficiency of P6. The results of this study can promote and facilitate the applicability of pillar[6]arene in organic functional materials and polymer materials.

Experimental

General methods and synthesis

All reactions were performed under argon atmosphere unless otherwise noted. All commercial reagents were used without further purification unless otherwise noted. All solvents, including dichloromethane and chloroform, were used without any further purification. NMR spectra were recorded on Varian 300 and 400 MHz NMR spectrometers. Mass spectra were recorded on Bruker Daltonics MALDI-TOF mass spectrometer. The 1,4 dialkyl benzene (alkyl = Ethyl, Propyl, n-Butyl, iso-Butyl, cyclohexylmethyl, Hexyl) were synthesized using the Hydroquinone and alkyl bromide according to the previously reported methods.[196] The product (white solid) has been

purified using the flash column using pure hexanes. The purity of the product has been confirmed using the ^{1}H-NMR and ^{13}C-NMR (see the NMR section).

Synthesis:

In order to have better understanding about the effects of the reaction concentration on the selectivity and yield, the reaction of 1,4-dihexoxybenzene and paraformaldehyde were carried out under the same condition (room temperature and 2 h) using different amount of $CHCl_3$. As listed in the Table S1, the 40 mL of $CHCl_3$ showed the best results and increasing the amount of solvent will not alter the selectivity and yield of the reaction significantly. Decreasing this amount to 20 mL can decrease the selectivity of the reaction. Also, using 10 mL $CHCl_3$ generated polymerized compound. Therefore, all condensation reactions were carried out using 40 mL of solvent.

Table 4.4 The effects of solvent amount ($CHCl_3$) on the selectivity and yield of the condensation reaction of 1,4-dihexoxybenzene and paraformaldehyde using $MeSO_3H$ as catalyst.

amount of $CHCl_3$ (mL)	%yield $^{Hex}P5$	$^{Hex}P6$
10	ND	ND
20	67	15
40	83	6
50	81	7

Moreover, to examine the applicability of this synthetic method for large scale synthesis of pillar[n]arene (n = 5, 6), the reactions repeated with 10 g scale (36 mmol) of 1,4-dihexoxybenzene and paraformaldehyde (2.1 g, 72 mmol, 2.0 equiv) under the same condition (room temperature, 2 h and solvent = 350 mL). As illustrated in the Table S2,

the results indicate that this method is reliable for large scale synthesis of P5 and P6 selectively.

Table 4.5 Large scale condensation of 1,4-dihexoxybenzene (10 g) and paraformaldehyde.

solvent	cat.	%yield	
		^{Hex}P5	^{Hex}P6
$CHCl_3$	$MeSO_3H$	7	78
DCM	$MeSO_3H$	68	10

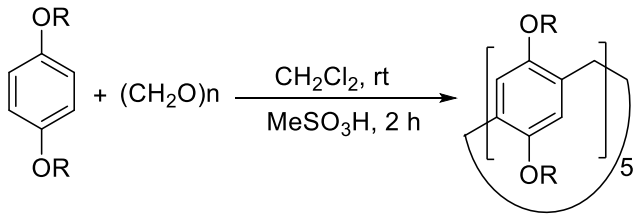

Pillar[5]arene synthesis: To a solution of 1,4-dialkyloxy benzene (5 mmol, R = Ethyl, Propyl, n-Butyl, i-Butyl, Hexyl and Cyclohexylmethyl) in dichloromethane (DCM, 40 mL), paraformaldehyde was added (0.3 g, 10 mmol, 2.0 equiv) under the Argon atmosphere. Then, the methanesulfonic acid (1 mL, 15 mmol, 3.0 equiv) was added at one portion. The mixture was stirred at the room temperature for 2 h. The reaction has been quenched by adding water to the Schlenk flask. The acid has been neutralized using sodium carbonate solution. The organic layer has been separated using the separation funnel. The dichloromethane has been evaporated under the vacuum. The pure product has been purified using the flash column (Hexane/Ethyl acetate = 100/3, yield = 75-85%).

$^{Et}P5^{200}$: mass 0.56 g, yield 65%; melting point (white solid): 156-158 °C; MALDI Mass (calculated: 890.50; experimental: 890.74); ^{1}H-NMR (CDCl3 at 20 °C) δ: 1.28 (t, 30H), 3.76 (s, 10H), 3.84 (q, 20H), 6.74 (s, 10H); ^{13}C-NMR (CDCl3 at 20 °C) δ: 15.30, 29.75, 63.82, 114.85, 128.65, 149.77.

$^{Pr}P5^{200}$: mass 0.74 g, yield 72%; melting point (white solid): 114-116 °C; MALDI Mass (calculated: 1030.65; experimental: 1030.61); ^{1}H-NMR (CDCl3 at 20 °C) δ: 1.05 (t, 30H), 1.79 (sext, 20H), 3.79 (s, 10H), 3.83 (t, 20H), 6.85 (s, 10H); ^{13}C-NMR (CDCl3 at 20 °C) δ: 10.91, 23.16, 29.64, 70.0, 114.92, 128.45, 149.85.

$^{i\text{-}Bu}P5^{194}$: mass 0.78 g, yield 67%; melting point (white solid): 144-146 °C; MALDI Mass (calculated: 1170.81; experimental: 1170.01); ^{1}H-NMR (CDCl3 at 20 °C) δ: 1.05 (t, 60H), 2.09 (sep, 10H), 3.50 (t, 10H), 3.74-3.79 (m, 20H) 6.84 (s, 10H); ^{13}C-NMR (CDCl3 at 20 °C) δ: 14.28, 19.64, 19.78, 22.76, 28.83, 29.51, 31.66, 115.03, 128.28, 149.95.

$^{n\text{-}Bu}P5^{200}$: mass 0.82 g, yield 71%; melting point (white solid): 133-135 °C; MALDI Mass (calculated: 1170.81; experimental: 1170.41); ^{1}H-NMR (CDCl3 at 20 °C) δ: 1.00 (t, 30H), 1.55 (sext, 20H), 1.81 (p, 20H), 3.77 (s, 10H), 3.88 (t, 20H), 6.87 (s, 10H); ^{13}C-NMR (CDCl3 at 20 °C) δ: 14.21, 19.68, 29.47, 32.19, 68.06, 114.65, 128.39, 149.79.

$^{Hex}P5^{192}$: mass 1.02 g, yield 71%; melting point (white solid): 103-105 °C; MALDI Mass (calculated:1451.12; experimental:1449.99); ^{1}H-NMR (CDCl3 at 20 °C) δ: 0.90 (t, 30H), 1.32-1.38 (m, 40H), 1.48-1.58 (m, 20H), 1.76-1.86 (m, 20H), 3.75 (s, 10H),

3.85 (t, 20H), 6.84 (s, 10H); ^{13}C-NMR (CDCl3 at 20 °C) δ: 14.22, 22.79,26.20, 29.49, 30.07, 31.97, 68.49, 114.85, 128.34, 149.94.

^{Cy}P5[69]: mass 1.14 g, yield 73%; melting point (white solid): 240-242 °C; MALDI Mass (calculated:1571.12; experimental:1570.24); ^{1}H-NMR (CDCl3 at 20 °C) δ: 1.08-1.40 (m, 50H), 1.72-2.07 (m, 60H), 3.51 (t, 10H), 3.76, (s, 10H), 3.86 (q, 10H), 6.84 (s, 10H); ^{13}C-NMR (CDCl3 at 20 °C) δ: 26.27, 26.86, 29.26, 30.31, 30.62, 38.62, 74.12, 114.86, 128.30, 149.95.

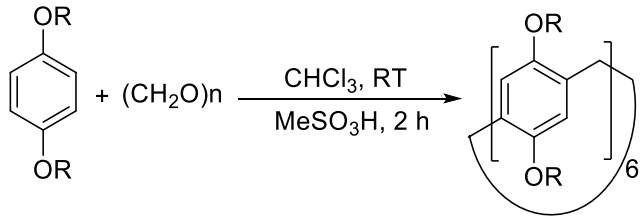

Pillar[6]arene synthesis. To a solution of 1,4-dialkyloxy benzene (5 mmol, R = Ethyl, Propyl, n-Butyl, i-Butyl, Hexyl and Cyclohexylmethyl) in chloroform ($CHCl_3$, 40 mL), paraformaldehyde (0.3 g, 10 mmol, 2.0 equiv) under the Argon atmosphere. Then, the methanesulfonic acid (1 mL, 15 mmol, 3.0 equiv) was added at one portion. The mixture was stirred at the room temperature for 2 h. The reaction has been quenched by adding water to the Schlenk flask. The acid has been neutralized using sodium carbonate solution. The organic layer has been separated using the separation funnel. The chloroform has been evaporated under the vacuum. The solid has been washed with acetone and ethyl acetate. For the 1,4-diethoxy benzene, the product has been further purified as described previously.[68] The pure products have been confirmed using the ^{1}HNMR, ^{13}CNMR and MALDI-TOF spectroscopy techniques (yield = 73-83%).

$^{Et}P6^{200}$: mass 0.65 g, yield 73%; melting point (white solid): 169-171 °C; MALDI Mass (calculated: 1068.60; experimental: 1068.04); ^{1}H-NMR (CDCl3 at 20 °C) δ: 1.29 (t, 36H), 3.81 (q, 36H), 6.70 (s, 12H); ^{13}C-NMR (CDCl3 at 20 °C) δ: 15.30, 29.87, 64.47, 115.07, 128.19, 150.76.

$^{Pr}P6^{200}$: mass 0.78 g, yield 76%; melting point (white solid): 120-122 °C; MALDI Mass (calculated: 1236.78; experimental: 1236.79); ^{1}H-NMR (CDCl3 at 20 °C) δ: 0.99 (t, 36H), 1.74 (sext, 24H), 3.79 (t, 24H), 3.92 (s, 12H), 6.69 (s, 12H); ^{13}C-NMR (CDCl3 at 20 °C) δ: 10.82, 23.05, 29.61, 70.52, 114.88, 128.17, 150.81.

$^{i\text{-}Bu}P6^{194}$: mass 0.93 g, yield 80%; melting point (white solid): 150-152 °C; MALDI Mass (calculated:1404.97; experimental:1403.86); ^{1}H-NMR (CDCl3 at 20 °C) δ: 0.96 (d, 72H), 2.02 (m, 12H), 3.85 (d, 24H), 3.90 (s, 12H), 6.67 (s, 12H); ^{13}C-NMR (CDCl3 at 20 °C) δ: 19.56, 28.68, 29.33, 75.38, 114.63, 128.12, 150.71.

$^{n\text{-}Bu}P6^{200}$: mass 0.96 g, yield 82%; melting point (white solid): 115-117 °C; MALDI Mass (calculated: 1404.97; experimental:1403.21); ^{1}H-NMR (CDCl3 at 20 °C) δ: 0.91 (t, 36H), 1.37-1.49 (m, 24H), 1.64-1.74 (m, 24H), 3.81 (t, 24H), 3.87 (s, 12H), 6.67 (s, 12H); ^{13}C-NMR (CDCl3 at 20 °C) δ: 14.06, 19.53, 29.62, 31.92, 68.66, 114.84, 128.18, 150.81.

$^{Hex}P6^{192}$: mass 1.20 g, yield 83%; melting point (white solid): 111-113 °C; MALDI Mass (calculated: 1741.35; experimental: 1739.94); ^{1}H-NMR (CDCl3 at 20 °C) δ: 0.87 (t, 36H), 1.28 (m, 48H), 1.39 (quin, 24H), 1.70 (p, 24H), 3.80 (t, 24H), 3.86 (s, 12H), 6.67 (s, 12H); ^{13}C-NMR (CDCl3 at 20 °C) δ: 14.20, 22.78, 26.05, 29.82, 31.87, 69.00, 114.83, 128.14, 150.82.

$^{Cy}P6^{69}$: mass 1.22 g, yield 78%; melting point (white solid): 190-192 °C; MALDI Mass (calculated:1885.35; experimental: 1883.36); ^{1}H-NMR (CDCl3 at 20 °C) δ: 0.85-1.30 (m, 60H), 1.63-1.83 (m, 72H), 3.61 (d, 24H), 3.87 (s, 12H); ^{13}C-NMR (CDCl3 at 20 °C) δ: 26.11, 26.76, 30.23, 38.25, 74.53, 114.65, 128.31, 150.72.

^{1}H- and ^{13}C-NMR spectra of P5, P6 and reactants.

^{1}H NMR spectrum of ^{Et}P5 at 20 °C in $CDCl_3$

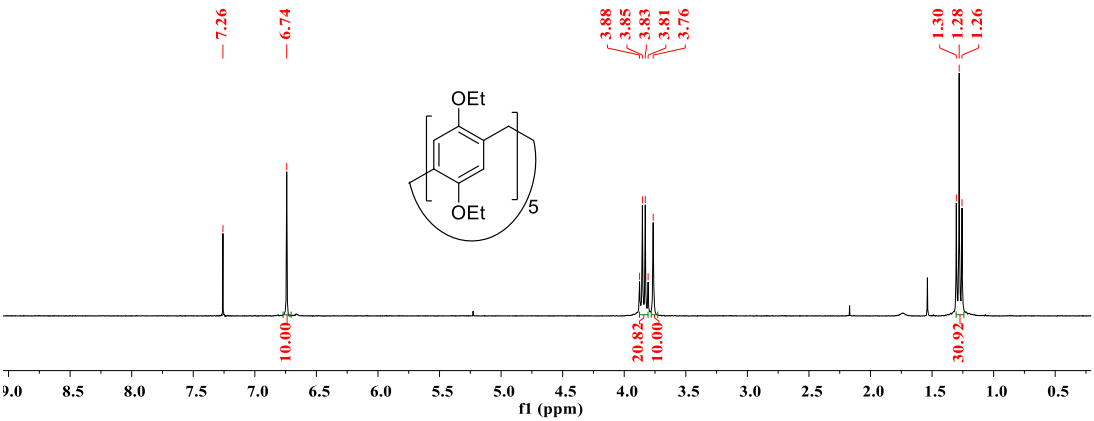

^{13}C NMR spectrum of ^{Et}P5at 20 °C in CDCl3

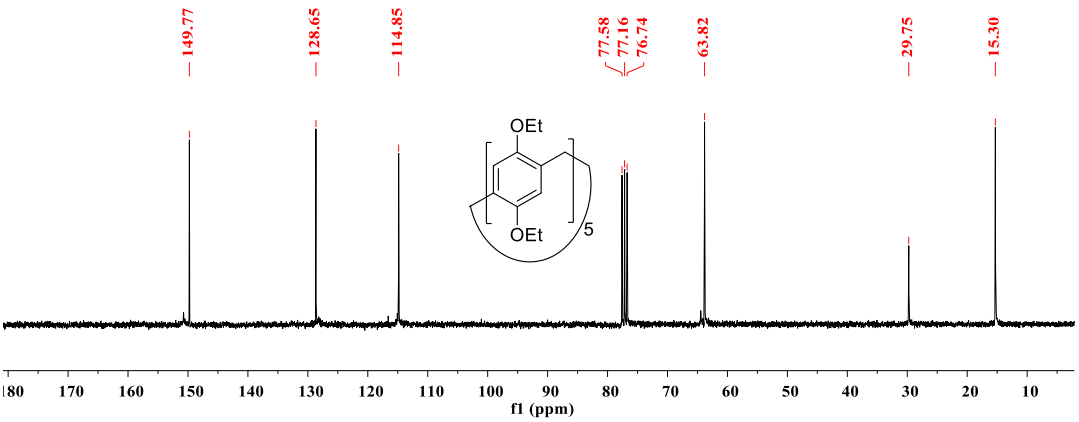

^{1}H NMR spectrum of ^{Pr}P5 at 20 °C in CDCl3

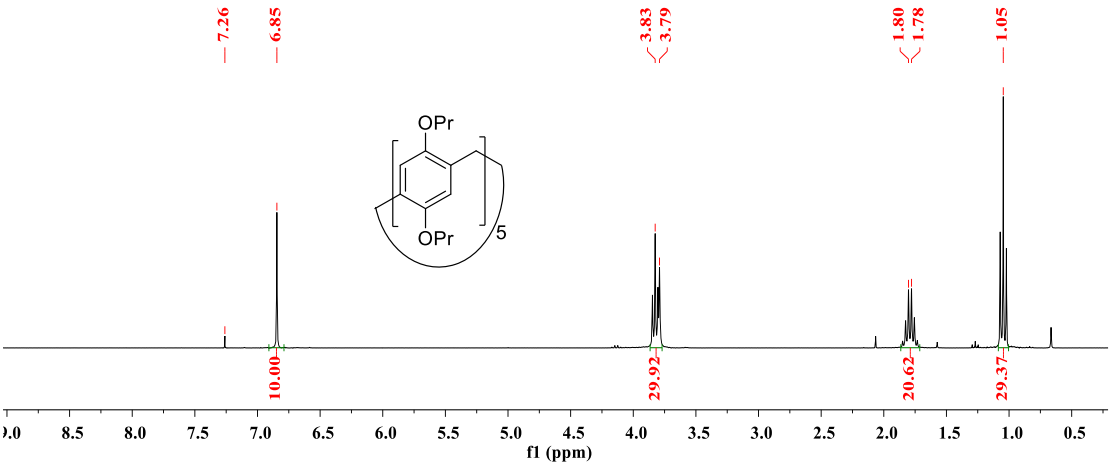

^{13}C NMR spectrum of ^{Pr}P5 at 20 °C in CDCl3

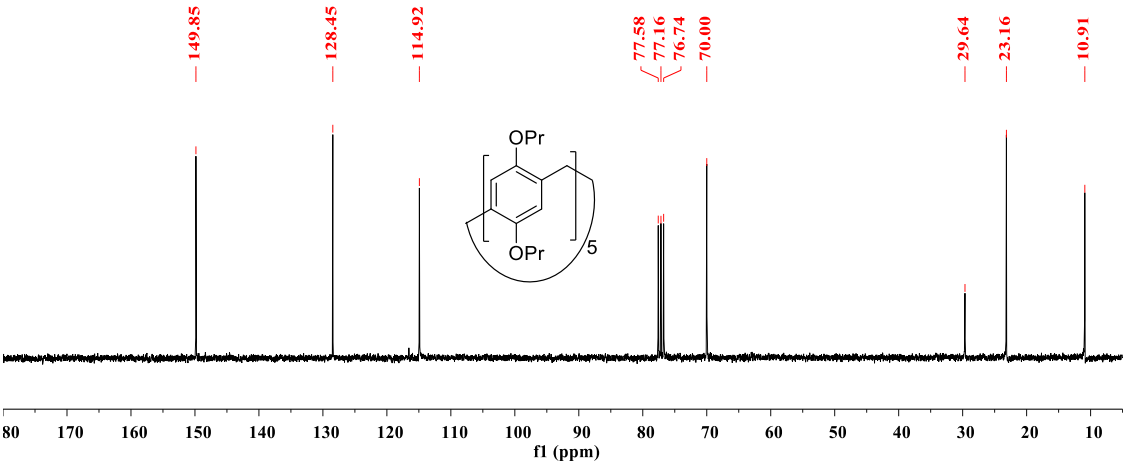

^{1}H NMR spectrum of $^{i\text{-Bu}}$P5 at 20 °C in CDCl3

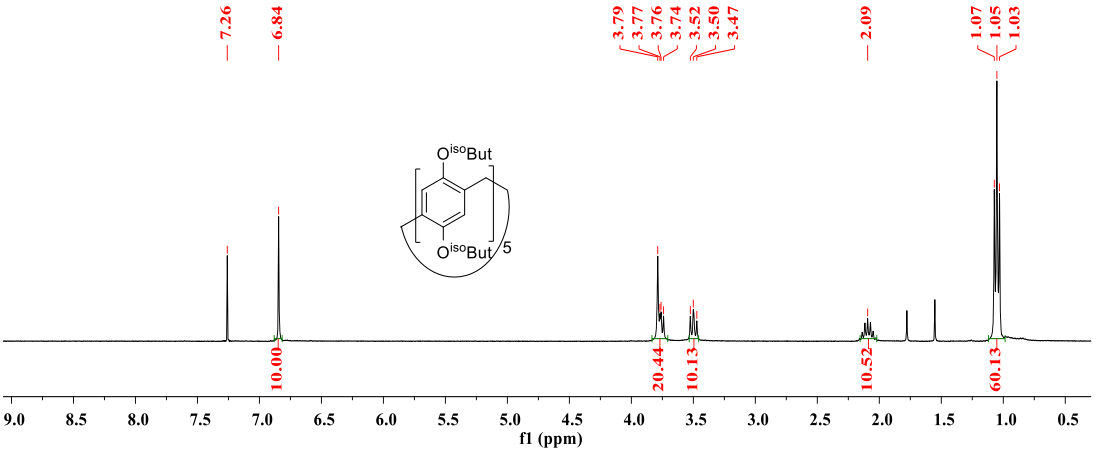

^{13}C NMR spectrum of $^{i\text{-Bu}}$P5 at 20 °C in CDCl3

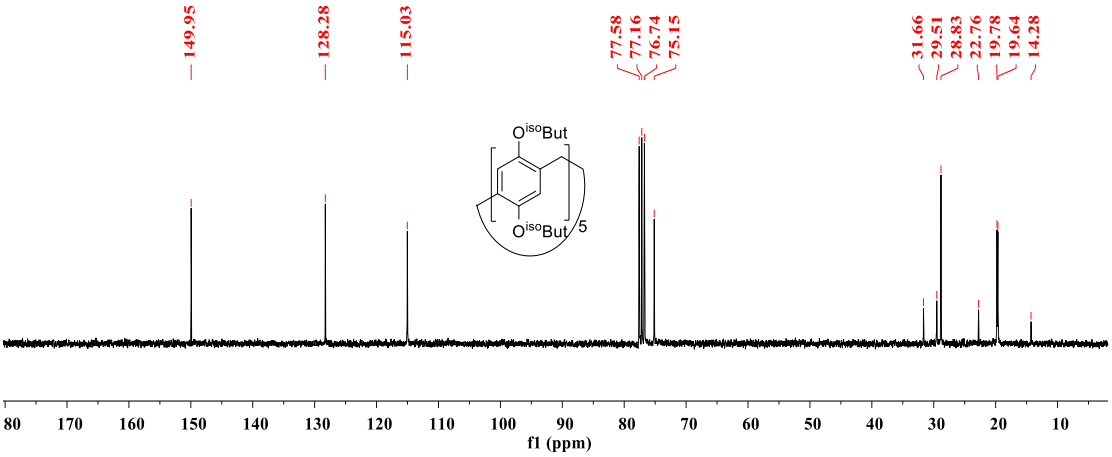

^{1}H NMR spectrum of $^{n\text{-}Bu}$P5 at 20 °C in CDCl3

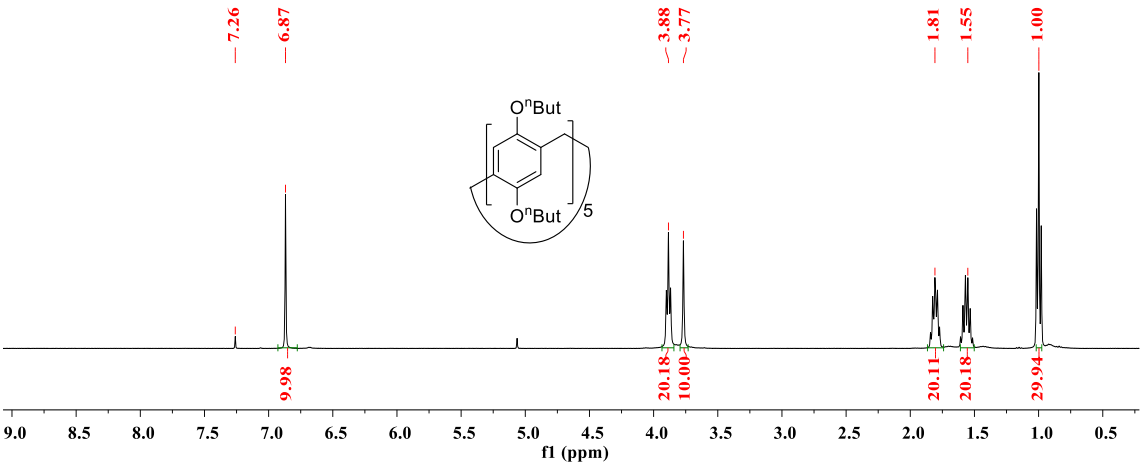

^{13}C NMR spectrum of $^{n\text{-}Bu}$P5 at 20 °C in CDCl3

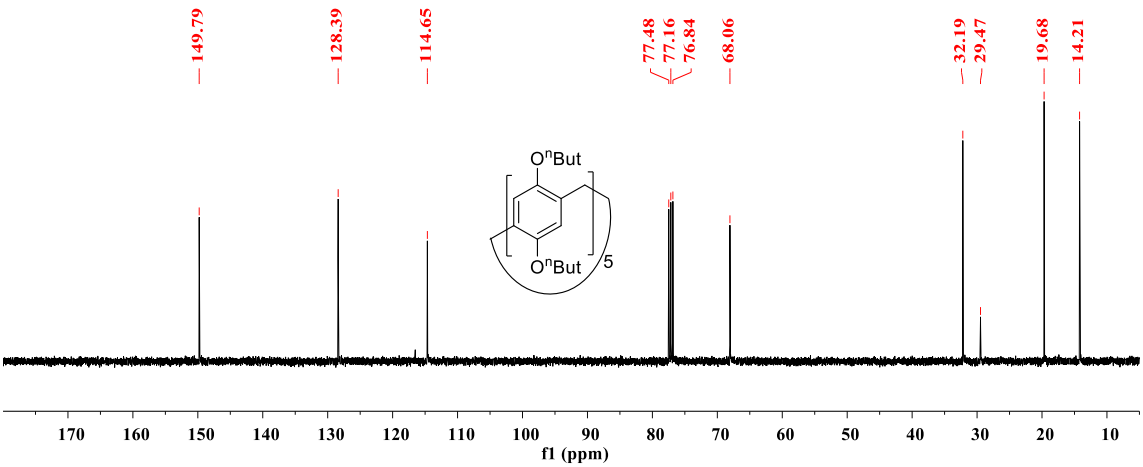

^{1}H NMR spectrum of ^{Cy}P5 at 20 °C in CDCl3

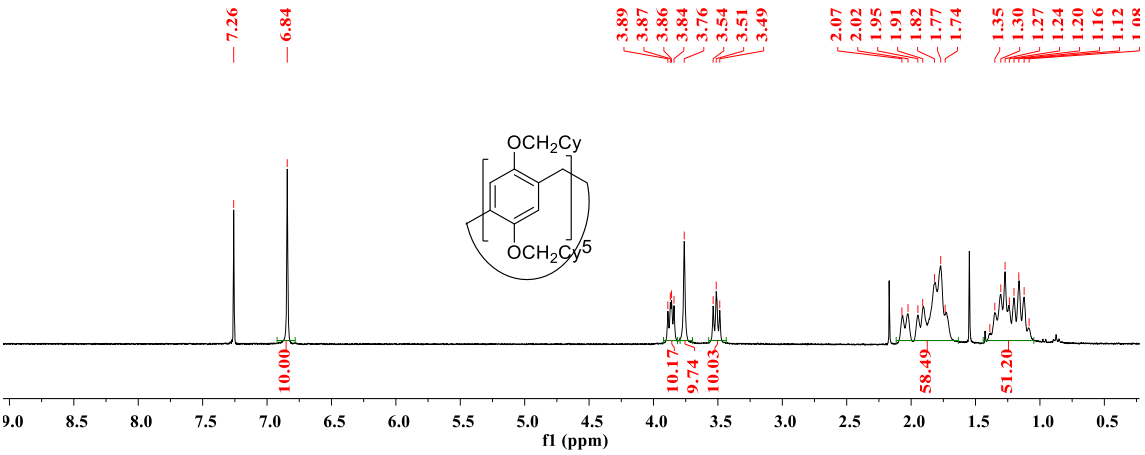

^{13}C NMR spectrum of ^{Cy}P5 at 20 °C in CDCl3

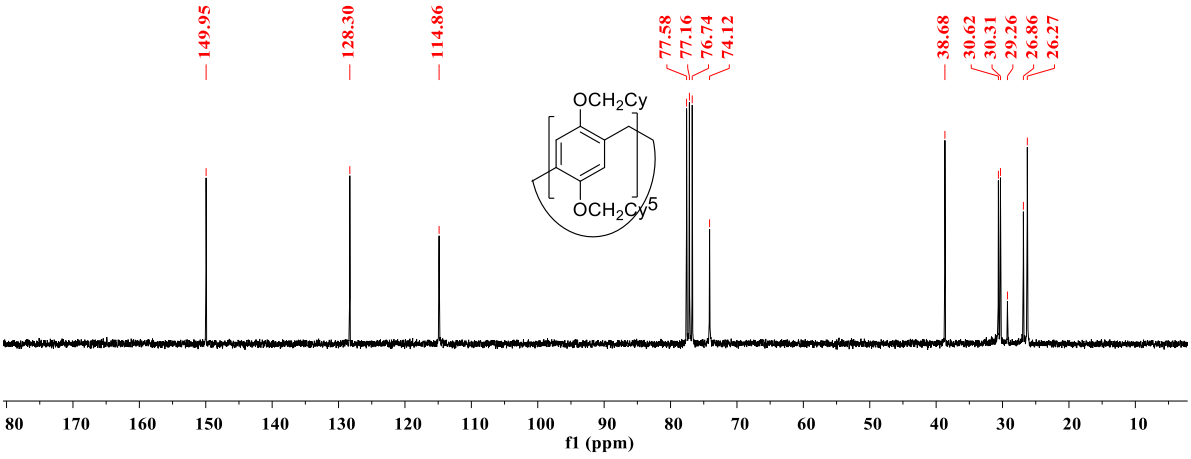

^{1}H NMR spectrum of ^{Hex}P5 at 20 °C in CDCl3

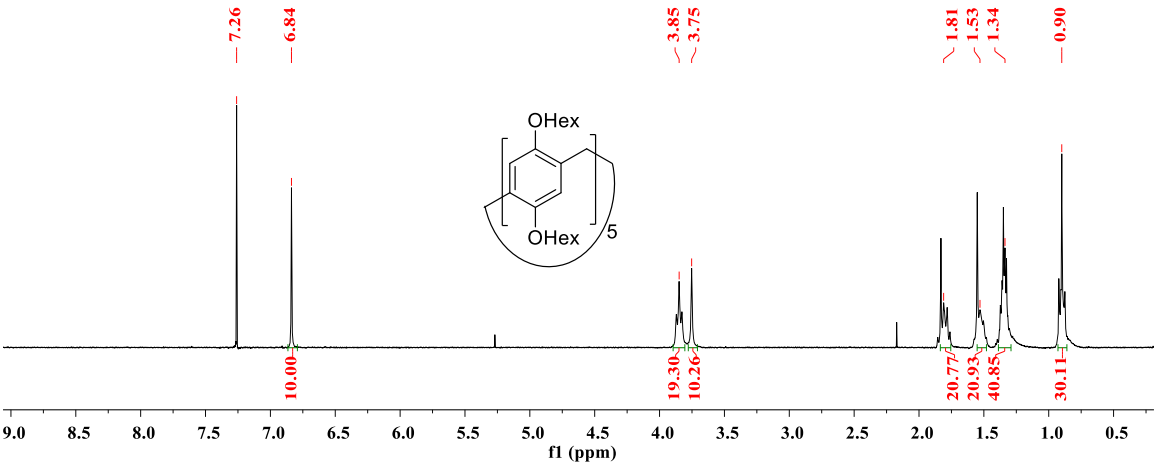

^{13}C NMR spectrum of ^{Hex}P5 at 20 °C in CDCl3

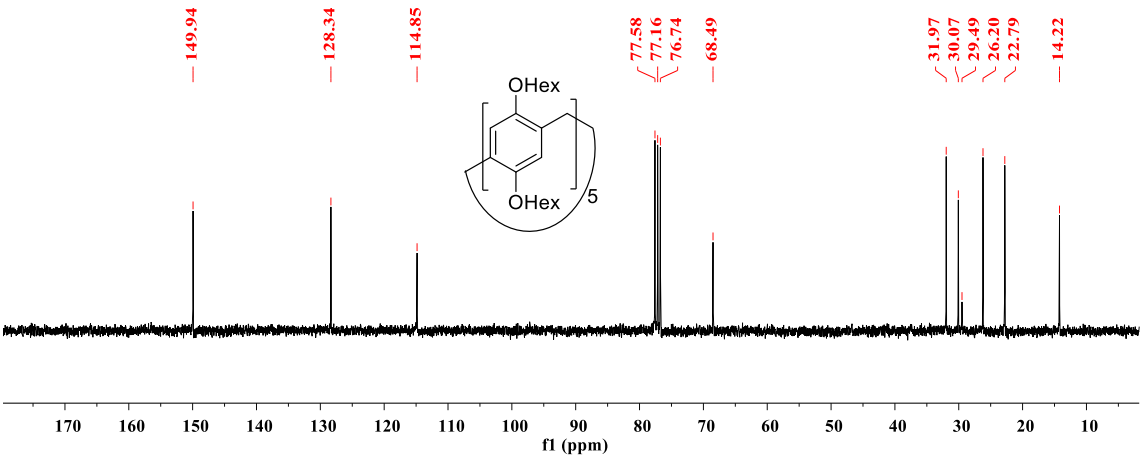

^{1}H NMR spectrum of ^{Et}P6 at 20 °C in CDCl3

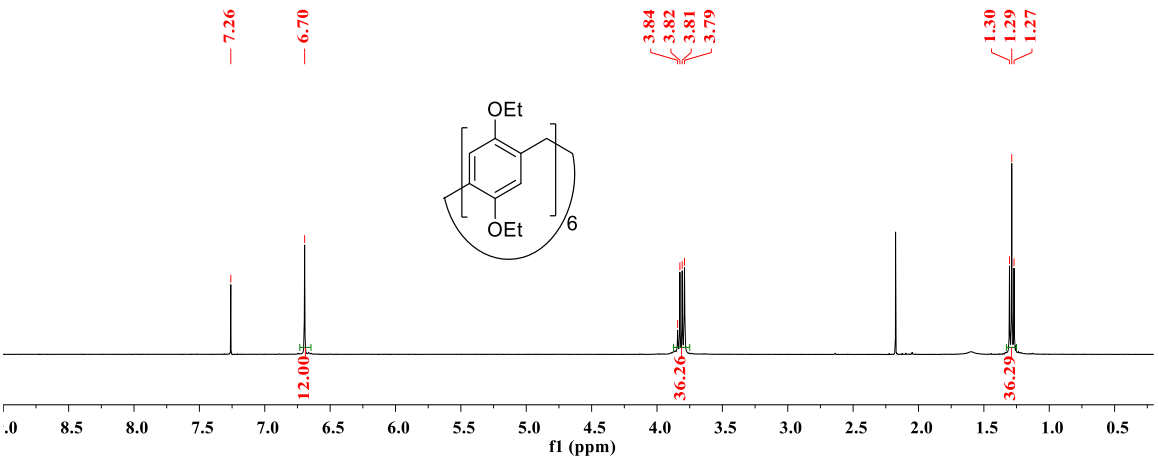

^{13}C NMR spectrum of ^{Et}P6 at 20 °C in CDCl3

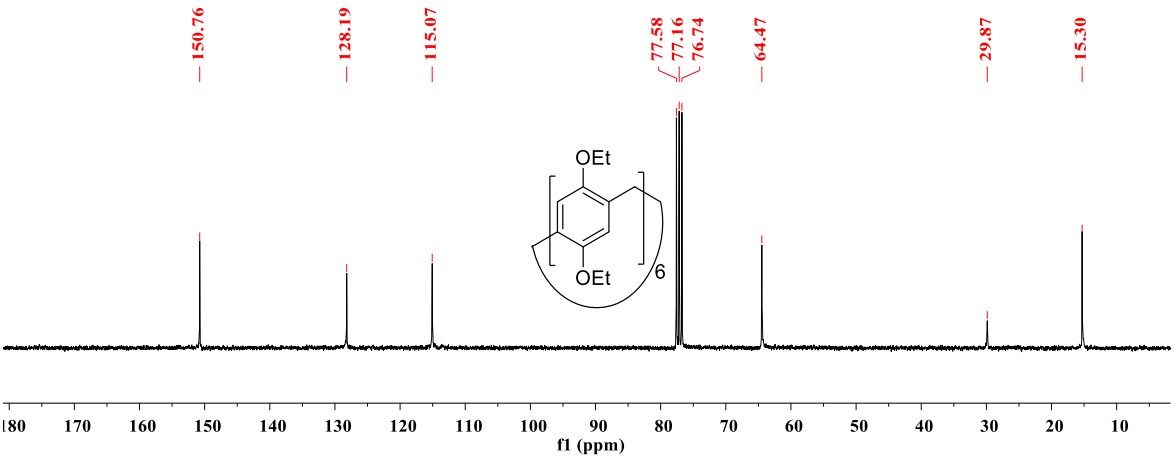

^{1}H NMR spectrum of ^{Pr}P6 at 20 °C in CDCl3

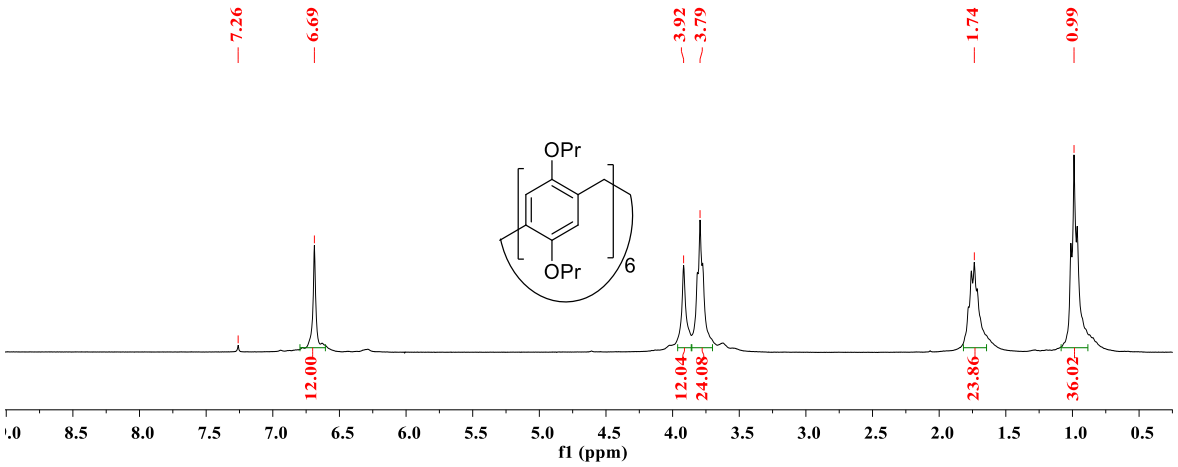

^{13}C NMR spectrum of ^{Pr}P6 at 20 °C in CDCl3

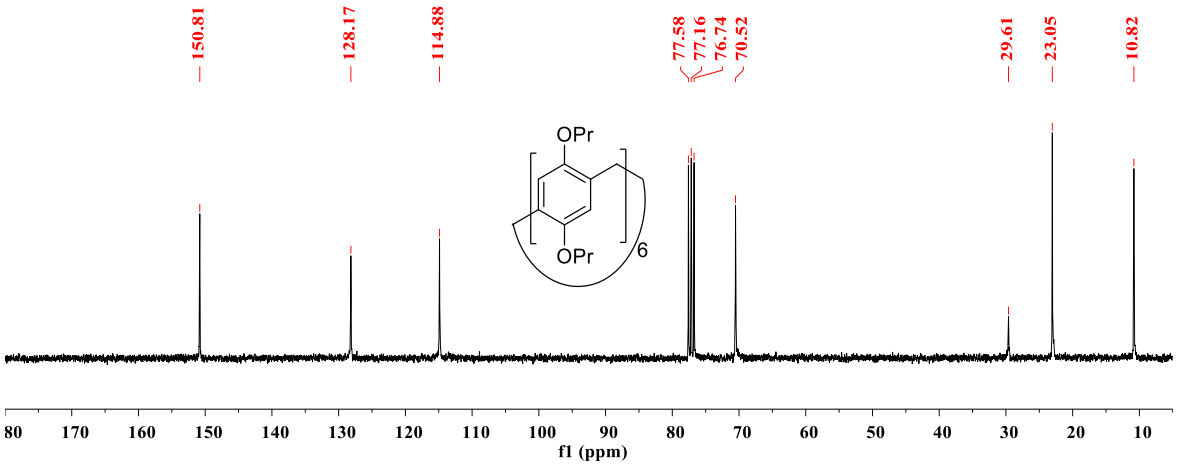

^{1}H NMR spectrum of $^{i\text{-Bu}}$P6 at 20 °C in CDCl3

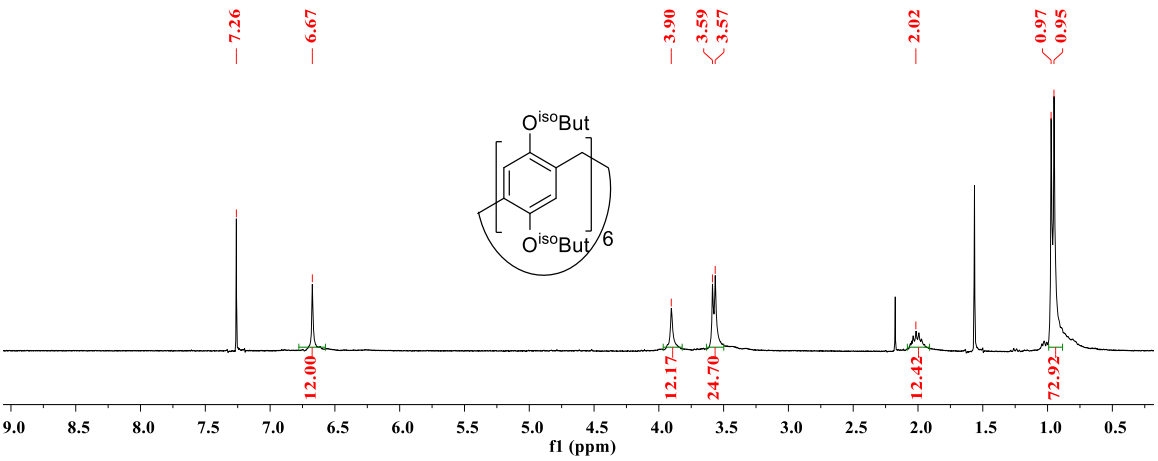

^{13}C NMR spectrum of $^{i\text{-Bu}}$P6 P6 at 20 °C in CDCl3

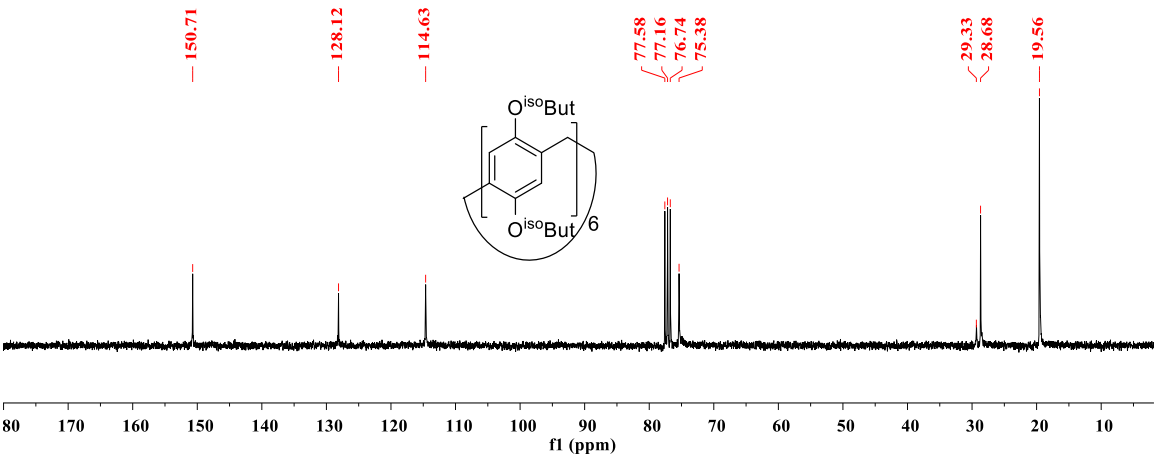

^{1}H NMR spectrum of $^{n\text{-Bu}}$P6 at 20 °C in CDCl3

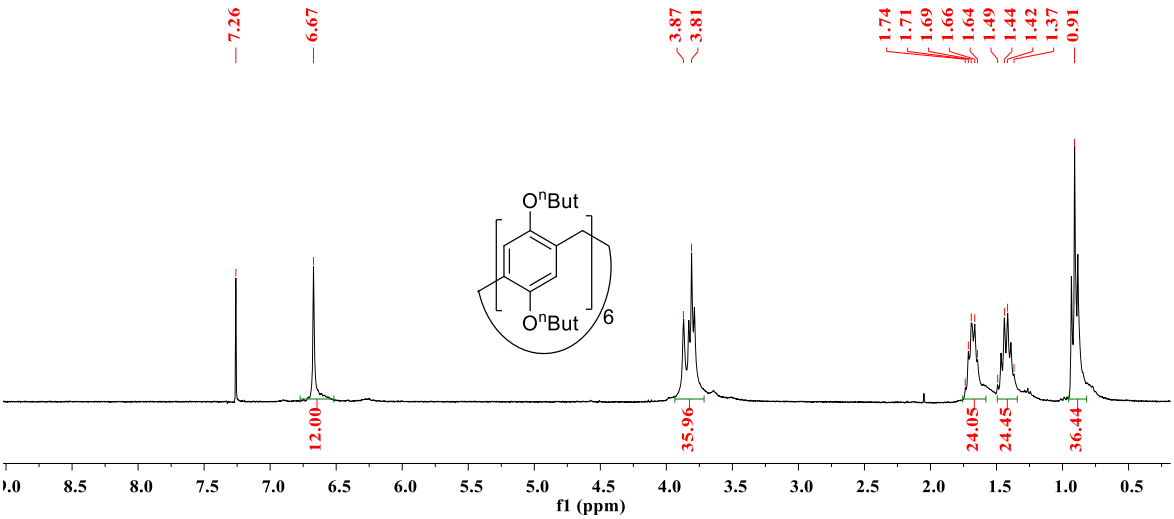

^{13}C NMR spectrum of $^{n\text{-Bu}}$P6 at 20 °C in CDCl3

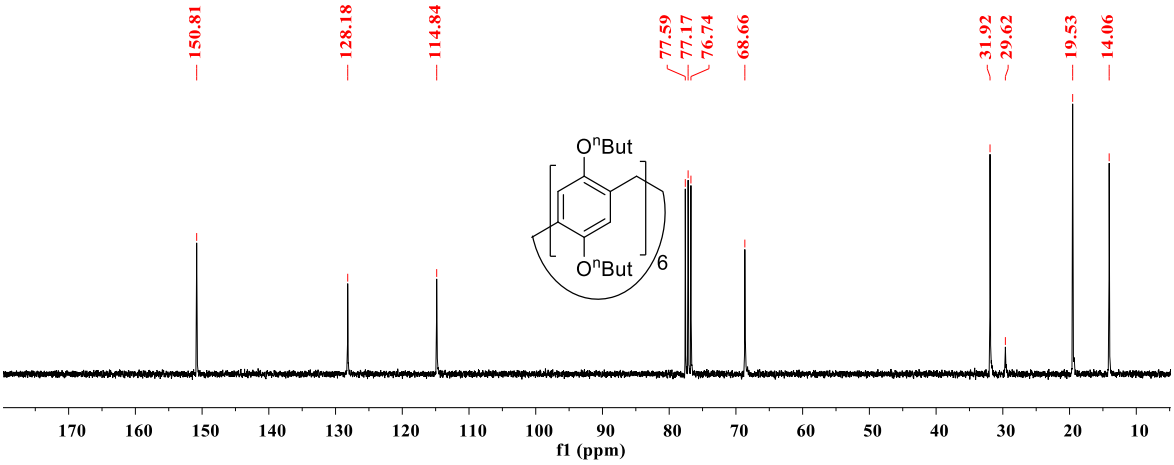

^{1}H NMR spectrum of ^{Cy}P6 at 20 °C in CDCl3

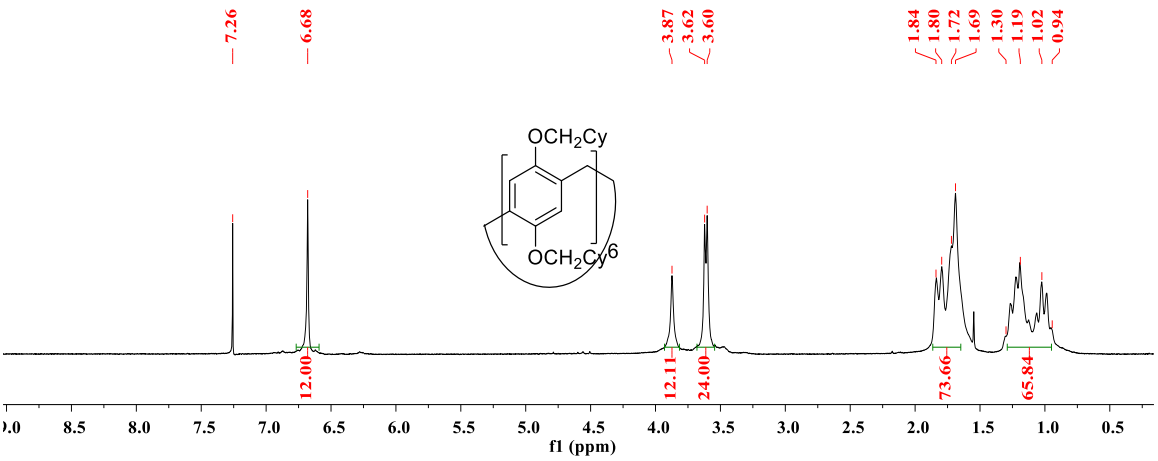

^{13}C NMR spectrum of ^{Cy}P6 at 20 °C in CDCl3

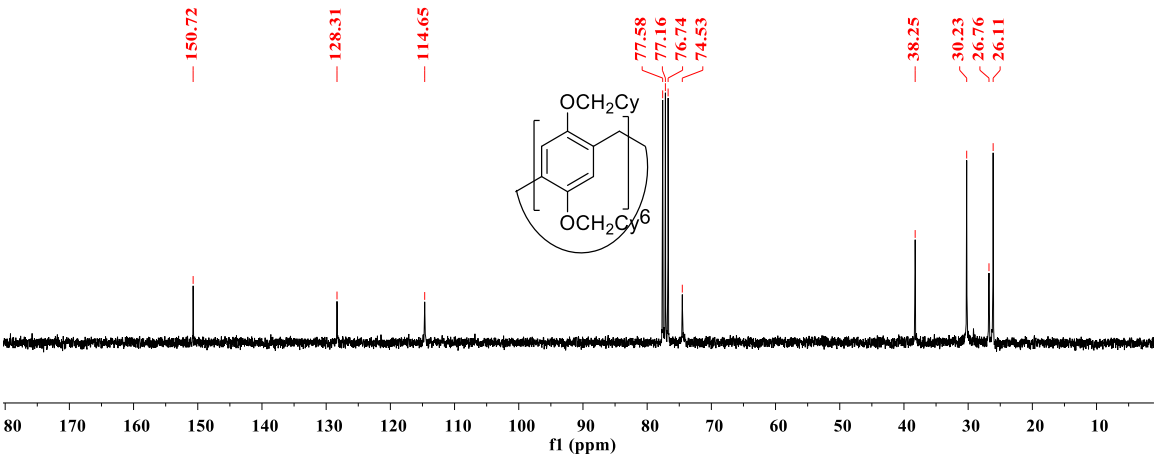

^{1}H NMR spectrum of ^{Hex}P6 at 20 °C in CDCl3

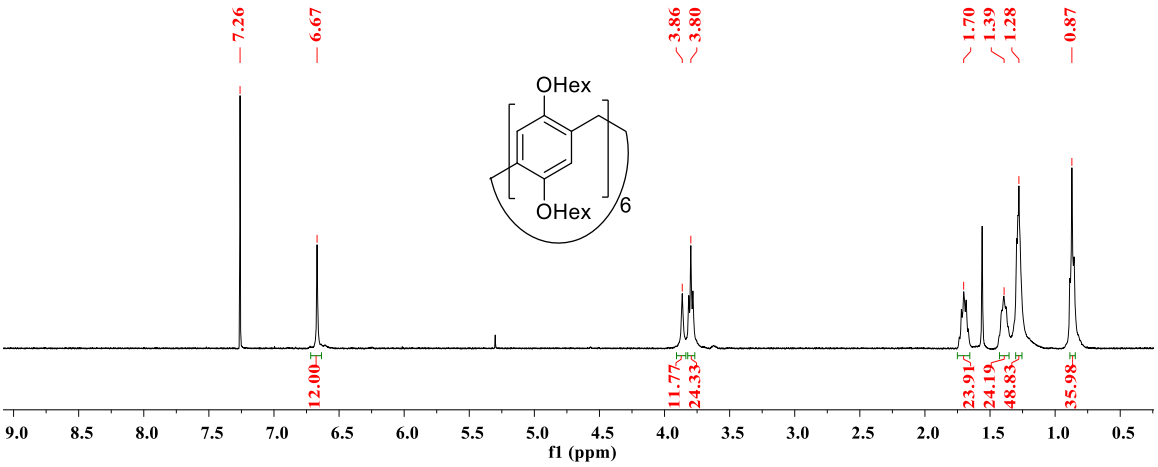

^{13}C NMR spectrum of ^{Hex}P6 at 20 °C in CDCl3

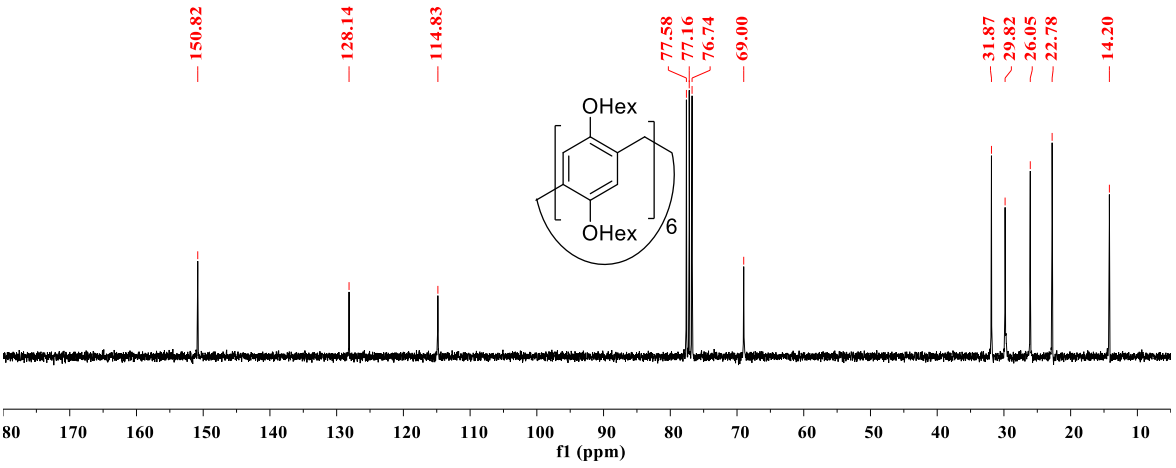

^{1}H NMR spectrum of 1,4-diethyloxybenzene at 20 °C in $CDCl_3$

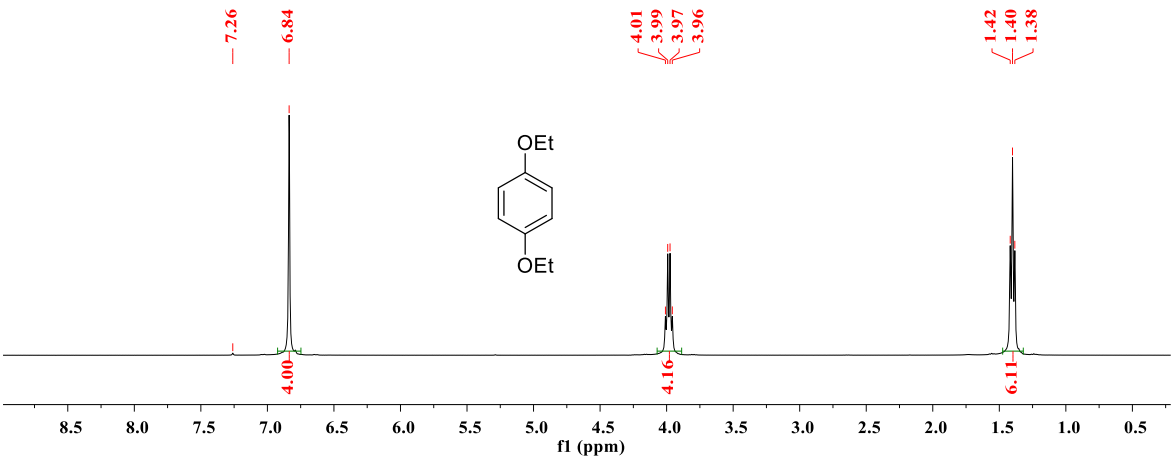

^{13}C NMR spectrum of 1,4-diethyloxybenzene at 20 °C in CDCl3

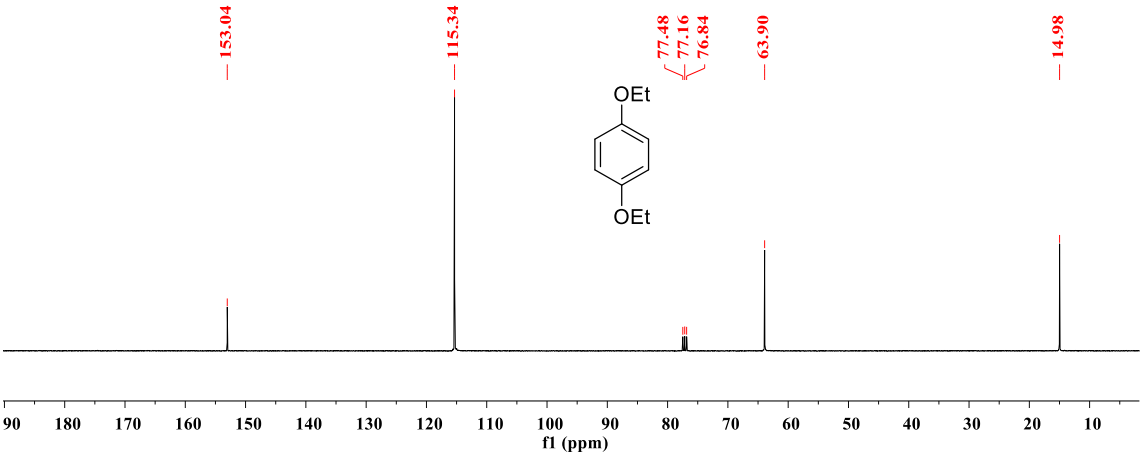

^{1}H NMR spectrum of 1,4-dipropyloxybenzene at 20 °C in CDCl3

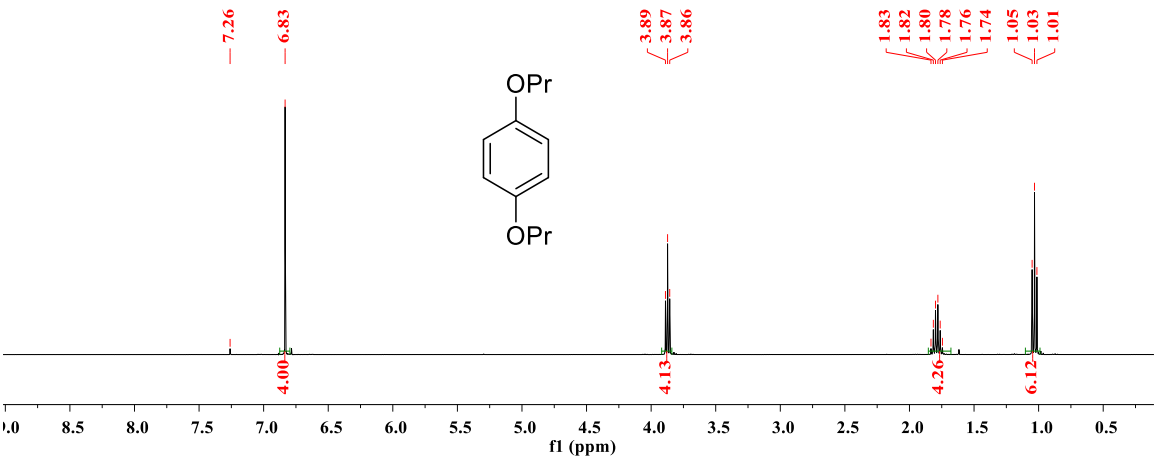

^{13}C NMR spectrum of 1,4-dipropyloxybenzene at 20 °C in CDCl3

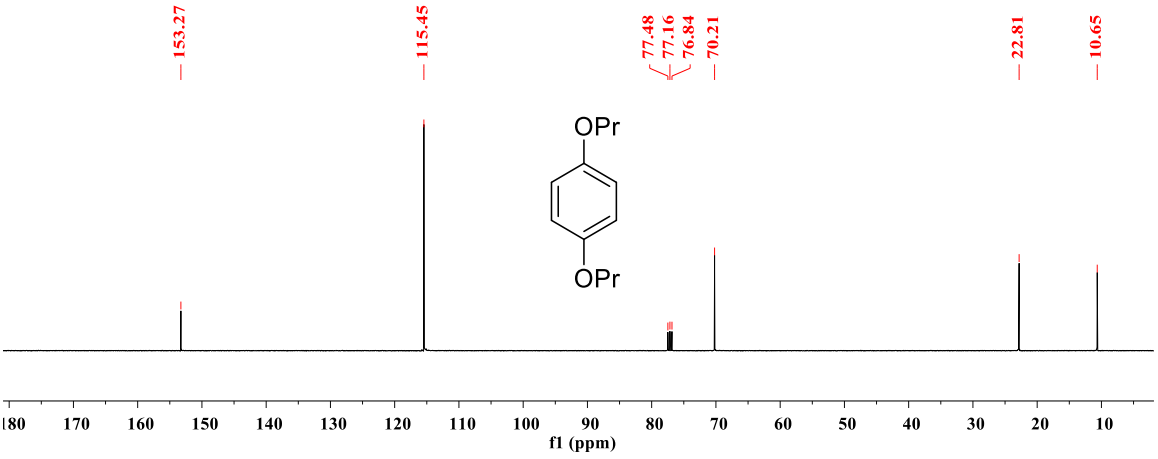

^{1}H NMR spectrum of 1,4-isobutyloxybenzene at 20 °C in CDCl3

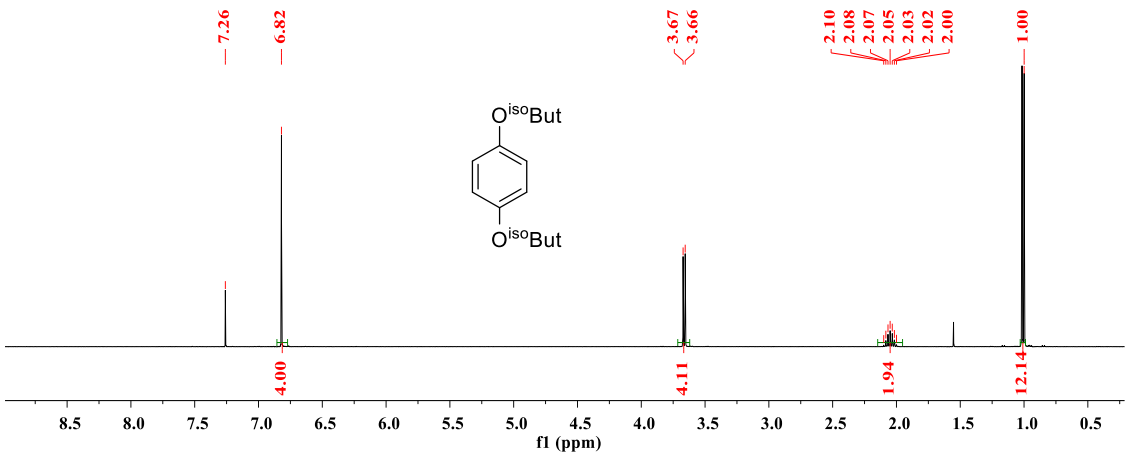

^{13}C NMR spectrum of 1,4-isobutyloxybenzene at 20 °C in CDCl3

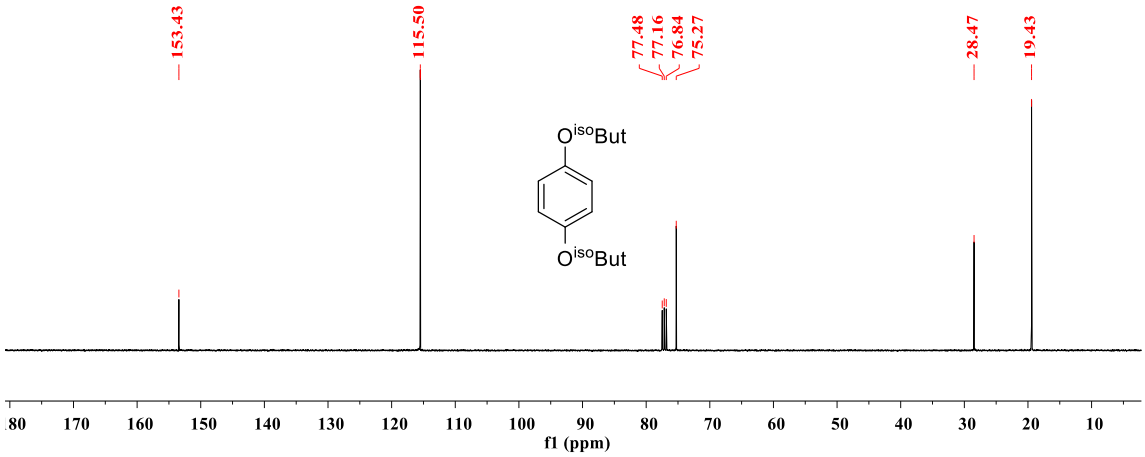

^{1}H NMR spectrum of 1,4-n-butyloxybenzene at 20 °C in CDCl3

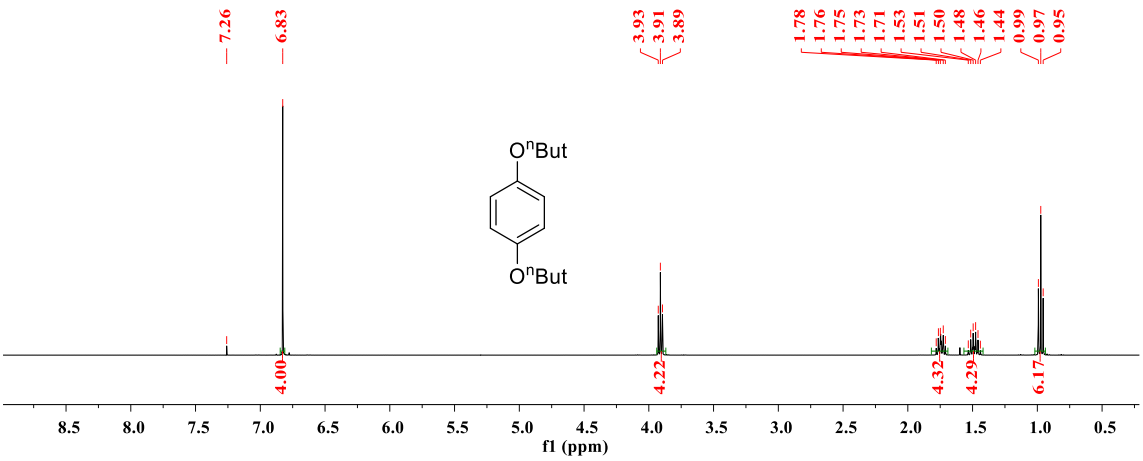

^{13}C NMR spectrum of 1,4-n-butyloxybenzene at 20 °C in CDCl3

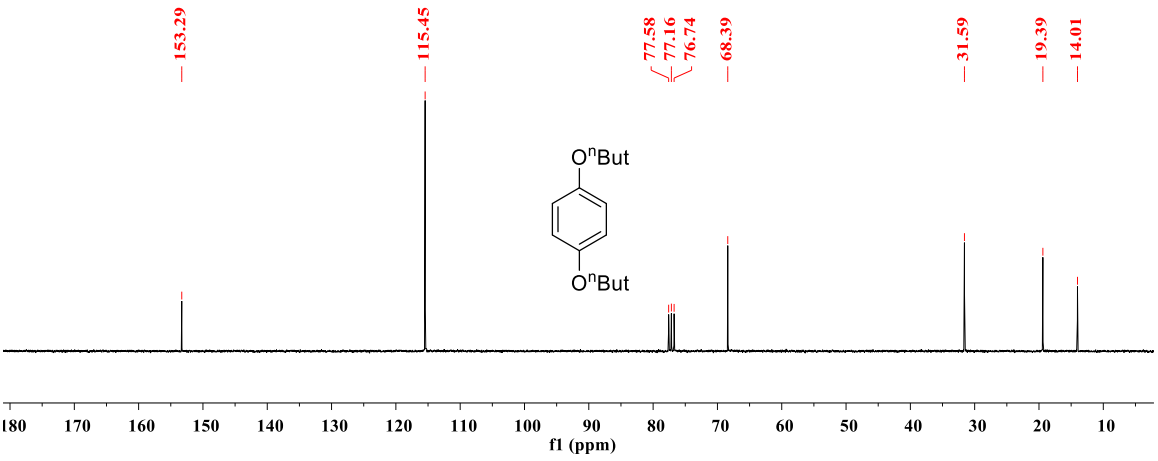

^{1}H NMR spectrum of 1,4-n-hexyloxybenzene at 20 °C in CDCl3

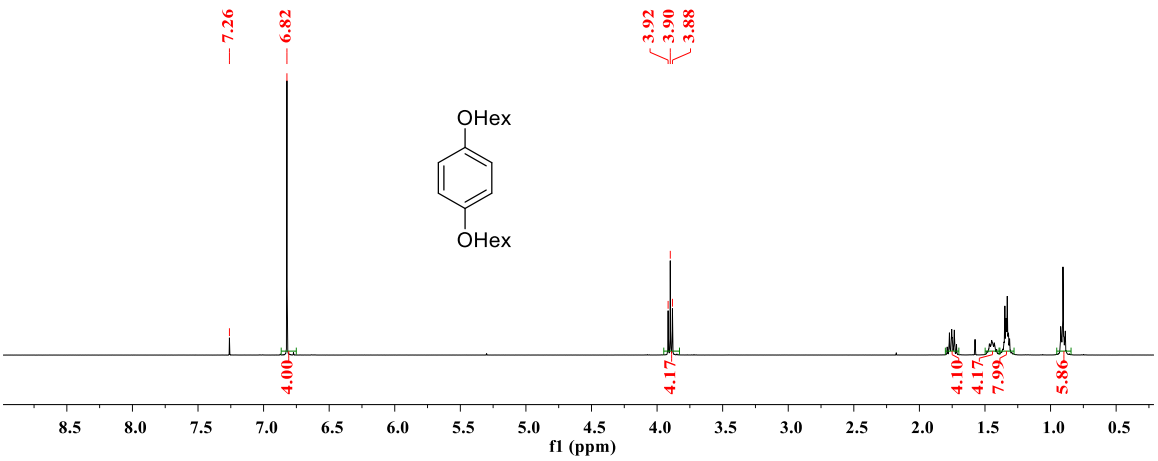

^{13}C NMR spectrum of 1,4-n-hexyloxybenzene at 20 °C in CDCl3

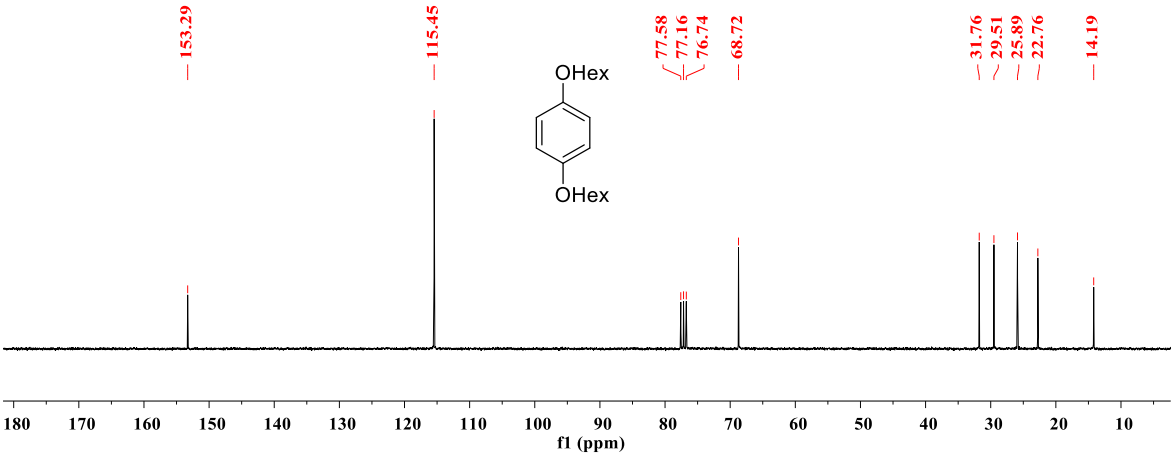

^{1}H NMR spectrum of 1,4-dicyclohexylmethylbenzene at 20 °C in CDCl3

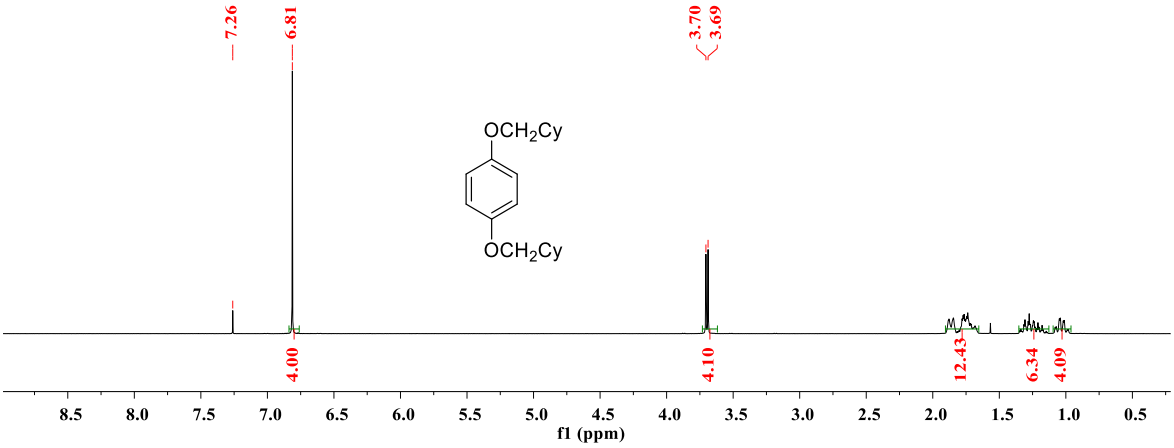

^{13}C NMR spectrum of 1,4-dicyclohexylmethylbenzene at 20 °C in CDCl3

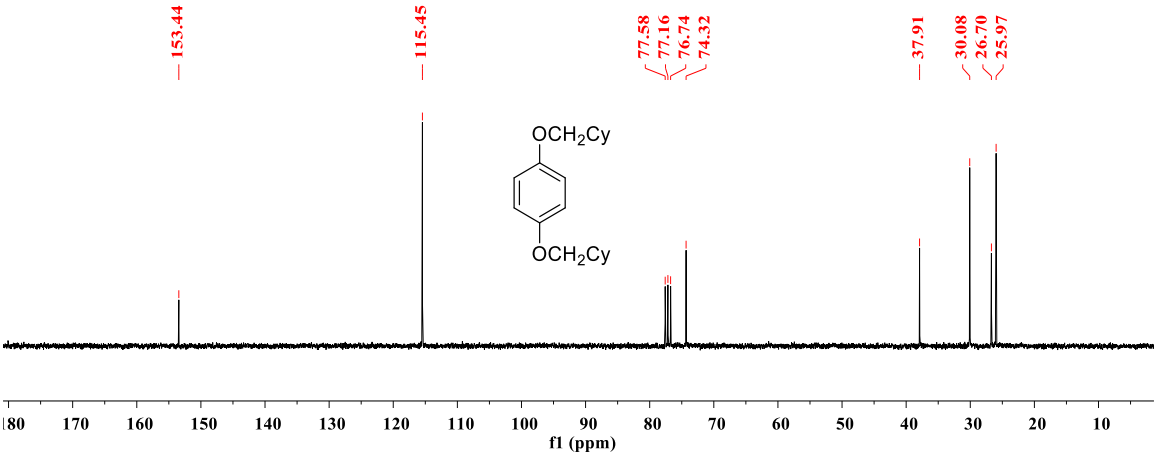

MALDI-TOF data for P5 and P6

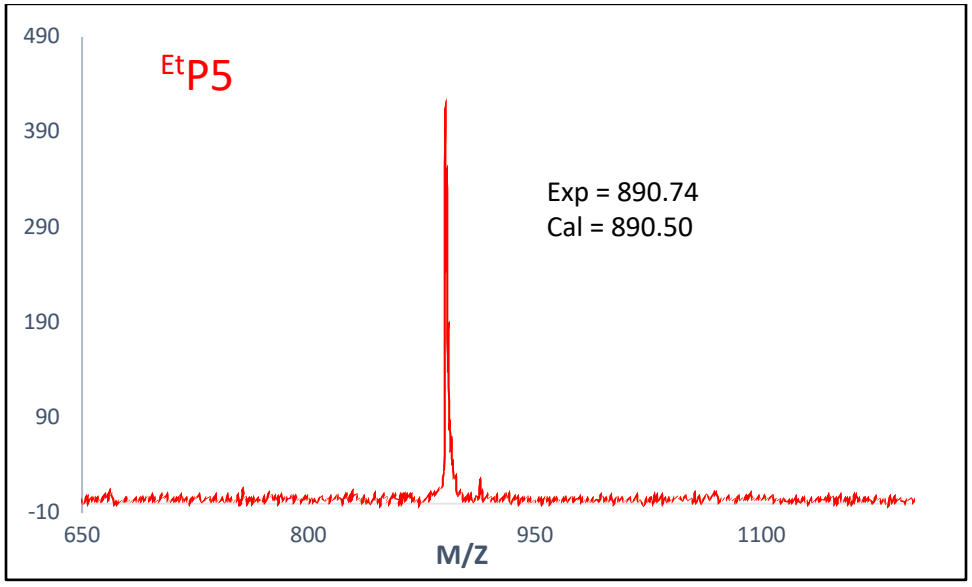

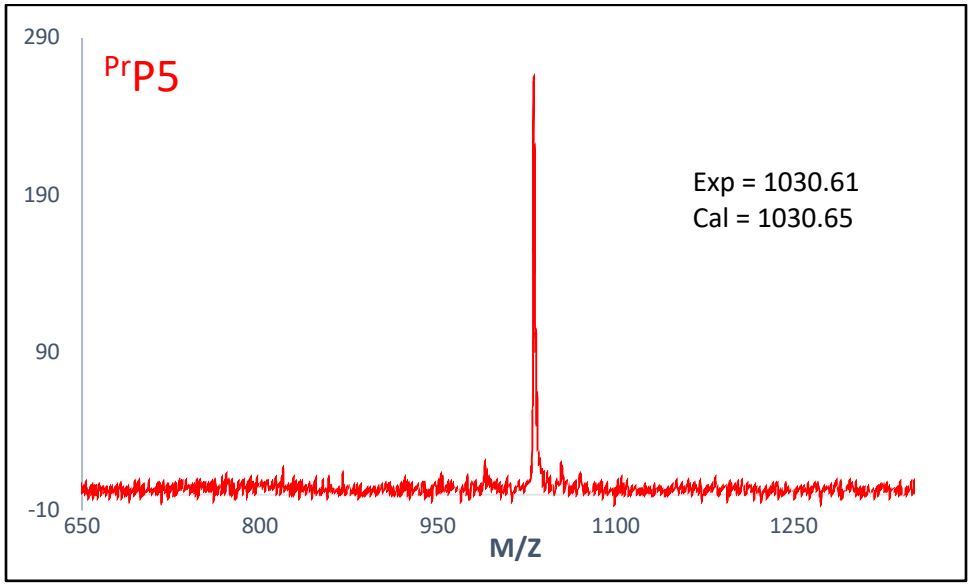

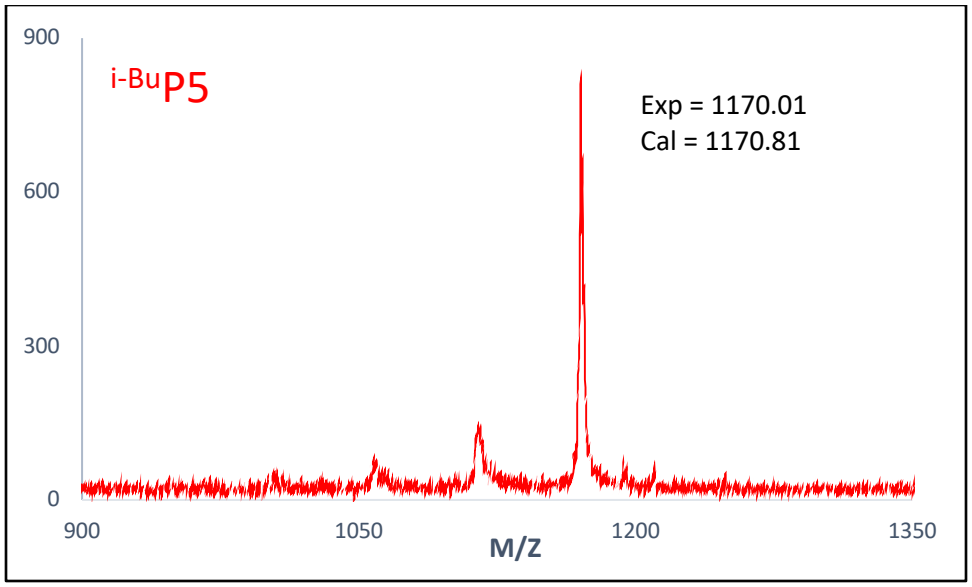
i-BuP5
Exp = 1170.01
Cal = 1170.81
900
600
300
0
900
1050
1200
1350
M/Z

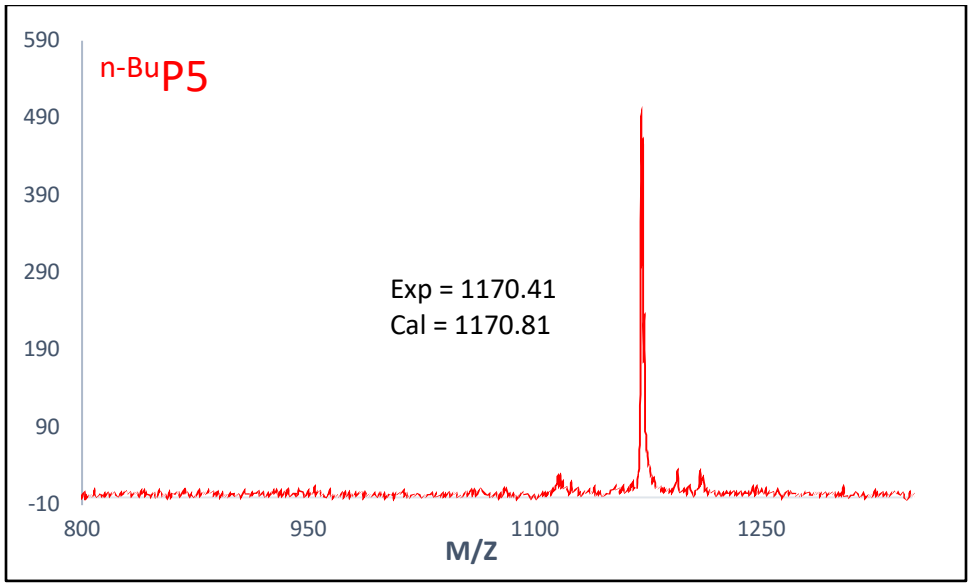
n-BuP5
Exp = 1170.41
Cal = 1170.81
590
490
390
290
190
90
-10
800
950
1100
1250
M/Z

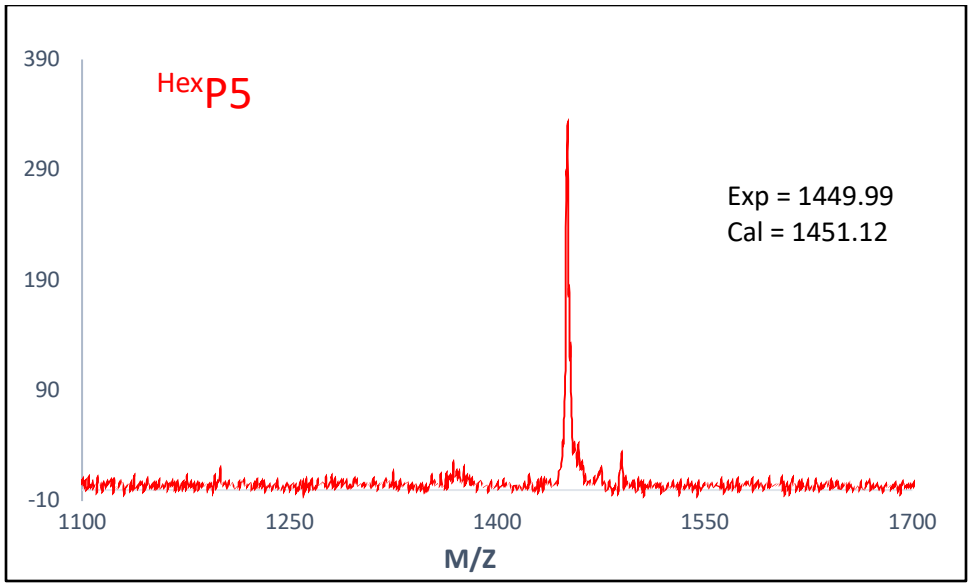
HexP5
Exp = 1449.99
Cal = 1451.12
390
290
190
90
-10
1100
1250
1400
1550
1700
M/Z

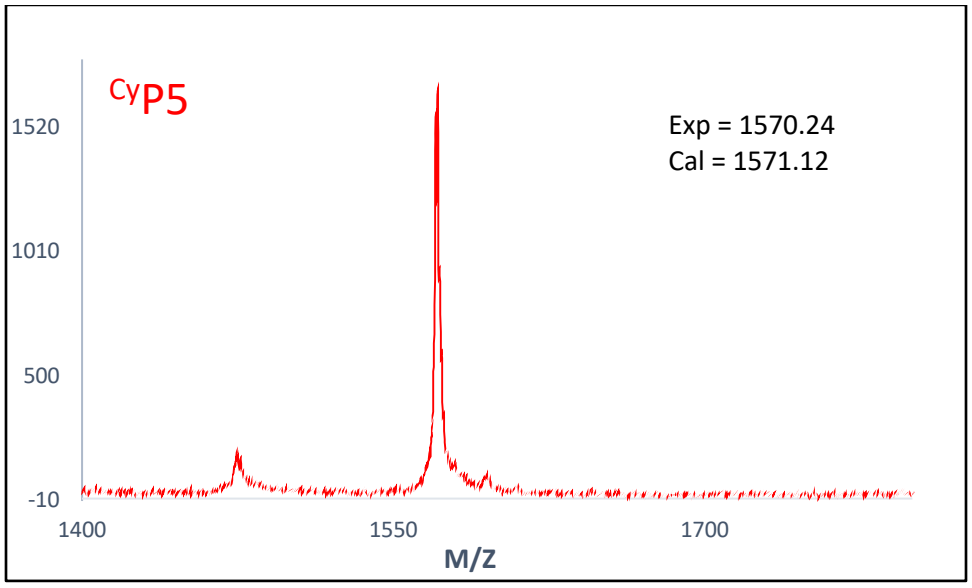
CyP5
Exp = 1570.24
Cal = 1571.12
1520
1010
500
-10
1400
1550
1700
M/Z

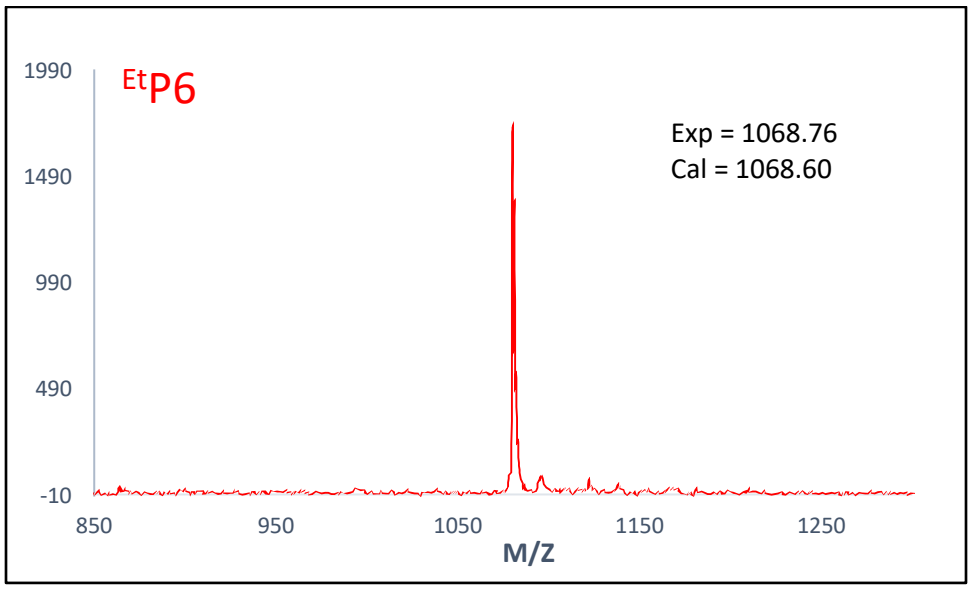
EtP6
Exp = 1068.76
Cal = 1068.60
1990
1490
990
490
-10
850
950
1050
1150
1250
M/Z

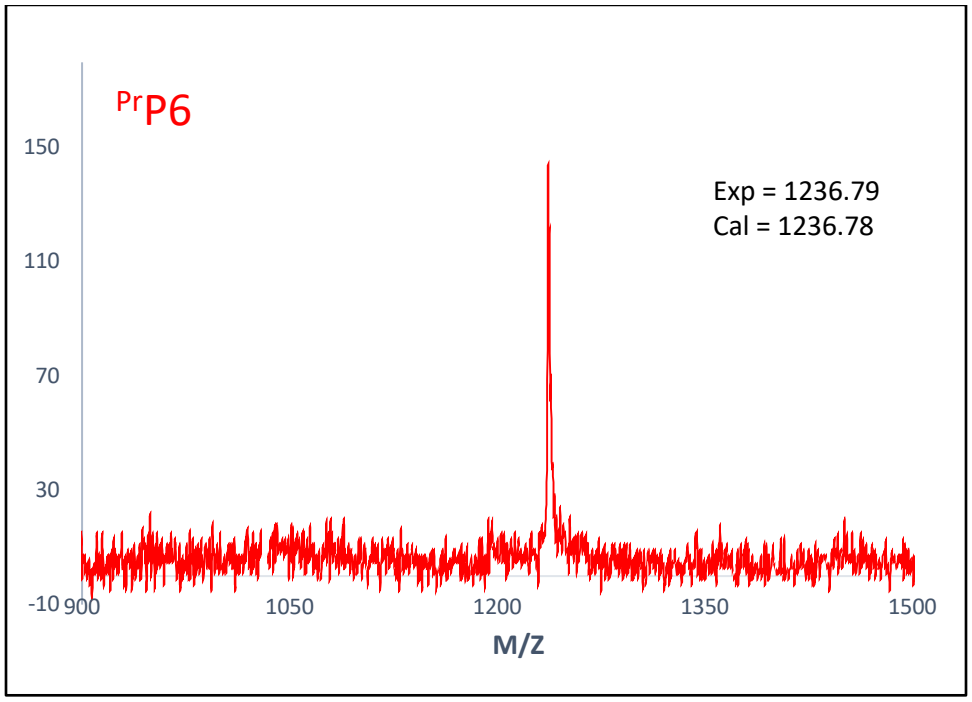
PrP6
Exp = 1236.79
Cal = 1236.78
150
110
70
30
-10
900
1050
1200
1350
1500
M/Z

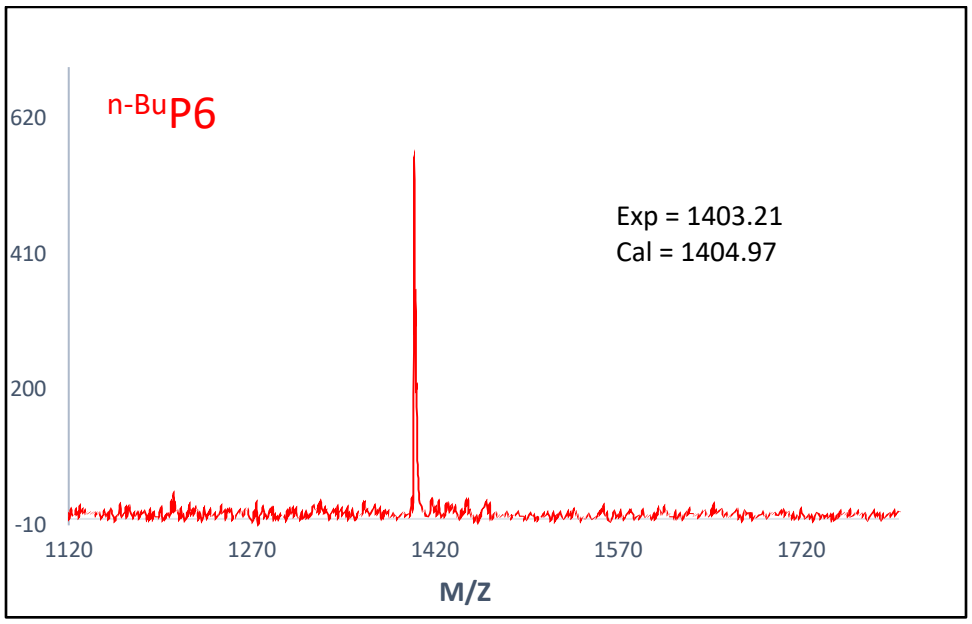
n-BuP6
620
410
200
-10
1120
1270
1420
1570
1720
M/Z
Exp = 1403.21
Cal = 1404.97

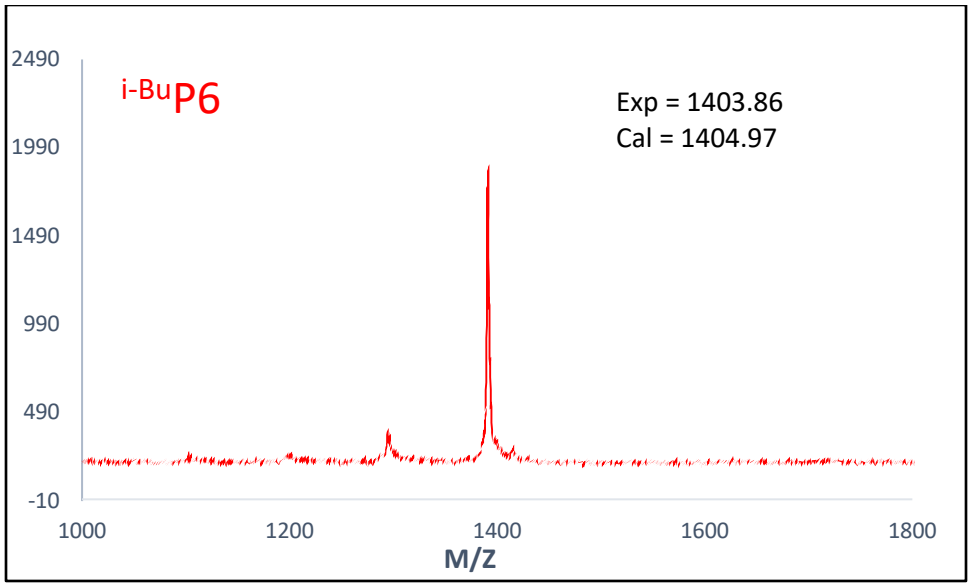
i-BuP6
2490
1990
1490
990
490
-10
1000
1200
1400
1600
1800
M/Z
Exp = 1403.86
Cal = 1404.97

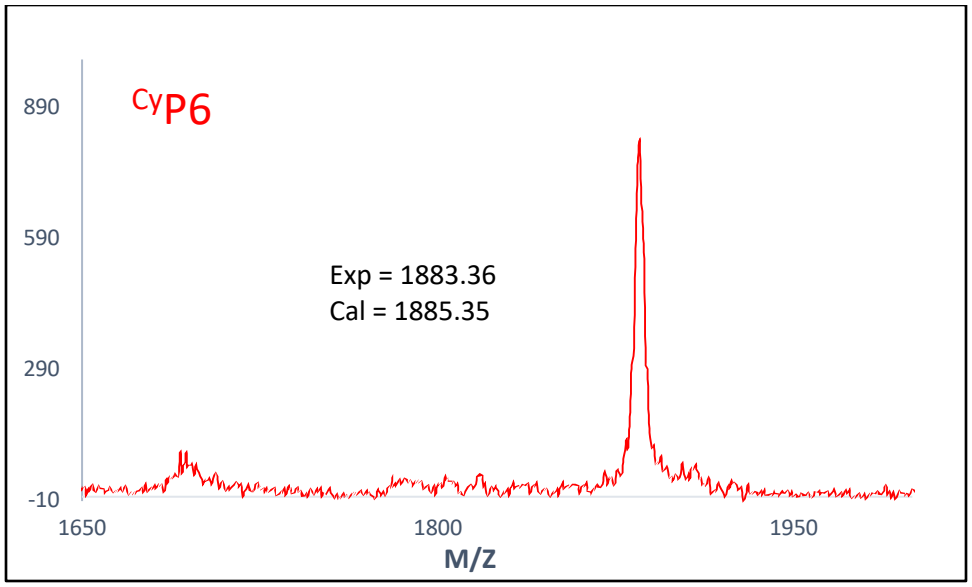
CyP6
890
590
290
-10
Exp = 1883.36
Cal = 1885.35
1650
1800
1950
M/Z

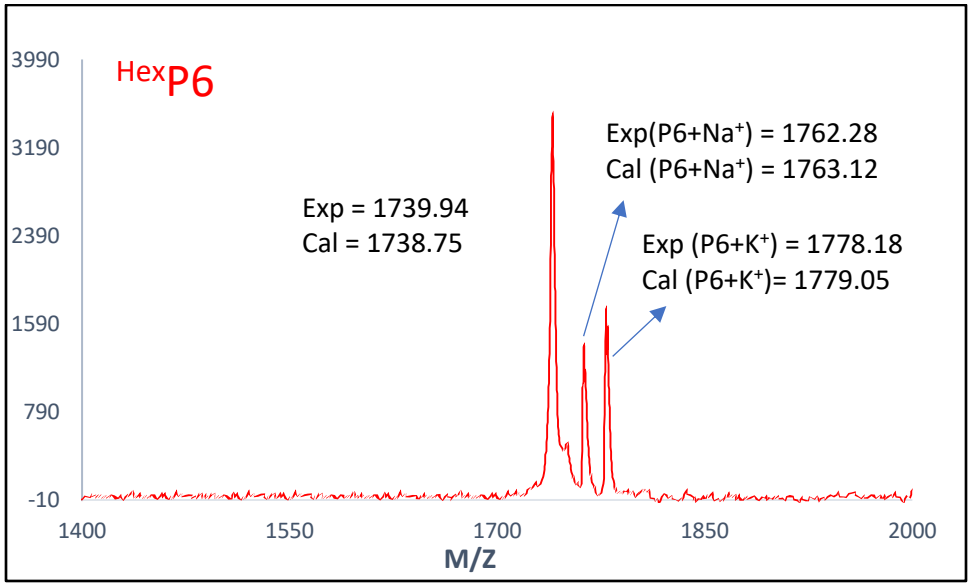
HexP6
3990
3190
2390
1590
790
-10
Exp = 1739.94
Cal = 1738.75
Exp(P6+Na+) = 1762.28
Cal (P6+Na+) = 1763.12
Exp (P6+K+) = 1778.18
Cal (P6+K+)= 1779.05
1400
1550
1700
1850
2000
M/Z

Table 4.6 Summary of X-ray crystallographic data of pillarenes.

Identification code	raj29o	raj29t5
Empirical formula	$C_{98.65}H_{155.65}Cl_{0.7}N_{1.65}O_{10}$	$C_{108.84}H_{156.66}Cl_{3.56}N_{1.03}O_{10}$
Formula weight	1549.78	1765.91
Temperature/K	100.15	100.15
Crystal system	triclinic	monoclinic
Space group	P-1	$P2_1/c$
a/Å	12.18936(18)	23.7051(2)
b/Å	20.5151(3)	16.51019(17)
c/Å	20.9676(3)	25.9498(2)
α/°	113.1244(12)	90
β/°	96.6891(12)	92.3922(9)
γ/°	97.9850(11)	90
Volume/Å^3	4690.28(12)	10147.27(17)
Z	2	4
ρ_{calc}g/cm^3	1.097	1.156
μ/mm^{-1}	0.712	1.394
F(000)	1702	3830
Crystal size/mm^3	0.341 × 0.288 × 0.116	0.419 × 0.223 × 0.181
Radiation	CuKα (λ = 1.54184)	CuKα (λ = 1.54184)
2Θ range for data collection/°	7.456 to 141.226	6.818 to 141.458
Index ranges	-14 ≤h≤14, -25≤k≤25, -25≤l≤25	-28≤h≤28, -20≤k≤20,-31≤l≤ 31
Reflections collected	85093	36252
Independent reflections	17789 [R_{int} = 0.0300, R_{sigma} =0.0177]	36252 [R_{int} = ?, R_{sigma} = 0.0159]
Data/restraints/parameters	17789/9/1053	36252/30/1180
Goodness-of-fit on F^2	1.038	1.023
Final R indexes [I>=2σ(I)]	R_1 = 0.0487, wR_2 = 0.1359	R_1 = 0.0518, wR_2 = 0.1498
Final R indexes [all data]	R_1 = 0.0525, wR_2 = 0.1401	R_1 = 0.0587, wR_2 = 0.1539
Largest diff. peak/hole / e Å^{-3}	0.36/-0.30	0.51/-0.47

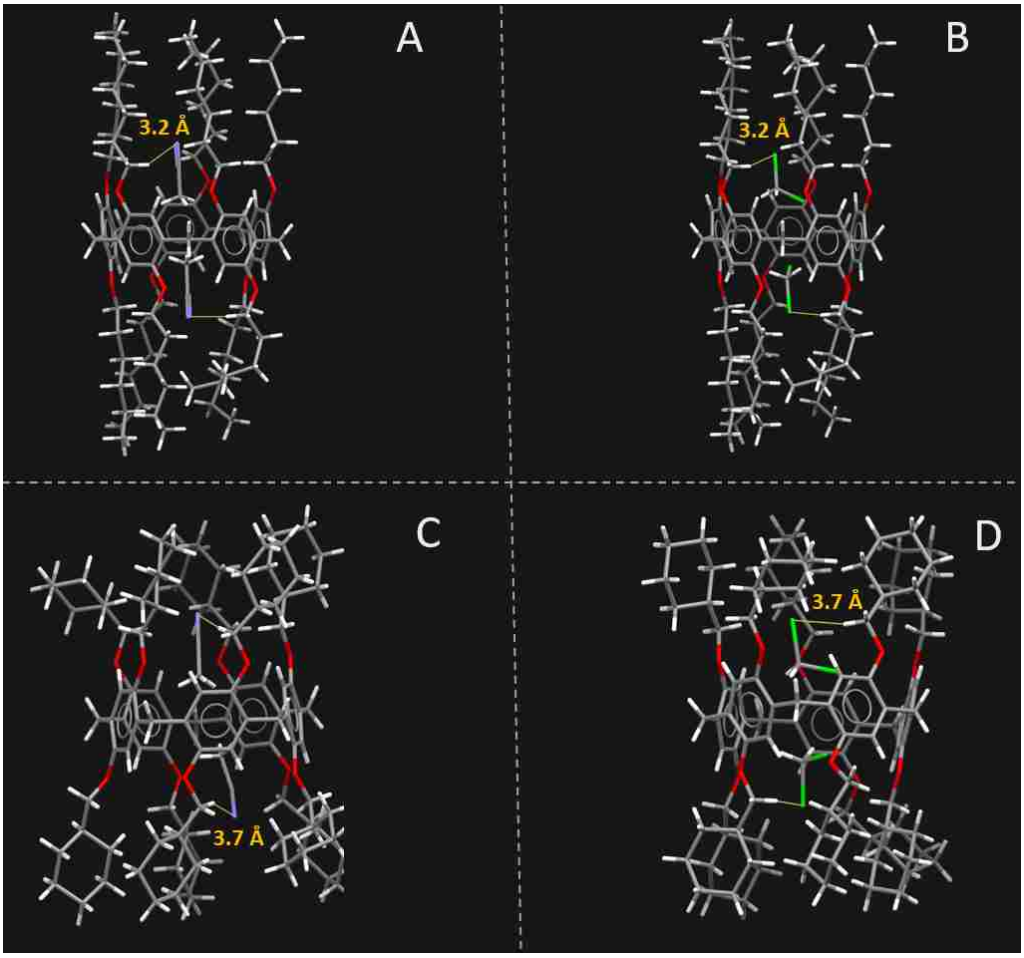

Figure 4.5 The average (all ten) interaction between H (O-CH_2) of ^{Hex}P5/^{Cy}P5 and N and Cl of CH_3CN and CH_2Cl_2, respectively. All values are based on the single x-ray crystal structures for ^{Hex}P5+2 CH_3CN (A), ^{Hex}P5+2 CH_2Cl_2 (B), ^{Cy}P5+2 CH_3CN (C), ^{Cy}P5+2 CH_2Cl_2 (D).

Table 4.7 The complexation free energies of P5 and P6 with CH_2Cl_2/$CHCl_3$ in kcal.mol^{-1} (the number in brackets are calculated using PBE0 functional)

	P5	P6
CH_2Cl_2	-5.1 [-5.3]	-0.9 [-1.2]
$CHCl_3$	-1.7 [-0.8]	-4.0 [-3.0]

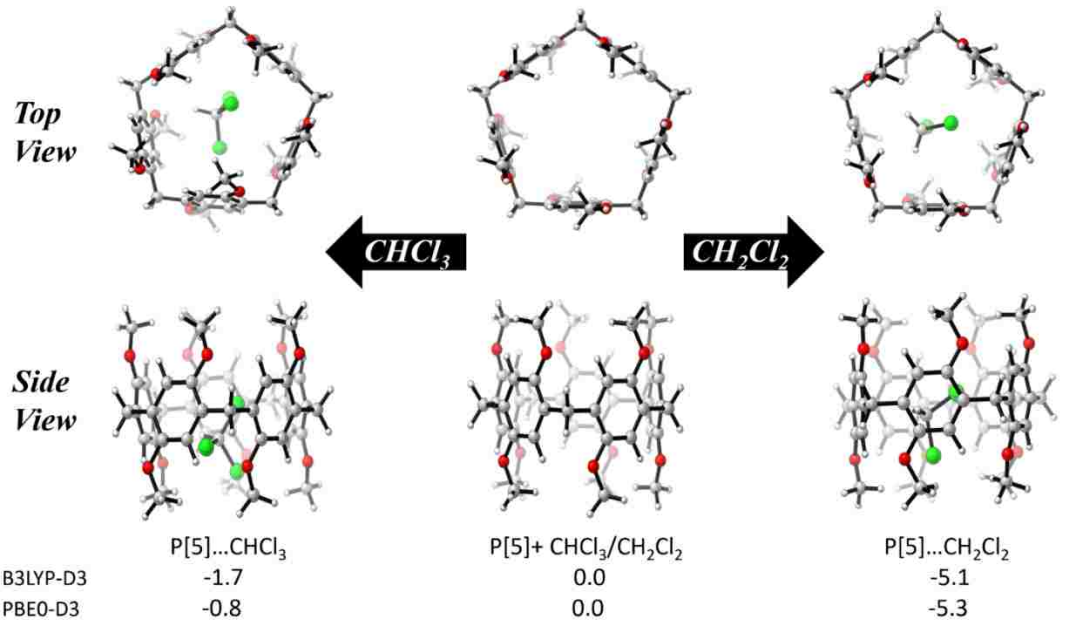

	P[5]...$CHCl_3$	P[5]+ $CHCl_3$/CH_2Cl_2	P[5]...CH_2Cl_2
B3LYP-D3	-1.7	0.0	-5.1
PBE0-D3	-0.8	0.0	-5.3

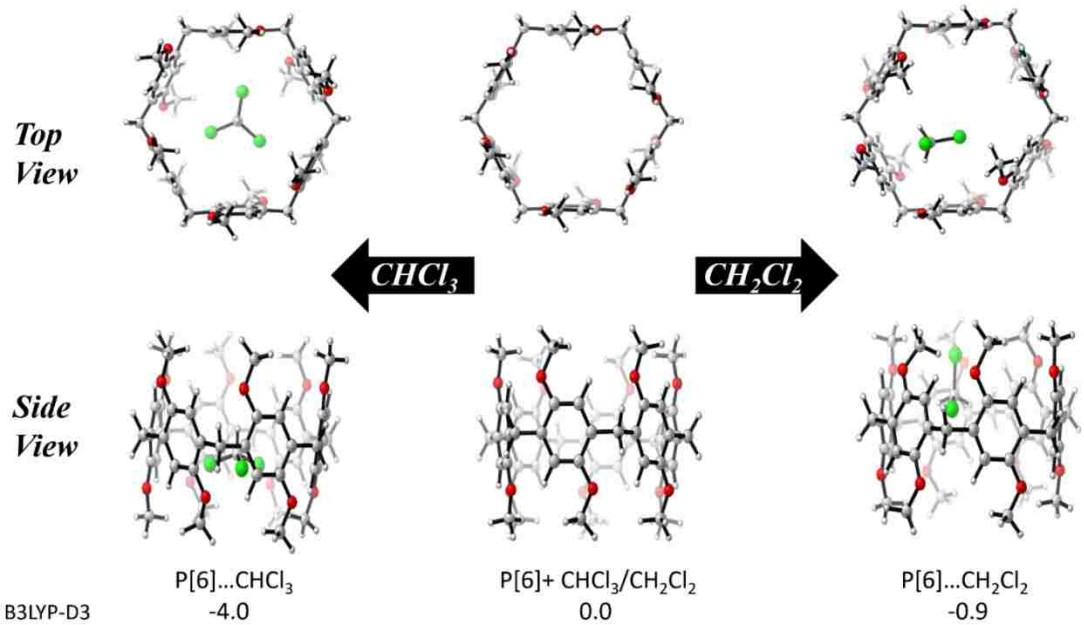

	P[6]...$CHCl_3$	P[6]+ $CHCl_3$/CH_2Cl_2	P[6]...CH_2Cl_2
B3LYP-D3	-4.0	0.0	-0.9
PBE0-D3	-3.0	0.0	-1.2

Figure 4.6 The complexation free energies (in kcal.mol^{-1}) for P5 and P6 with CH_2Cl_2 and $CHCl_3$ (6-31+G(d,p)-PCM(CH_2Cl_2)//6-31G(d)-gas).

BIBLIOGRAPHY

1 G. Crini, *Chem. Rev.*, 2014, **114**, 10940–10975.

2 A. Harada, *Acc. Chem. Res.*, 2001, **34**, 456–464.

3 J. Anthony Semlyen, *Large Ring Molecules*, Wiley-VCH; Weinheim, 1996.

4 A. Harada, H. Adachi, Y. Kawaguchi, M. Okada and M. Kamachi, *Polym. J.*, 1996, **28**, 159–163.

5 Y. K. And and A. Harada, *Org. Lett.*, 2000, **2**, 1353–1356.

6 A. Harada and S. Takahashi, *J. Chem. Soc., Chem. Commun.*, 1984, **0**, 645–646.

7 C. J. Pedersen, *J. Am. Chem. Soc.*, 1967, **89**, 7017–7036.

8 B. O. Strasser and A. I. Popov, *J. Am. Chem. Soc.*, 1985, **107**, 7921–7924.

9 D. G. Lee and V. S. Chang, *J. Org. Chem.*, 1978, **43**, 1532–1536.

10 D. Landini, A. Maia, F. Montanari and P. Tundo, *J. Am. Chem. Soc.*, 1979, **101**, 2526–2530.

11 S. Maleknia and J. Brodbelt, *J. Am. Chem. Soc.*, 1993, **115**, 2837–2843.

12 V. Rüdiger, H.-J. Schneider, V. P. Solov'ev, V. P. Kazachenko and O. A. Raevsky, *European J. Org. Chem.*, 1999, **1999**, 1847–1856.

13 B. L. Williamson and C. S. Creaser, *Int. J. Mass Spectrom.*, 1999, **188**, 53–61.

14 W. A. Freeman, W. L. Mock and N. Y. Shih, *J. Am. Chem. Soc.*, 1981, **103**, 7367–7368.

15 J. Lagona, P. Mukhopadhyay, S. Chakrabarti and L. Isaacs, *Angew. Chemie - Int. Ed.*, 2005, **44**, 4844–4870.

16 R. Behrend, E. Meyer and F. Rusche, *Justus Liebig's Ann. der Chemie*, 1905, **339**, 1–37.

17 J. Kim, I.-S. Jung, S.-Y. Kim, E. Lee, J.-K. Kang, S. Sakamoto, K. Yamaguchi and K. Kim, *J. Am. Chem. Soc.*, 2000, **122**, 540–541.

18 A. Day, A. P. Arnold, Rodney J. Blanch and B. Snushall, *J. Org. Chem.*, 2001, **66**, 8094–8100.

19 A. I. Day, R. J. Blanch, A. P. Arnold, S. Lorenzo, G. R. Lewis and I. Dance, *Angew. Chemie*, 2002, **114**, 285–287.

20 J. W. Lee, S. Samal, N. Selvapalam, H.-J. Kim and K. Kim, *Acc. Chem. Res.*, 2003, **36**, 621–630.

21 K. Kim, *Chem. Soc. Rev.*, 2002, **31**, 96–107.

22 K. Kim, *Self-Assembly of Interlocked Structures with Cucurbituril, Metal Ions and Metal Complexes*, John Wiley & Sons, Ltd, 2007.

23 R. Kumar, Y. Jung and J. S. Kim, *Calixarenes and Beyond*, 2016.

24 C. D. Gutsche, *Calixarenes: An Introdution*, Royal Society of Chemistry, 2nd edn., 2008.

25 L. Mandolini and R. Ungaro, *Calixarenes in action*, world scientific, 2000.

26 T. Ogoshi, *Pillararenes*, Royal Society of Chemistry, 2016.

27 M. J. Hardie, *Chem. Soc. Rev.*, 2010, **39**, 516–527.

28 J. L. Scott, D. R. MacFarlane, C. L. Raston and C. M. Teoh, *Green Chem.*, 2000, **2**, 123–126.

29 D. Wang, M. V Ivanov, S. Mirzaei, S. V. Lindeman and R. Rathore, 2018, **16**, 5712–5717.

30 T. Brotin, Vincent Roy and J.-P. Dutasta, *J. Org. Chem.*, 2005, **70**, 6187–6195.

31 H. Zhang, J. W. Steed and J. L. Atwood, *Supramol. Chem.*, 1994, **4**, 185–190.

32 B. T. Ibragimov, K. K. Makhkamov and K. M. Beketov, *J. Incl. Phenom. Macrocycl. Chem.*, 1999, **35**, 583–593.

33 M. R. Caira, A. Jacobs and L. R. Nassimbeni, *Supramol. Chem.*, 2004, **16**, 337–342.

34 M. J. Hardie, R. Ahmad and C. J. Sumby, *New J. Chem.*, 2005, **29**, 1231–1240.

35 K. T. Holman, J. L. Atwood and J. W. Steed, *Angew. Chemie Int. Ed. English*, 1997, **36**, 1736–1738.

36 E. Huerta, G. A. Metselaar, A. Fragoso, E. Santos, C. Bo and J. de Mendoza, *Angew. Chemie Int. Ed.*, 2007, **46**, 202–205.

37 M. Martínez García, P. Arroyo Ortega, F. Lara Ochoa, G. Espinosa Pérez, S. Hernández Ortega, M. I. Chávez Uribe, M. Salmón and R. Cruz-Almanza, *Tetrahedron*, 1997, **53**, 17633–17642.

38 G. Cafeo, D. Garozzo, F. H. Kohnke, S. Pappalardo, M. F. Parisi, R. Pistone Nascone and D. J. Williams, *Tetrahedron*, 2004, **60**, 1895–1902.

39 V. Král, P. A. Gale, P. Anzenbacher Jr., K. Jursíková, V. Lynch, J. L. Sessler, V. Král and P. Anzenbacher Jr., *Chem. Commun.*, 1998, **0**, 9–10.

40 R. Chen, K. Somphol, M. Bhadbhade, N. Kumar and D. Black, *Synlett*, 2013, **24**, 1497–1500.

41 L.-P. Yang, W.-E. Liu and W. Jiang, *Tetrahedron Lett.*, 2016, **57**, 3978–3985.

42 P. Thuéry, J. Tae Gil and T. Yamato, *Supramol. Chem.*, 2003, **15**, 359–365.

43 M.-X. Wang, X.-H. Zhang and Q.-Y. Zheng, *Angew. Chemie Int. Ed.*, 2004, **43**, 838–842.

44 P. Lhoták, *European J. Org. Chem.*, 2004, **2004**, 1675–1692.

45 J. L. Katz, Bram J. Geller and R. R. Conry, *Org. Lett.*, 2006, **8**, 2755–2758.

46 M. Kirsch, H.-G. Korth, R. Sustmann and H. de Groot, *Biol. Chem.*, 2002, **383**, 389–399.

47 C. C. Addison, *Chem. Rev.*, 1980, **80**, 21–39.

48 D. M. Rudkevich, *Angew. Chemie Int. Ed.*, 2004, **43**, 558–571.

49 B. Botta, I. D'Acquarica, G. D. Monache, L. Nevola, D. Tullo, F. Ugozzoli and M. Pierini, *J. Am. Chem. Soc.*, 2007, **129**, 1202–11212.

50 Grigory V. Zyryanov, Yanlong Kang and D. M. Rudkevich, *J. Am. Chem. Soc.*, 2003, **125**, 2997–3007.

51 G. V. Zyryanov, Y. Kang, S. P. Stampp and D. M. Rudkevich, *Chem. Commun.*, 2002, **0**, 2792–2793.

52 R. Rathore, S. H. Abdelwahed and I. A. Guzei, *J. Am. Chem. Soc.*, 2004, **126**, 13582–13583.

53 D. Wang, L. V Ivanova, M. Ivanov, S. Mirzaei, Q. Timerghazin, S. Reid and R. Rathore, *Chem. - A Eur. J.*, 2018, **24**, 17439–17443.

54 R. Rathore, S. V. Lindeman, K. S. S. P. Rao, D. Sun and J. K. Kochi, *Angew. Chemie Int. Ed.*, 2000, **39**, 2123–2127.

55 D. Wang, D. Zhang, S. V Lindeman and R. Rathore, *Chem. – An Asian J.*, 201AD, **14**, 542–546.

56 R. Assmus, V. Böhmer, J. M. Harrowfield, M. I. Ogden, W. R. Richmond, B. W. Skelton and A. H. White, *J. Chem. Soc., Dalt. Trans.*, 1993, **0**, 2427–2433.

57 A. Casnati, S. Barboso, H. Rouquette, M.-J. Schwing-Weill, F. Arnaud-Neu, J.-F. Dozol and R. Ungaro, *J. Am. Chem. Soc.*, 2001, **123**, 12182–12190.

58 P. Rao, O. Enger, E. Graf, M. W. Hosseini, A. De Cian and J. Fischer, *Eur. J. Inorg. Chem.*, 2000, **2000**, 1503–1508.

59 R. J. Forster, A. Cadogan, M. Telting Diaz, D. Diamond, S. J. Harris and M. A. McKervey, *Sensors Actuators B Chem.*, 1991, **4**, 325–331.

60 K. M. O'Connor, G. Svehla, S. J. Harris and M. A. McKervey, *Talanta*, 1992, **39**, 1549–1554.

61 F. Cadogan, P. Kane, M. A. McKervey and D. Diamond, *Anal. Chem.*, 1999, **71**,

5544–5550.

62 T. Grady, A. Cadogan, T. McKittrick, S. J. Harris, D. Diamond and M. A. McKervey, *Anal. Chim. Acta*, 1996, **336**, 1–12.

63 M. A. Markowitz, R. Bielski and S. L. Regen, *J. Am. Chem. Soc.*, 1988, **110**, 7545–7546.

64 W. H. Chan, P. X. Cai and X. H. Gu, *Analyst*, 1994, **119**, 1853–1857.

65 T. Ogoshi, S. Kanai, S. Fujinami, T. Yamagishi and Y. Nakamoto, *J. Am. Chem. Soc.*, 2008, **130**, 5022–5023.

66 T. Ogoshi, T. Aoki, K. Kitajima, S. Fujinami, T. Yamagishi and Y. Nakamoto, *J. Org. Chem.*, 2011, **76**, 328–331.

67 T. Boinski and A. Szumna, *Tetrahedron*, 2012, **68**, 9419–9422.

68 X. B. Hu, Z. Chen, L. Chen, L. Zhang, J. L. Hou and Z. T. Li, *Chem. Commun.*, 2012, **48**, 10999–11001.

69 T. Ogoshi, N. Ueshima, T. Akutsu, D. Yamafuji, T. Furuta, F. Sakakibara and T. A. Yamagishi, *Chem. Commun.*, 2014, **50**, 5774–5777.

70 M. Holler, N. Allenbach, J. Sonet and J.-F. Nierengarten, *Chem. Commun.*, 2012, **48**, 2576–2578.

71 T. Ogoshi, D. Yamafuji, D. Kotera, T. Aoki, S. Fujinami and T. Yamagishi, *J. Org. Chem.*, 2012, **77**, 11146–11152.

72 P. Wei, X. Yan and F. Huang, *Chem. Commun.*, 2014, **50**, 14105–14108.

73 C. Han, Z. Zhang, G. Yu and F. Huang, *Chem. Commun.*, 2012, **48**, 9876–9878.

74 I. Nierengarten, S. Guerra, M. Holler, L. Karmazin-Brelot, J. Barberá, R. Deschenaux and J.-F. Nierengarten, *European J. Org. Chem.*, 2013, **2013**, 3675–3684.

75 Z. Zhang, B. Xia, C. Han, Y. Yu and F. Huang, *Org. Lett.*, 2010, **12**, 3285–3287.

76 Z. Zhang, L. Shao and J. Yang, *Tetrahedron Lett.*, 2018, **59**, 3000–3004.

77 L. Liu, D. Cao, Y. Jin, H. Tao, Y. Kou and H. Meier, *Org. Biomol. Chem.*, 2011, **9**, 7007–7010.

78 X.-B. Hu, Z. Chen, L. Chen, L. Zhang, J.-L. Hou and Z.-T. Li, *Chem. Commun.*, 2012, **48**, 10999–11001.

79 T. Ogoshi, K. Demachi, K. Kitajima and T. Yamagishi, *Chem. Commun.*, 2011, **47**, 10290–10292.

80 B. Xia and M. Xue, *Chem. Commun.*, 2014, **50**, 1021–1023.

81 J. Fan, H. Deng, J. Li, X. Jia and C. Li, *Chem. Commun.*, 2013, **49**, 6343–6345.

82 N. L. Strutt, H. Zhang, S. T. Schneebeli and J. F. Stoddart, *Chem. - A Eur. J.*, 2014, **20**, 10996–11004.

83 T. S. Navale, M. R. Talipov, R. Shukla and R. Rathore, *J. Phys. Chem. C*, 2016, **120**, 19558–19565.

84 K. Iwaso, Y. Takashima and A. Harada, *Nat. Chem.*, 2016, **8**, 625–632.

85 S. C. Everhart, U. K. Jayasundara, H. Kim, R. Procúpez-Schtirbu, W. A. Stanbery, C. H. Mishler, B. J. Frost, J. I. Cline and T. W. Bell, *Chem. - A Eur. J.*, 2016, **22**, 11291–11302.

86 H. J. Shepherd, I. A. Gural'skiy, C. M. Quintero, S. Tricard, L. Salmon, G. Molnár and A. Bousseksou, *Nat. Commun.*, 2013, **4**, 2607–2616.

87 V. J. Chebny, R. Shukla, S. V. Lindeman and R. Rathore, *Org. Lett.*, 2009, **11**, 1939–1942.

88 C. Song and T. M. Swager, *Org. Lett.*, 2008, **10**, 3575–3578.

89 R. Rathore, V. J. Chebny, E. J. Kopatz and I. A. Guzei, *Angew. Chemie Int. Ed.*, 2005, **44**, 2771–2774.

90 C. Li, N. Gunari, K. Fischer, A. Janshoff and M. Schmidt, *Angew. Chemie Int. Ed.*, 2004, **43**, 1101–1104.

91 B. Rout, L. Motiei and D. Margulies, *Synlett*, 2014, **25**, 1050–1054.

92 I. Leray and B. Valeur, *Eur. J. Inorg. Chem.*, 2009, **2009**, 3525–3535.

93 D. Wang, M. V. Ivanov, D. Kokkin, J. Loman, J.-Z. Cai, S. A. Reid and R. Rathore, *Angew. Chemie Int. Ed.*, 2018, **57**, 8189–8193.

94 P. A. Pieniazek, A. I. Krylov and S. E. Bradforth, *J. Chem. Phys.*, 2007, **127**, 044317–044328.

95 R. Shukla, K. Thakur, V. J. Chebny, S. A. Reid and R. Rathore, *J. Phys. Chem. B*, 2010, **114**, 14592–14595.

96 D. Wang, M. R. Talipov, M. V. Ivanov, S. Mirzaei, S. V. Lindeman, S. Cai, R. Rathore and S. A. Reid, *J. Phys. Chem. Lett.*, 2018, **9**, 4233–4238.

97 Y. Liu, S. Yan, J. Li and H. Shan, *Polym. Bull.*, 2018, **75**, 3667–3678.

98 E. Al-Farhan, P. M. Keehn and R. Stevenson, *Tetrahedron Lett.*, 1992, **33**, 3591–3594.

99 V. Percec, C. G. Cho and C. Pugh, *Macromolecules*, 1991, **24**, 3227–3234.

100 B. Umezawa, O. Hoshino, H. Hara, K. Ohyama, S. Mitsubayashi and J. Sakakibara, *Chem. Pharm. Bull. (Tokyo).*, 1969, **17**, 2240–2244.

101 J. D. White and B. D. Gesner, *Tetrahedron Lett.*, 1968, **9**, 1591–1594.

102 Gaussian 09, Revision D.01, M. J. Frisch, G. W. Trucks, H. B. Schlegel, G. E. Scuseria, M. A. Robb, J. R. Cheeseman, G. Scalmani, V. Barone, B. Mennucci, G. A. Petersson, H. Nakatsuji, M. Caricato, X. Li, H. P. Hratchian, A. F. Izmaylov, J. Bloino, G. Zheng, J. L. Sonnenberg, M. Hada, M. Ehara, K. Toyota, R. Fukuda, J. Hasegawa, M. Ishida, T. Nakajima, Y. Honda, O. Kitao, H. Nakai, T. Vreven, J. A. Montgomery, Jr., J. E. Peralta, F. Ogliaro, M. Bearpark, J. J. Heyd, E. Brothers, K. N. Kudin, V. N. Staroverov, R. Kobayashi, J. Normand, K. Raghavachari, A. Rendell, J. C. Burant, S. S. Iyengar, J. Tomasi, M. Cossi, N. Rega, J. M. Millam, M. Klene, J. E. Knox, J. B. Cross, V. Bakken, C. Adamo, J. Jaramillo, R. Gomperts, R. E. Stratmann, O. Yazyev, A. J. Austin, R. Cammi, C. Pomelli, J. W.

Ochterski, R. L. Martin, K. Morokuma, V. G. Zakrzewski, G. A. Voth, P. Salvador, J. J. Dannenberg, S. Dapprich, A. D. Daniels, Ö. Farkas, J. B. Foresman, J. V. Ortiz, J. Cioslowski, and D. J. Fox, Gaussian, Inc., Wallingford CT, 2009.

103 D. S. Ranasinghe, J. T. Margraf, Y. Jin and R. J. Bartlett, *J. Chem. Phys.*, 2017, **146**, 034102–034110.

104 M. Lundberg and P. E. M. Siegbahn, *J. Chem. Phys.*, 2005, **122**, 224103–224112.

105 Y. Zhang and W. Yang, *J. Chem. Phys.*, 1998, **109**, 2604–2608.

106 M. R. Talipov, A. Boddeda, Q. K. Timerghazin and R. Rathore, *J. Phys. Chem. C*, 2014, **118**, 21400–21408.

107 C. Adamo and V. Barone, *Chem. Phys. Lett.*, 1997, **274**, 242–250.

108 S. Grimme, A. Hansen, J. G. Brandenburg and C. Bannwarth, *Chem. Rev.*, 2016, **116**, 5105–5154.

109 B. Uhler, M. V. Ivanov, D. Kokkin, N. Reilly, R. Rathore and S. A. Reid, *J. Phys. Chem. C*, 2017, **121**, 15580–15588.

110 D. Kokkin, M. V. Ivanov, J. Loman, J.-Z. Cai, R. Rathore and S. A. Reid, *J. Phys. Chem. Lett.*, 2018, **9**, 2058–2061.

111 E. Cancès, B. Mennucci and J. Tomasi, *J. Chem. Phys.*, 1998, **107**, 3032–3041.

112 R. Ditchfield, *Mol. Phys.*, 1974, **27**, 789–807.

113 M. Martínez, F. L. Ochoa, R. Cruz-Almanza and R. A. Toscano, *J. Chem. Crystallogr.*, 1996, **26**, 451–456.

114 A. Maliniak, Z. Luz, R. Poupko, C. Krieger and H. Zimmermann, *J. Am. Chem. Soc.*, 1990, **112**, 4277–4283.

115 N. E. Burlinson and J. A. Ripmeester, *J. Incl. Phenom.*, 1985, **3**, 95–98.

116 A. J. Cohen, P. Mori-Sánchez and W. Yang, *Chem. Rev.*, 2012, **112**, 289–320.

117 S. Ehrlich, J. Moellmann and S. Grimme, *Acc. Chem. Res.*, 2013, **46**, 916–926.

118 J. L. Bao, L. Gagliardi and D. G. Truhlar, *J. Phys. Chem. Lett.*, 2018, **9**, 2353–2358.

119 M. Renz, K. Theilacker, C. Lambert and M. Kaupp, *J. Am. Chem. Soc.*, 2009, **131**, 16292–16302.

120 M. V. Ivanov, S. H. Wadumethrige, D. Wang and R. Rathore, *J. Phys. Chem. C*, 2017, **121**, 15639–15643.

121 T. Nishinaga, *Organic redox systems : synthesis, properties, and applications*, Wiley-VCH; Weinheim, 2015.

122 T. S. Navale, K. Thakur, V. S. Vyas, S. H. Wadumethrige, R. Shukla, S. V. Lindeman and R. Rathore, *Langmuir*, 2012, **28**, 71–83.

123 M. R. Talipov, M. M. Hossain, A. Boddeda, K. Thakur and R. Rathore, *Org. Biomol. Chem.*, 2016, **14**, 2961–2968.

124 R. Rathore, A. S. V. Lindeman and J. K. Kochi, *J. Am. Chem. Soc.*, 1997, **119**, 9393–9404.

125 Jay K. Kochi, A. Rajendra Rathore and P. Le Maguères, *J. Org. Chem.*, 2000, **65**, 6826–6836.

126 Jian-Ming Lü, A. Sergiy V. Rosokha and J. K. Kochi, *J. Am. Chem. Soc.*, 2003, **125**, 12161–12171.

127 H. A. Benesi and J. H. Hildebrand, *J. Am. Chem. Soc.*, 1949, **71**, 2703–2707.

128 Sergey V. Lindeman, A. Jürgen Hecht and J. K. Kochi, *J. Am. Chem. Soc.*, 2003, **125**, 11597–11606.

129 H. Günther, *NMR spectroscopy : basic principles, concepts, and applications in chemistry*, 3rd edn., 2013.

130 R. Rathore, C. L. Burns and M. I. Deselnicu, in *Organic Syntheses*, John Wiley & Sons, Inc., Hoboken, NJ, USA, 2005, pp. 1–9.

131 M. R. Talipov, A. Boddeda, M. M. Hossain and R. Rathore, *J. Phys. Org. Chem.*,

2016, **29**, 227–233.

132 S. E. Matthews, P. Schmitt, V. Felix, M. G. B. Drew and P. D. Beer, *J. Am. Chem. Soc.*, 2002, **124**, 1341–1353.

133 H. J. Kim, M. H. Lee, L. Mutihac, J. Vicens and J. S. Kim, *Chem. Soc. Rev.*, 2012, **41**, 1173–1190.

134 A. Mattiuzzi, I. Jabin, C. Mangeney, C. Roux, O. Reinaud, L. Santos, J. F. Bergamini, P. Hapiot and C. Lagrost, *Nat. Commun.*, 2012, **3**, 1130–1137.

135 F. De Riccardis, I. Izzo, D. Montesarchio and P. Tecilla, *Acc. Chem. Res.*, 2013, **46**, 2781–2790.

136 B. S. Creaven, D. F. Donlon and J. McGinley, *Coord. Chem. Rev.*, 2009, **253**, 893–962.

137 Y. Zafrani and Y. Cohen, *Org. Lett.*, 2017, **19**, 3719–3722.

138 W. P. Van Hoorn, M. G. H. Morshuis, F. C. J. M. Van Veggel and D. N. Reinhoudt, *J. Phys. Chem. A*, 1998, **5639**, 1130–1138.

139 S. Simaan and S. E. Biali, *J. Org. Chem.*, 2004, **69**, 95–98.

140 C. Alema, *J. Phys. Chem. A*, 2005, **109**, 8049–8054.

141 S. E. Biali and V. Bo, *J. Org. Chem.*, 1997, **3263**, 8350–8360.

142 D. Wang, L. V. Ivanova, M. V. Ivanov, S. Mirzaei, Q. K. Timerghazin, S. A. Reid and R. Rathore, *Chem. - A Eur. J.*, 2018, **24**, 17439–17443.

143 O. Morikawa, T. Ishizaka and H. Sakakibara, *Polym. Bull.*, 2005, **107**, 97–107.

144 J. Stursa, H. Dvorakova, J. Smidrkal and J. Moravcova, *Tetrahedron Lett.*, 2004, **45**, 2043–2046.

145 C. Leonhardt, S. Brumm, A. Seifert, G. Cox, A. Lange, T. Rüffer, D. Schaarschmidt, H. Lang, N. Jöhrmann, M. Hietschold, F. Simon and M. Mehring, *Chempluschem*, 2013, **78**, 1400–1412.

146 W. Iwanek, M. Urbaniak and M. Bocheńska, *Tetrahedron*, 2002, **58**, 2239–2243.

147 P. Della Sala, C. Gaeta, W. Navarra, C. Talotta, M. De Rosa, G. Brancatelli, S. Geremia, F. Capitelli, P. Neri, U. Salerno, V. Giovanni, P. Ii, I.-F. Salerno, U. Trieste and L. Giorgieri, *J. Org. Chem.*, 2016, **81**, 5726–5731.

148 M. I. Ogden, A. L. Rohl, J. D. Gale, A. Chemistry, G. P. O. Box, S. Kensington, U. K. Sw and R. Bsse, *Chem. Commun.*, 2001, **0**, 1626–1627.

149 J. A. Ripmeester, G. D. Enright, C. I. Ratcliffe, K. A. Udachin and I. L. Moudrakovski, *Chem. Commun.*, 2006, **0**, 4986–4996.

150 A. D. Becke, *Phys. Rev. A*, 1988, **38**, 3098–3100.

151 Y. Zhao and D. G. Truhlar, *Theor. Chem. Acc.*, 2008, **120**, 215–241.

152 C. Adamo and V. Barone, *J. Chem. Phys.*, 1999, **110**, 6158–6170.

153 J.-D. Chai and M. Head-Gordon, *Phys. Chem. Chem. Phys.*, 2008, **10**, 6615–6620.

154 T. Yanai, D. P. Tew and N. C. Handy, *Chem. Phys. Lett.*, 2008, **393**, 51–57.

155 F. Weigend, R. Ahlrichs and F. K. Gmbh, *Phys. Chem. Chem. Phys.*, 2005, **7**, 3297–3305.

156 S. Grimme, S. Ehrlich and L. Goerigk, *J. Comput. Chem.*, 2011, **32**, 1456–1465.

157 A. V Marenich, C. J. Cramer and D. G. Truhlar, *J. Phys. Chem. B*, 2009, **113**, 6378–6396.

158 J. R. Cheeseman, G. W. Trucks, T. A. Keith, M. J. Frisch, J. R. Cheeseman, G. W. Trucks, T. A. Keith and M. J. Frisch, *J. Chem. Phys.*, 1996, **104**, 5497–5509.

159 J. Lii and N. L. Allinger, *J. Am. Chem. Soc.*, 1989, **111**, 8576–8582.

160 J. Lii and N. L. Allinger, *J. Am. Chem. Soc.*, 1989, **111**, 8566–8575.

161 L. Norman and H. Young, *J. Am. Chem. Soc.*, 1989, **111**, 8551–8557.

162 J. W. Ponder, et al., Tinker software tools for molecular design.

163 S. Mirzaei, D. Wang, S. V Lindeman, C. M. Sem and R. Rathore, *Org. Lett.*, 2018,

20, 6583–6586.

164 L. W. Chung, W. M. C. Sameera, R. Ramozzi, A. J. Page, M. Hatanaka, G. P. Petrova, T. V. Harris, X. Li, Z. Ke, F. Liu, H.-B. Li, L. Ding and K. Morokuma, *Chem. Rev.*, 2015, **115**, 5678–5796.

165 A. K. Rappe, C. J. Casewit, K. S. Colwell, W. A. Goddard and W. M. Skiff, *J. Am. Chem. Soc.*, 1992, **114**, 10024–10035.

166 A. J. Rybarczyk-pirek, M. Z. Zgierski and A. J. Rybarczyk-pirek, *J. Chem. Phys.*, 2001, **115**, 9346–9351.

167 P. Dauber and A. T. Hagler, *Acc. Chem. Res.*, 1980, **13**, 105–112.

168 S. Carlotto and M. Zerbetto, *J. Chem. Educ.*, 2014, **91**, 96–102.

169 W. K. Den Otter and W. J. Briels, *J. Am. Chem. Soc.*, 1998, **2**, 13167–13175.

170 D. Cao, Y. Kou, J. Liang, Z. Chen, L. Wang and H. Meier, *Angew. Chemie Int. Ed.*, 2009, **48**, 9721–9723.

171 M. Guo, X. Wang, C. Zhan, P. Demay-Drouhard, W. Li, K. Du, M. A. Olson, H. Zuilhof and A. C.-H. Sue, *J. Am. Chem. Soc.*, 2018, **140**, 74–77.

172 Y. Yao, M. Xue, J. Chen, M. Zhang and F. Huang, *J. Am. Chem. Soc.*, 2012, **134**, 15712–15715.

173 N. L. Strutt, H. Zhang, S. T. Schneebeli and J. F. Stoddart, *Acc. Chem. Res.*, 2014, **47**, 2631–2642.

174 K. Jie, Y. Zhou, E. Li and F. Huang, *Acc. Chem. Res.*, 2018, **51**, 2064–2072.

175 W. Si, P. Xin, Z.-T. Li and J.-L. Hou, *Acc. Chem. Res.*, 2015, **48**, 1612–1619.

176 S. Guo, Y. Song, Y. He, X.-Y. Hu and L. Wang, *Angew. Chemie Int. Ed.*, 2018, **57**, 3163–3167.

177 T. Ogoshi, K. Saito, R. Sueto, R. Kojima, Y. Hamada, S. Akine, A. M. P. Moeljadi, H. Hirao, T. Kakuta and T. Yamagishi, *Angew. Chemie Int. Ed.*, 2018, **57**, 1592–1595.

178 T. Ogoshi, K. Yoshikoshi, R. Sueto, H. Nishihara and T. Yamagishi, *Angew. Chemie Int. Ed.*, 2015, **54**, 6466–6469.

179 R. Joseph, D. Kaizerman, I. M. Herzog, M. Hadar, M. Feldman, M. Fridman and Y. Cohen, *Chem. Commun.*, 2016, **52**, 10656–10659.

180 Q. Lin, Y.-Q. Fan, P.-P. Mao, L. Liu, J. Liu, Y.-M. Zhang, H. Yao and T.-B. Wei, *Chem. - A Eur. J.*, 2018, **24**, 777–783.

181 Y. Cao, Y. Li, X.-Y. Hu, X. Zou, S. Xiong, C. Lin and L. Wang, *Chem. Mater.*, 2015, **27**, 1110–1119.

182 L.-L. Tan, H. Li, Y.-C. Qiu, D.-X. Chen, X. Wang, R.-Y. Pan, Y. Wang, S. X.-A. Zhang, B. Wang and Y.-W. Yang, *Chem. Sci.*, 2015, **6**, 1640–1644.

183 G. Yu, J. Zhou, J. Shen, G. Tang and F. Huang, *Chem. Sci.*, 2016, **7**, 4073–4078.

184 H. Gu, S. Mu, G. Qiu, X. Liu, L. Zhang, Y. Yuan and D. Astruc, *Coord. Chem. Rev.*, 2018, **364**, 51–85.

185 Y. Cao, X.-Y. Hu, Y. Li, X. Zou, S. Xiong, C. Lin, Y.-Z. Shen and L. Wang, *J. Am. Chem. Soc.*, 2014, **136**, 10762–10769.

186 K. Jie, M. Liu, Y. Zhou, M. A. Little, A. Pulido, S. Y. Chong, A. Stephenson, A. R. Hughes, F. Sakakibara, T. Ogoshi, F. Blanc, G. M. Day, F. Huang and A. I. Cooper, *J. Am. Chem. Soc.*, 2018, **140**, 6921–6930.

187 T. Ogoshi, R. Sueto, K. Yoshikoshi, K. Yasuhara and T. Yamagishi, *J. Am. Chem. Soc.*, 2016, **138**, 8064–8067.

188 G. Yu, C. Han, Z. Zhang, J. Chen, X. Yan, B. Zheng, S. Liu and F. Huang, *J. Am. Chem. Soc.*, 2012, **134**, 8711–8717.

189 T. Ogoshi, N. Ueshima, F. Sakakibara, T. Yamagishi and T. Haino, *Org. Lett.*, 2014, **16**, 2896–2899.

190 M. V. Ivanov, D. Wang, T. S. Navale, S. V. Lindeman and R. Rathore, *Angew. Chemie - Int. Ed.*, 2018, **57**, 2144–2149.

191 K. Wang, L.-L. Tan, D.-X. Chen, N. Song, G. Xi, S. X.-A. Zhang, C. Li and Y.-W. Yang, *Org. Biomol. Chem.*, 2012, **10**, 9405–9409.

192 H. Tao, D. Cao, L. Liu, Y. Kou, L. Wang and H. Meier, *Sci. China Chem.*, 2012, **55**, 223–228.

193 S. Santra, I. S. Kovalev, D. S. Kopchuk, G. V. Zyryanov, A. Majee, V. N. Charushin and O. N. Chupakhin, *RSC Adv.*, 2015, **5**, 104284–104288.

194 C. Han, F. Ma, Z. Zhang, B. Xia, Y. Yu and F. Huang, *Org. Lett.*, 2010, **12**, 4360–4363.

195 Y. Kou, D. Cao, H. Tao, L. Wang, J. Liang, Z. Chen and H. Meier, *J. Incl. Phenom. Macrocycl. Chem.*, 2013, **77**, 279–289.

196 M. Da Pian, O. De Lucchi, G. Strukul, F. Fabris and A. Scarso, *RSC Adv.*, 2016, **6**, 48272–48275.

197 A. D. Becke, *Phys. Rev. A*, 1988, **38**, 3098–3100.

198 S. Grimme, J. Antony, S. Ehrlich and H. Krieg, *J. Chem. Phys.*, 2010, **132**, 154104–154123.

199 X. Shu, J. Fan, J. Li, X. Wang, W. Chen, X. Jia and C. Li, *Org. Biomol. Chem.*, 2012, **10**, 3393–3397.

200 S. Santra, D. S. Kopchuk, I. S. Kovalev, G. V. Zyryanov, A. Majee, V. N. Charushin and O. N. Chupakhin, *Green Chem.*, 2016, **18**, 423–426.